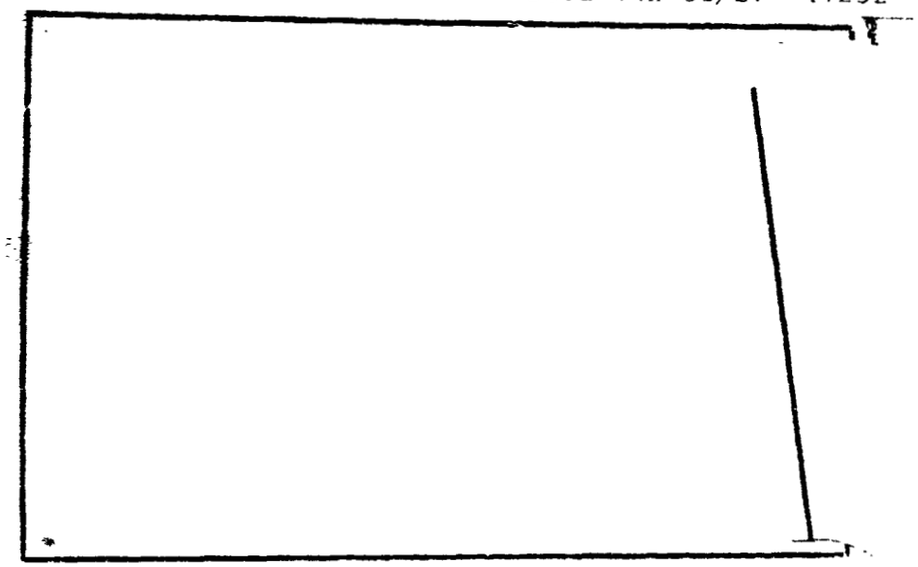

Virginia Polytechnic Institute and State University

Chemistry Department

Blacksburg, Virginia 24061

FINAL REPORT

A FUNDAMENTAL APPROACH TO ADHESION: SYNTHESIS, SURFACE ANALYSIS, THERMODYNAMICS AND MECHANICS

by

Wen Chen and James P. Wightman

Prepared for

National Aeronautics and Space Administration

January, 1979

Grant NSG-1124

NASA-Langley Research Center
Hampton, Virginia 23665
Materials Division
Donald J. Progar

Department of Chemistry
Virginia Polytechnic Institute and State University
Blacksburg, Virginia 24061

TABLE OF CONTENTS

LIST OF TABLES

LIST OF FIGURES

GLOSSARY

TECHNIQUES

AES - Auger electron spectroscopy

CMA - Cylindrical mirror analyzer

EDAX - Energy dispersive analysis of x-rays

ESCA - Electron spectroscopy for chemical analysis

SEM - Scanning electron microscopy

CHEMICALS

MEPPQ - Polyphenylquinoxaline

OTHERS

AMR - Advanced Metals Research

LaRC - Langley Research Center

PHI - Physical Electronics Industries

I. INTRODUCTION

During the current grant period, our experimental program has emphasized mainly the study of adherend surfaces and fractography using Electron Spectroscopy for Chemical Analysis (ESCA) and Scanning Electron Microscopy/Energy Dispersive Analysis of X-rays (SEM/EDAX). In addition, Auger Electron Spectroscopy (AES) with depth profiling capability has been used. The scope of the program is outlined in Table I.

Contamination of adhesion systems can play an important role not only in determining initial bond strengths but also in the durability of adhesive bonds. Sources of contamination effecting adhesive bonding and bond properties are listed in Table II. The analytical techniques used in our research program are suited uniquely to characterize and monitor such contamination.

Selected results of the research under the grant were presented in three papers at two national meetings described in Appendix I. Copies of the manuscript of three papers submitted for publication are included in Appendix II.

TABLE I

SCOPE OF EXPERIMENTAL PROGRAM

A. Graphite Fibers

SEM, ESCA

B. Kapton Film

1. Metallized Kapton

ESCA, AES/Depth Profiling

2. Fractography of Bonded Kapton Film

SEM

C. LaRC Monomers

ESCA

D. Contamination of Ti 6-4

AES/Depth Profiling

1. Anodized Ti 6-4
2. Phosphate/Fluoride Ti 6-4

E. Fracture Surface Analysis

SEM, ESCA

1. LaRC-13/no elastomer
2. LaRC-13/elastomer
3. Sample No. 1499 P-1

F. Surface Analysis of Primed Ti 6-4

SEM/EDAX, ESCA

1. MEPPQ Primer
2. Phosphate/Fluoride Treatment with BR-34 Primer
3. Phosphate/Fluoride Treatment with MEPPQ Primer
4. Phosphate/Fluoride Treatment with MEPPQ Primer-Boeing

TABLE II

SOURCES OF CONTAMINATION EFFECTING ADHESIVE BONDING AND BOND PROPERTIES

Raw Materials Processing

  Adherend

  Adhesive

Prebonding Treatment

  Chemical Solution Contributions

  Alloy Constituents

Environment

  Storage and Handling

  Bonding

II. EXPERIMENTAL

A. Methods and Procedures

1. Electron Spectroscopy for Chemical Analysis (ESCA)--ESCA data were collected on a DuPont 650 photoelectron spectrometer with a magnesium anode ($K\alpha_{1,2}$ = 1253.6 eV) and direct display of the spectra on an x-y recorder. The carbon 1s level (taken as 284.0 eV) was used to evaluate the work function of the spectrometer. Circular (6.4 mm or 32 mm^2) samples were mounted on the copper sample probes using double sided adhesive tape.

2. Scanning Electron Microscopy/Energy Dispersive Analysis of X-rays (SEM/EDAX)--SEM photomicrographs at various magnifications were obtained on an AMR scanning electron microscope (Advanced Metals Research Corporation Model 900). Approximate vertical dimensions of each photomicrograph appear at the right in the figures, and the corresponding magnification is listed in each caption. Most SEM samples were run after ESCA analysis. A thin ($\sim$ 20 nm) film of Au-Pd Alloy was vacuum-evaporated onto the samples to enhance conductivity of insulating samples. A rapid semi-quantitative elemental analysis was obtained on selected samples with an EDAX International Model 707A energy-dispersive X-ray fluorescence analyzer attached to the AMR-900 SEM. A photographic record of each EDAX spectrum was made using a camera specially adapted for the EDAX oscilloscope.

3. Auger Electron Spectroscopy (AES) with Ion-sputtering Depth Profiling--A PHI combined ESCA/Auger spectrometer (Physical Electronics Industries Model 550) with a double pass cylindrical mirror analyzer (CMA) described by Palmberg was used (1). Auger depth profiles were obtained with a coaxial electron gun and simultaneous ion beam etching using 2 keV Ar^+ ions from a differentially pumped PHI gun.

B. Materials

1. Graphite fibers--Four sets of graphite fibers (HMS, HTS-2, Celion 6000, and Thornel 300) were obtained from NASA-LaRC. Three sets of graphite fibers coded NASA 1 (only a single fiber), NASA 2 and NASA 3 were electrocoated by B. Y. Subramanian, Washington State University. The coating parameters were not specified. All the structures of the graphite fibers are described in Table III. The graphite fibers charge extensively in the ESCA spectrometer. In order to prevent electrical shorts in the analyzer section, a custom sample probe was used. Here, a set of graphite fibers was mounted on tape and then mechanically fastened to the probe at both ends with gold staples.

2. Metallized Kapton and Kapton film.--A sheet of metallized Kapton 203x127 mm was supplied by A. K. StClair at NASA-LaRC. A 100 nm aluminum film had been deposited on one side and a 15 nm chromium film deposited on the opposite side. A piece of 3 mil Kapton 38.1 x 25.4 mm was wiped with ethanol and was coated with a 15% diglyme solution of LaRC-3 under B stage at 443K. The adhesive area was about 9 x 25 mm on bonding to another piece of Kapton under contact pressure for 20 sec at 616K. The two films were then peeled apart and the mating surfaces analyzed.

3. LaRC Model Compounds. A number of new fluoro monomers were supplied by P. M. Hergenrother (2) at the NASA-LaRC. The monomers were run as powders.

4. Anodized and phosphate/fluoride treated Ti 6-4.--Samples of both anodized and phosphate/fluoride treated Ti 6-4 which analysis had been reported previously (3), were analyzed by Auger electron spectroscopy and also depth profiled with argon sputtering.

5. Fractured lap shear and T-peel specimens.--Two fractured T-peel specimen were supplied by personnel at NASA-LaRC. The adhesive in one

TABLE III

DESCRIPTION OF GRAPHITE FIBERS

Graphite Fibers	Structure
HMS	Batch No. 92-2 No surface finish
HTS-2	Batch No. 94-3 No surface finish
Celion 6000	Lot #HTA-7-7711 1.2% polyimide finish
Thornel 300	Grade WYP 30% Epoxy finish, UC 309
NASA-1	Unspecified fiber coated with styrene/maleic anhydride
NASA-2	CG-3 fiber coated with styrene/maleic anhydride
NASA-3	HTS fiber coated with nadic anhydride

specimen was LaRC-13 with no elastomer. LaRC-13 adhesive containing 15% of a florosiloxane elastomer was used in the second specimen. The third was a lap shear specimen coded 1499 P-1 which had a low strength. No other details were available.

6. Primed Ti 6-4 specimens--A sample coded #813-11-5 was reportedly given a phosphate/fluoride treatment and then primed with MEPPQ. Mr. Donald J. Progar supplied eight Ti 6-4 coupons which had been pretreated in the following ways:

(i) phosphate/fluoride etch;

(ii) heated to 483K for 45 min after (i);

(iii) primed with BR-34 (Batch B-169) and heated to 483K for 45 min after (i); and,

(iv) primed with MEPPQ (m-cresol/xylene solvent system) and heated to 343K for 30 min after (i).

The primer was dissolved partially in chloroform.

A final Ti 6-4 specimen primed with MEPPQ was supplied by the Boeing Aerospace Co.

III. RESULTS AND DISCUSSION

A. Graphite Fibers (SEM and ESCA)

SEM photomicrographs of seven graphite fibers are shown in Figures 1-7. The HMS fiber (Fig. 1) is characterized by surface striations whereas the HTS-2 fiber (Fig. 2) appears smooth. The other fibers were coated as noted in Table III. The epoxy coated Thornel fiber (Fig. 3) clearly shows striations. Although the Celion 600 fibers are coated (Fig. 4), surface striations are apparent both before and after solvent washing. The striations may be somewhat more marked after washing. The SEM of the styrene-maleic anhydride graphite fiber (Fig. 5) has a patchy appearance not noticed for the other fibers. Again, striations are apparent in the CG-3 fibers (Fig. 6) before and after solvent rinse. Coated HT-S fibers in Fig. 7 are quite different to the uncoated fibers shown in Fig. 2.

In summary, the SEM photomicrographs do not show marked changes in surface morphology between uncoated, coated and solvent rinsed graphite fibers.

The ESCA results for the graphite fibers are listed in Table IV. The binding energies (BE), atomic percents (AP), carbon-oxygen (C/O) and carbon-nitrogen (C/N) intensity ratios are tabulated. The oxygen and nitrogen intensities were corrected by the appropriate photoelectric cross-section (4). The HTS-2 fiber is characterized by the largest C/O and C/N ratios indicative of minimal amounts of surface oxygen and nitrogen compared to the two other uncoated fibers (HMS and Thornel 300). The C/O and C/N ratios for Thornel 300 fibers decrease sharply after coating with epoxy which is consistent with the increased oxygen and nitrogen content of epoxy.

There is no apparent removal of the coatings on solvent rinse as gauged by the constancy in both the C/O and C/N ratios of the unrinsed and rinsed fibers.

The C 1s photopeak in the coated fibers and Thornel 300 shows a small shoulder on the high binding side. This result is consistent with the higher oxygen content of these fibers.

Figure 1.

SEM photomicrographs (2,000x, 10,000x) of
HMS graphite fiber (Batch #32-2).

Figure 2.

SEM photomicrographs (2,000x, 10,000x) of HTS-2 graphite fiber (Batch #94-3).

Figure 3.

SEM photomicrographs (200x, 10,000x) of
Thornel 300 graphite fiber (Grade WYP 30%).

Figure 3. SEM photomicrographs (200x, 10,000x) of Thornel 300 graphite fiber (Grade WYP 30%).

Fiber has been coated with epoxy (UC 309 finish). Surface striations are clearly visible.

Figure 4.

SEM photomicrographs (2,000x, 10,000x) of Celion 6000 graphite fiber (Lot #HTA-7-7711).

Figure 4. SEM photomicrographs (2,000x, 10,000x) of Celion 6000 graphite fiber (Lot #HTA-7-7711).

Fiber has been treated with 1.2% PI solution.
A. Before solvent rinse. B. After rinsing with methyl ethyl ketone for 30 min at ambient temperature. There appears to be no apparent change in surface morphology.

Figure 5.

SEM photomicrographs (2,000x, 10,000x) of NASA-1 graphite fiber.

Figure 5. SEM photomicrographs (2,000x, 10,000x) of NASA-1 graphite fiber.

Fiber is coated with a polymer of styrene-maleic anhydride having a low to medium molecular weight. Surface roughness is apparent.

10μm

50μm

FIGURE 6.

SEM photomicrographs (2,000x, 5,000x) of
NASA-2 graphite fiber.

Figure 6. SEM photomicrographs (2,000x, 5,000x) of NASA-2 graphite fiber.

This CG-3 based fiber is a low tensile strength fiber coated with a polymer of styrene and maleic anhydride.

A. Before solvent rinse. B. After solvent rinsing with toluene for 30 min at ambient temperature. There appears to be no apparent change in surface morphology.

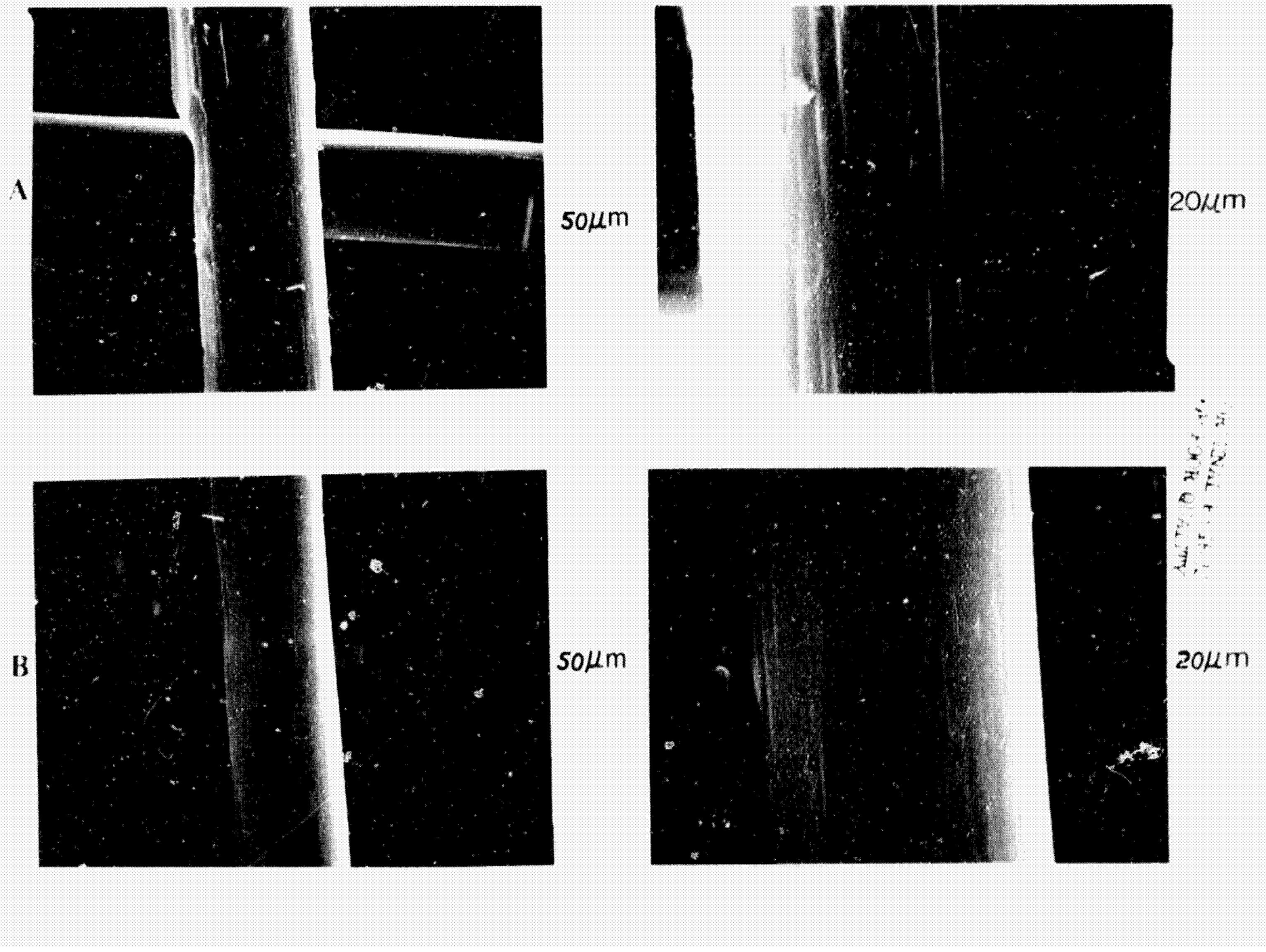
A
50μm
20μm
B
50μm
20μm

FIGURE 7.

SEM photomicrographs (2,000x, 10,000x) of NASA-3 graphite fiber.

Figure 7. SEM photomicrographs (2,000x, 10,000x) of NASA-3 graphite fiber.

This HT-S based fiber is a high tensile strength fiber coated with a polymer of nadic anhydride.

A. Before solvent rinse. B. After solvent rinsing with toluene for 30 min at ambient temperature there appears to be no change in surface morphology.

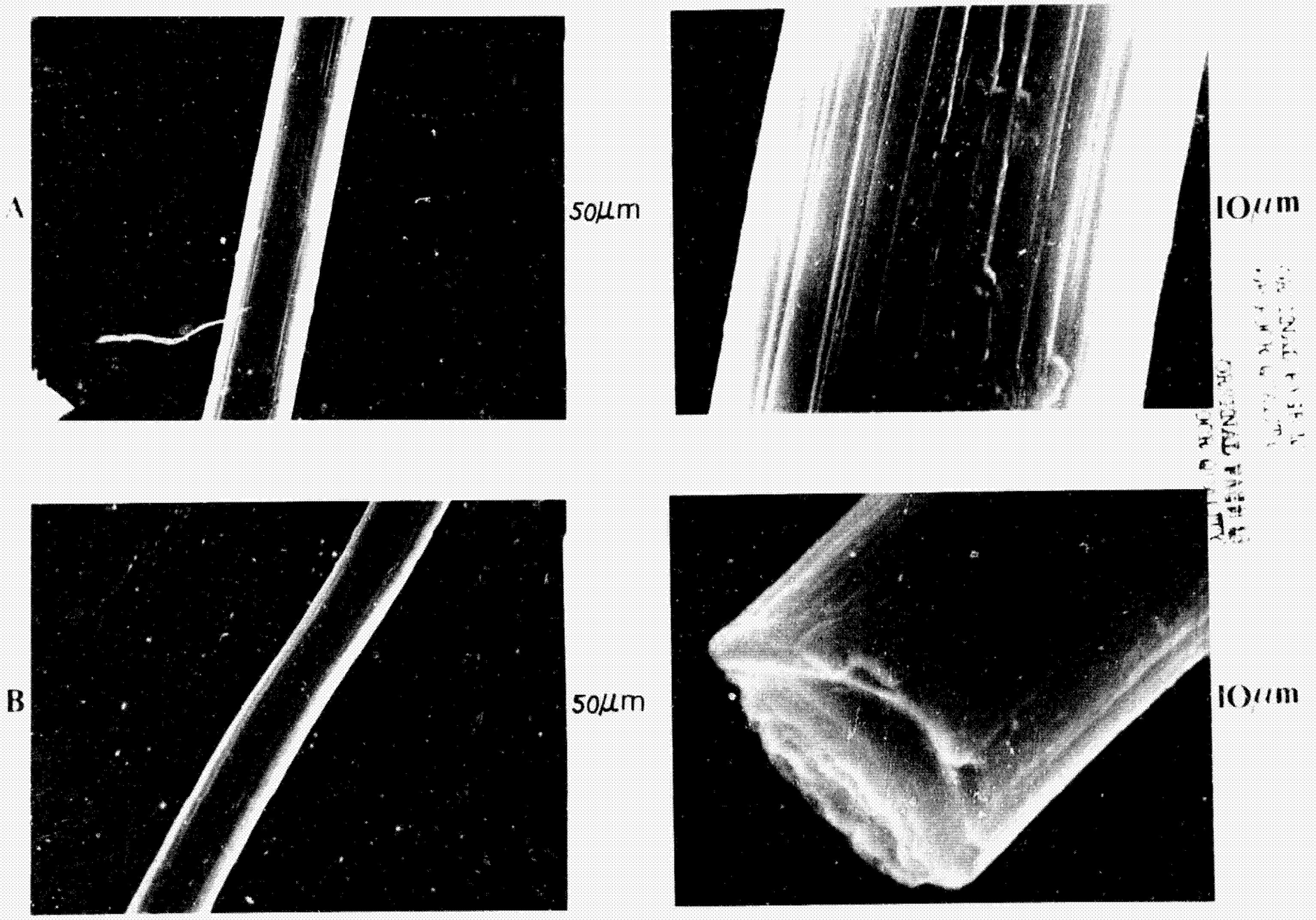
A
50μm
10μm
B
50μm
10μm

TABLE IV

ESCA ANALYSIS OF GRAPHITE FIBERS.

Fiber	C_{1s} BE(ev)	C_{1s} AP	O_{1s} BE(ev)	O_{1s} AP	N_{1s} BE(ev)	N_{1s} AP	C/O	C/N
1. HMS	(284.0)	88.6	532.4	9.7	399.5	1.7	9.	52.
2. HTS-2	(284.0)	92.9	532.2	6.7	399.4	0.4	14.*	232.*
3. Thornel 300	(284.0)	85.0	532.3	13.4	399.8	1.6	6.	53.
4. Thornel 300 (epoxy finish UC 300)	(284.0)	72.4	531.9	23.1	399.0	4.5	3.	16.
5. Celion 6000 (1.2% PI)	(284.0)	85.3	531.4	11.8	398.4	2.9	7.	29.
6. Celion 6000 (MEK rinse)	(284.0)	85.3	531.8	13.0	399.0	1.7	7.	50.
7. NASA-2	(284.0)	83.0	531.6	16.0	398.6	1.0	5.	83.
8. NASA-2 (toluene rinse)	(284.0)	84.2	532.0	14.5	399.4	1.3	6.	65.
9. NASA-3	(284.0)	81.0	531.8	17.6	399.1	1.4	5.	58.
10. NASA-3 (toluene rinse)	(284.0)	82.0	531.6	16.4	398.6	1.6	5.	51.
					Average		$\overline{6\pm1}$	$\overline{51\pm13}$

*values not included in average

B. Kapton Film

1. Metallized Kapton (ESCA and AES/Depth Profiling)

The ESCA spectra for metallized Kapton is shown in Figure 8. Spectra A is the Cr $2p_{3/2}$ photopeak (B.E. 581.4 eV) on opposite sides of the film. Spectra B is the Al 2p photopeak on opposite sides of the films. There is no Al noted on the Cr side nor any Cr noted on the Al side. Significantly, a doublet is noted in the Al photopeak which may be explained as follows. The higher binding energy peak at 118.4 eV is due to Al(III) in the aluminum oxide surface layer. Photoelectrons from elemental aluminum [Al(0)] penetrate the thin surface oxide layer ($\sim$ 20 nm) and give rise to the smaller binding energy peak at 115.8 eV. The difference of 2.6 eV between the two peaks is consistent with reported values (5).

The metallized Kapton film was also subjected to Auger electron spectroscopy (AES) with depth profiling. The Auger spectra from the aluminum and chromium sides are shown in Figure 9 and 10, respectively. Carbon and oxygen are also noted in both Auger spectra. The depth profile results for the aluminum side are shown in Figure 11. The sputter rate in this case was about 200 nm/min. The atomic concentrations (in percent) of carbon, aluminum and oxygen before sputtering were 17, 41, 43, respectively. The carbon signal drops to nearly zero within the aluminum oxide surface layer while the alunimum and oxygen signals increase to a maximum. Thereafter, the aluminum and oxygen signals decrease indicating that the aluminum coating has been penetrated. There is a concomittant increase in the carbon signal as the Kapton substrate is reached.

It is noteworthy that the O/Al ratio was 1.0 at the surface but through the aluminum coating remained fairly constant at a value of 0.67. The fact that Al(0) was observed in the ESCA spectra would suggest an even lower value of the O/Al ratio. The estimated thickness of the aluminum

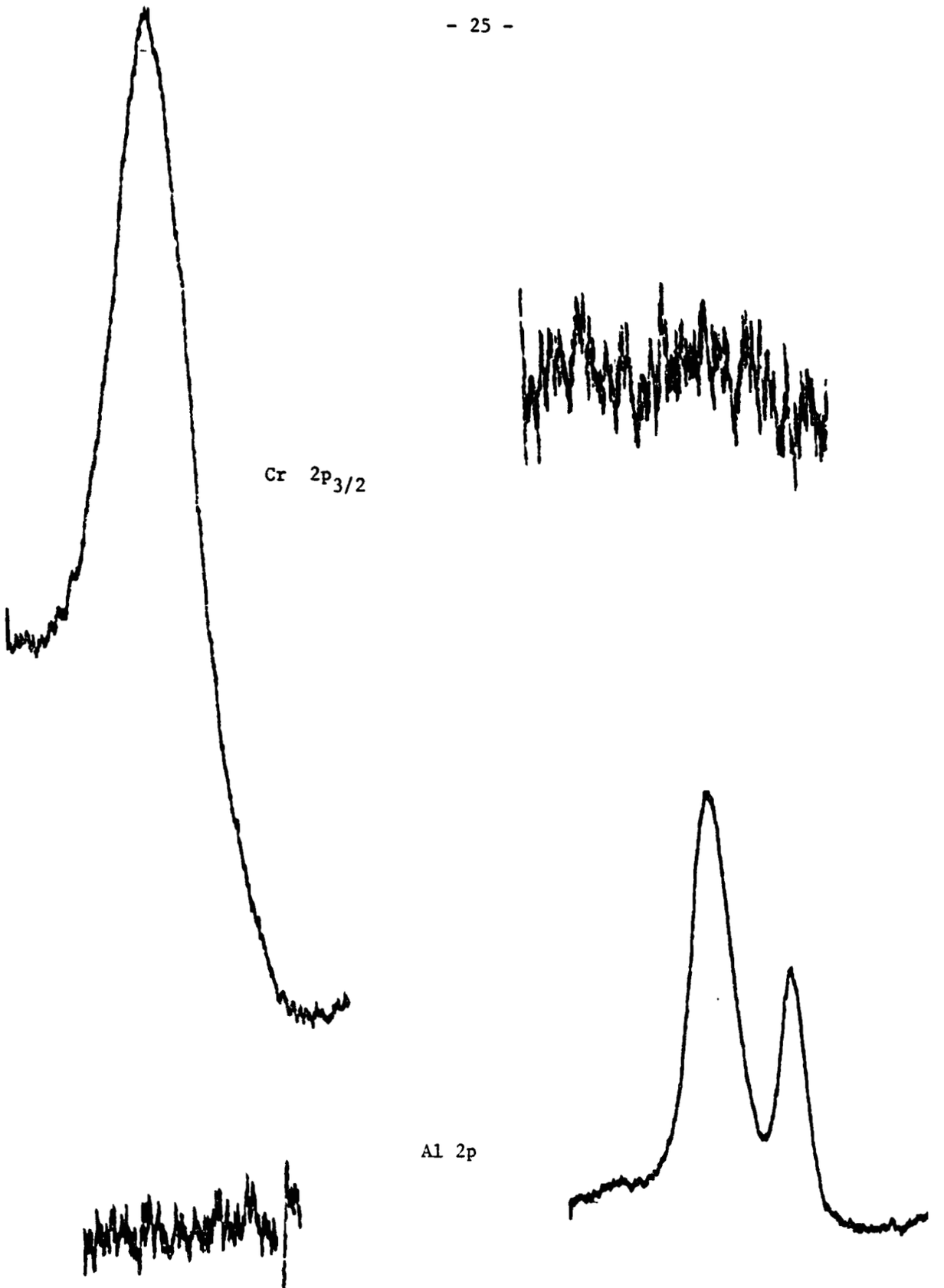

Figure 8. ESCA spectra of metallized Kapton film. A. Cr side B. Al side.

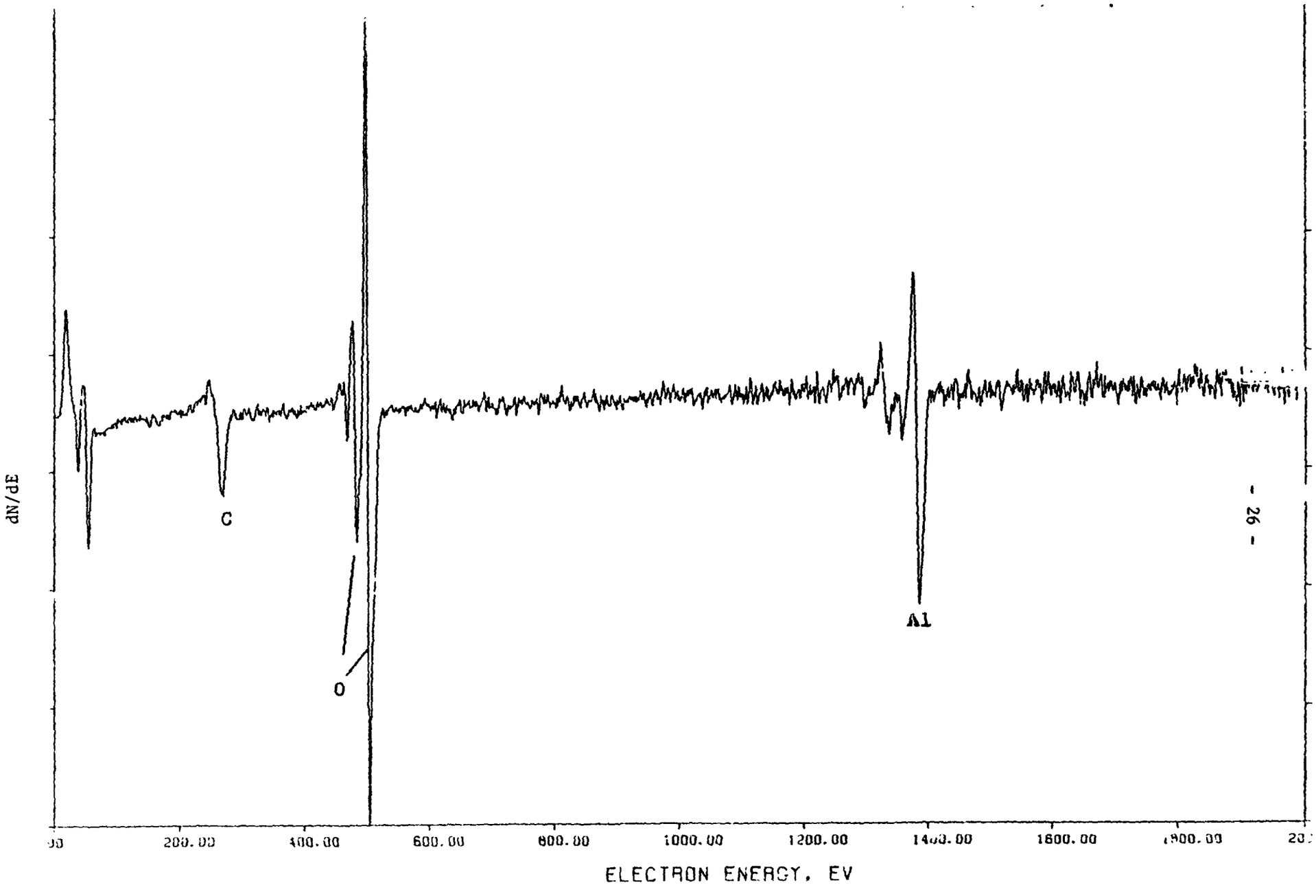

Figure 9. AES spectrum of metallized Kapton film (Al side).

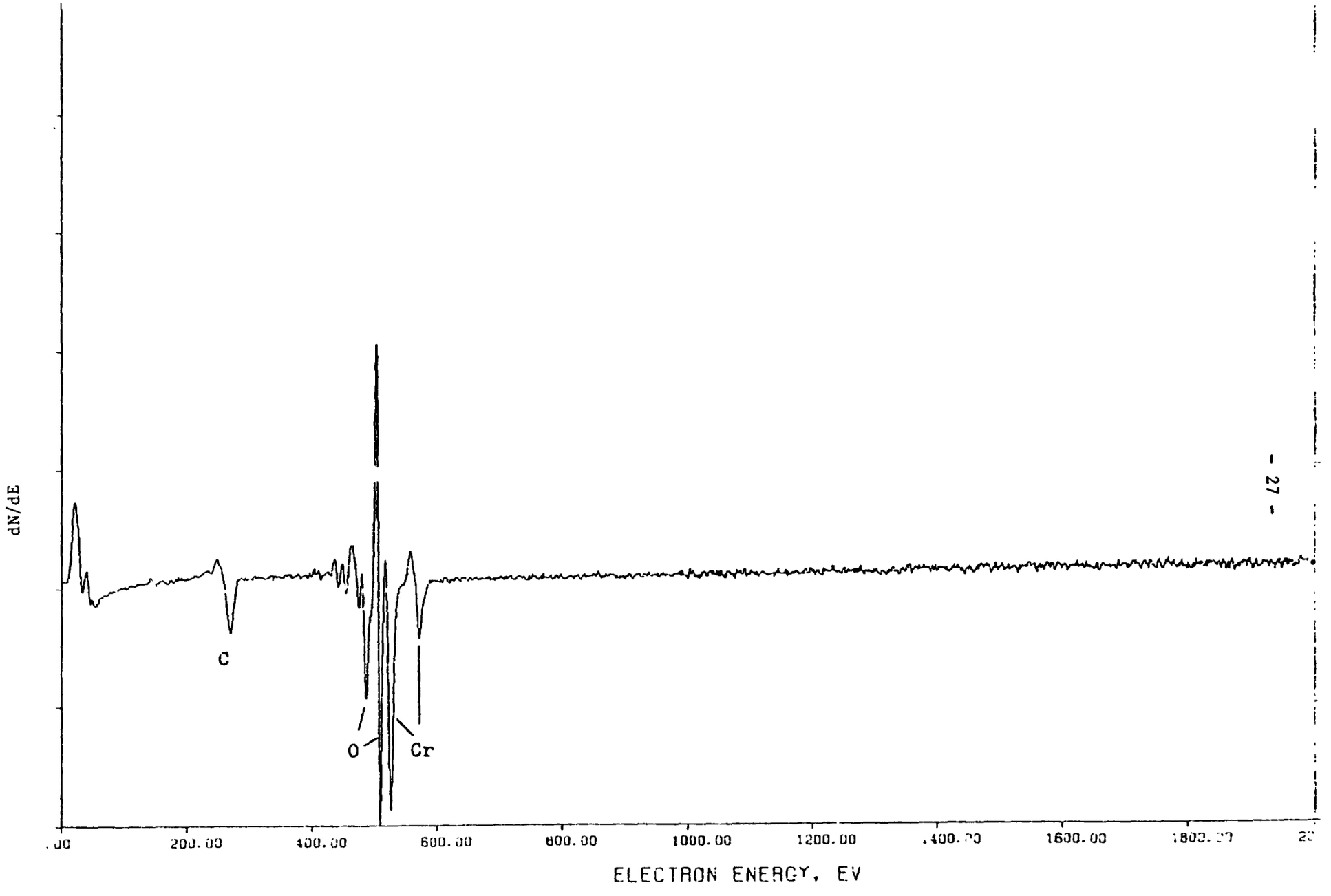

Figure 10. AES spectrum of metallized Kapton film (Cr side).

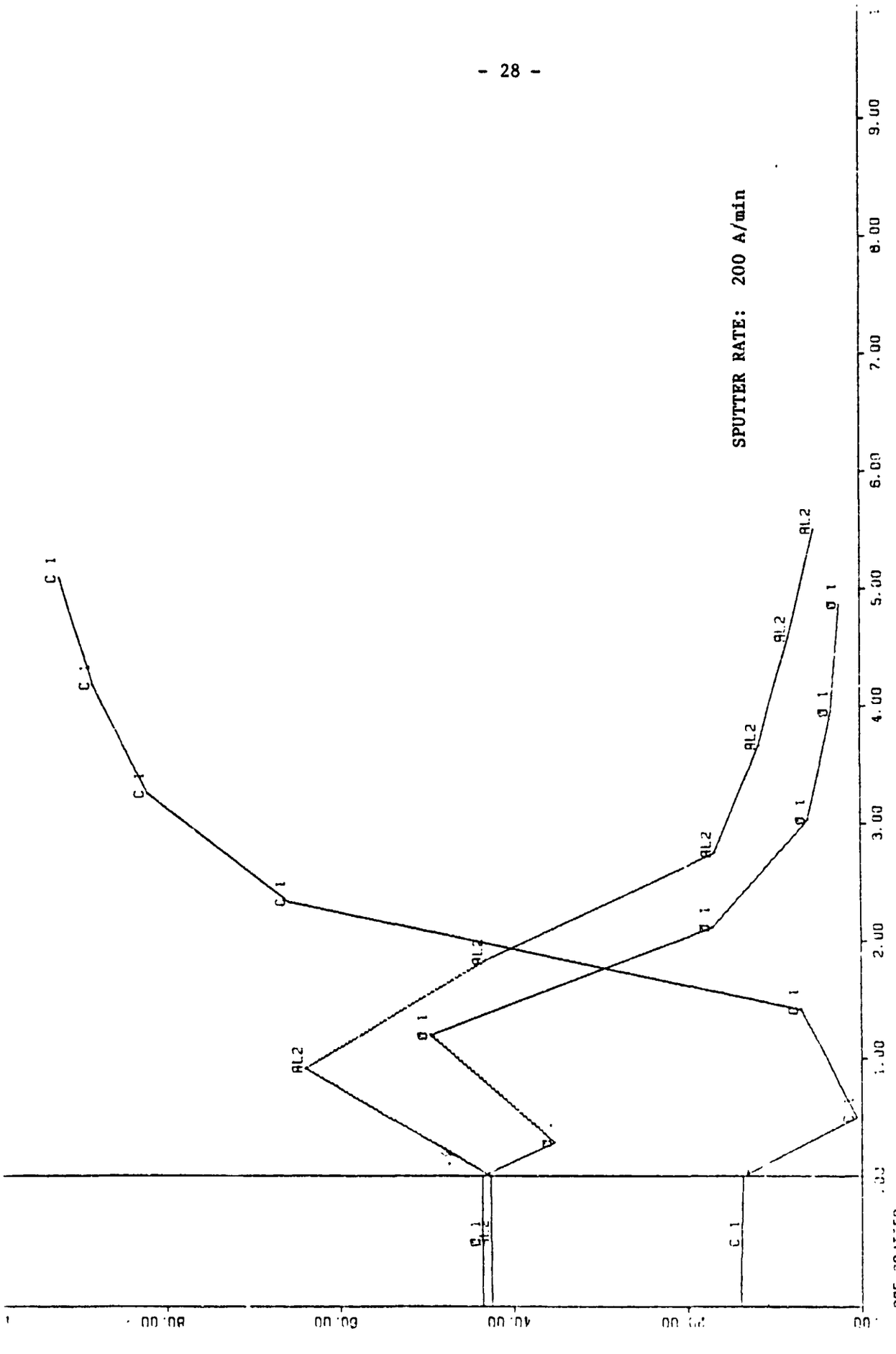

Figure 11. Composition-depth profiles of metallized Kapton film (Al side).

coating is about 40 nm based on a sputtering time of 2 minutes.

Similar depth profile results for the chromium side are shown in Figure 12. In contrast to the aluminum coating, the O/Cr ratio of the outer chromium coating was > 1 whereas the ratio was < 1 for the inner chromium coating. The estimated thickness of the chromium coating is about 14 nm based on a sputtering time of 7 minutes.

2. Fractography of bonded Kapton film (SEM)

SEM photomicrographs of fracture surfaces of Kapton film bonded with LaRC-3 adhesive are shown in Figure 13. The fracture surfaces are riddled with voids (1 μm < d < 10 μm) suggesting vapor release on curing.

C. LaRC Model Compounds (ESCA)

To demonstrate the versatility of ESCA and to gain additional experience, model compounds of known composition were analyzed. These findings are reported in the following discussion.

Narrow scan ESCA spectra were obtained for six fluorinated heterocyclic model compounds and are shown in Figures 14-19 along with the structures. Parameters obtained from the ESCA spectra and constituent ratios are listed in Tables V and VI, respectively. The higher B.E. peak at 290.3 ± 0.3 eV in the C 1s spectra is due to carbon bonded to fluorine. Average binding energies of 400.1 ± 0.1 eV and 398.6 ± 0.3 eV in the N 1s spectra are assigned to two different bonding states of nitrogen. The atomic ratios calculated from the ESCA spectra $[(F/C)_E, (N/C)_E]$ are in reasonable agreement with the value calculated from the ratio of elements in the empirical formula $[(F/C)_S, (N/C)_S]$.

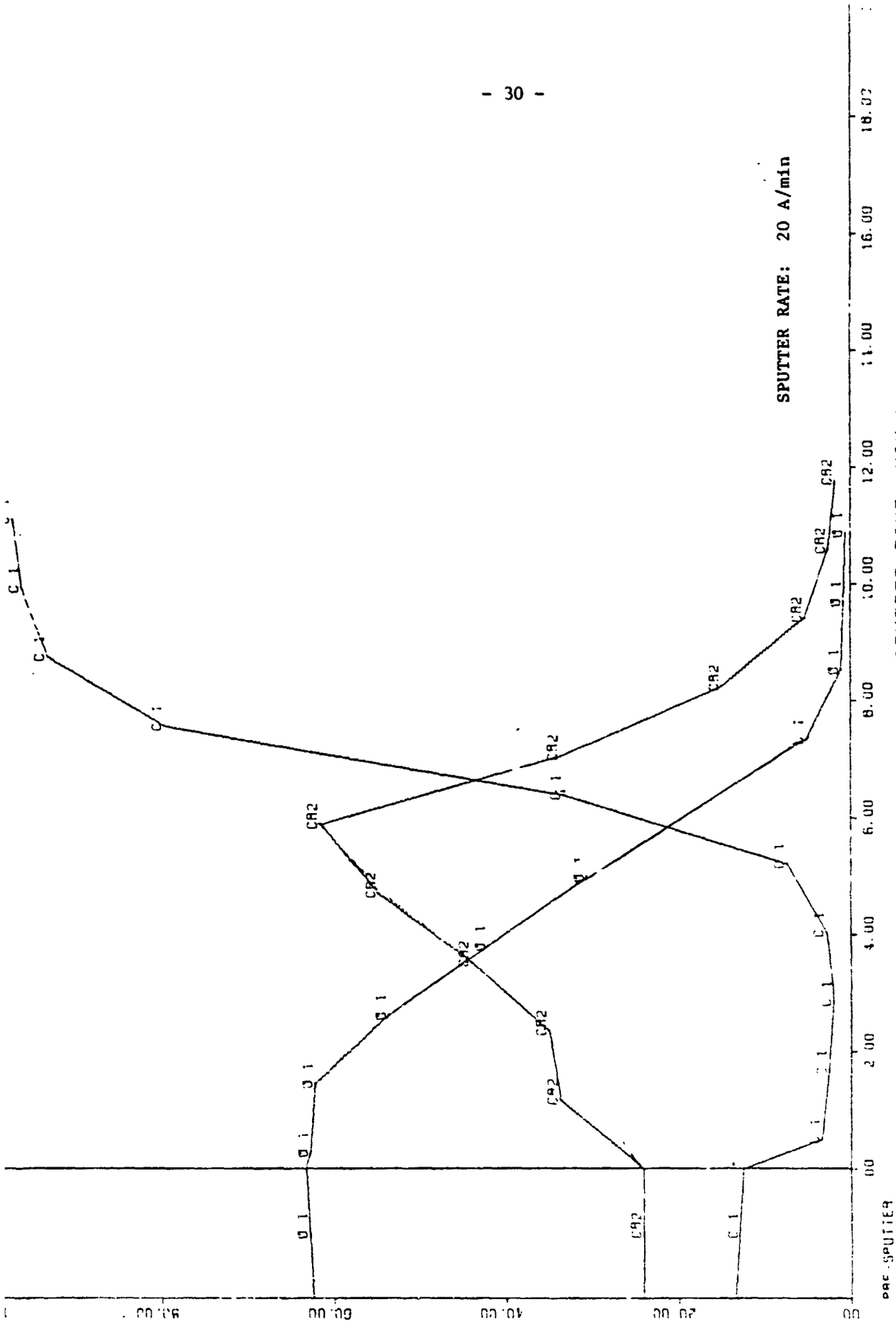

Figure 12. Composition-depth profiles of metallized Kapton film (Cr side).

FIGURE 13.

SEM photomicrographs (100x, 500x) of bonded Kapton fracture surfaces.

Figure 13, SEM photomicrographs (100x, 500x) of bonded Kapton fracture surfaces.

A and B represent opposite sides of the fractured bond. Note the honeycomb structure due to vapor generated voids.

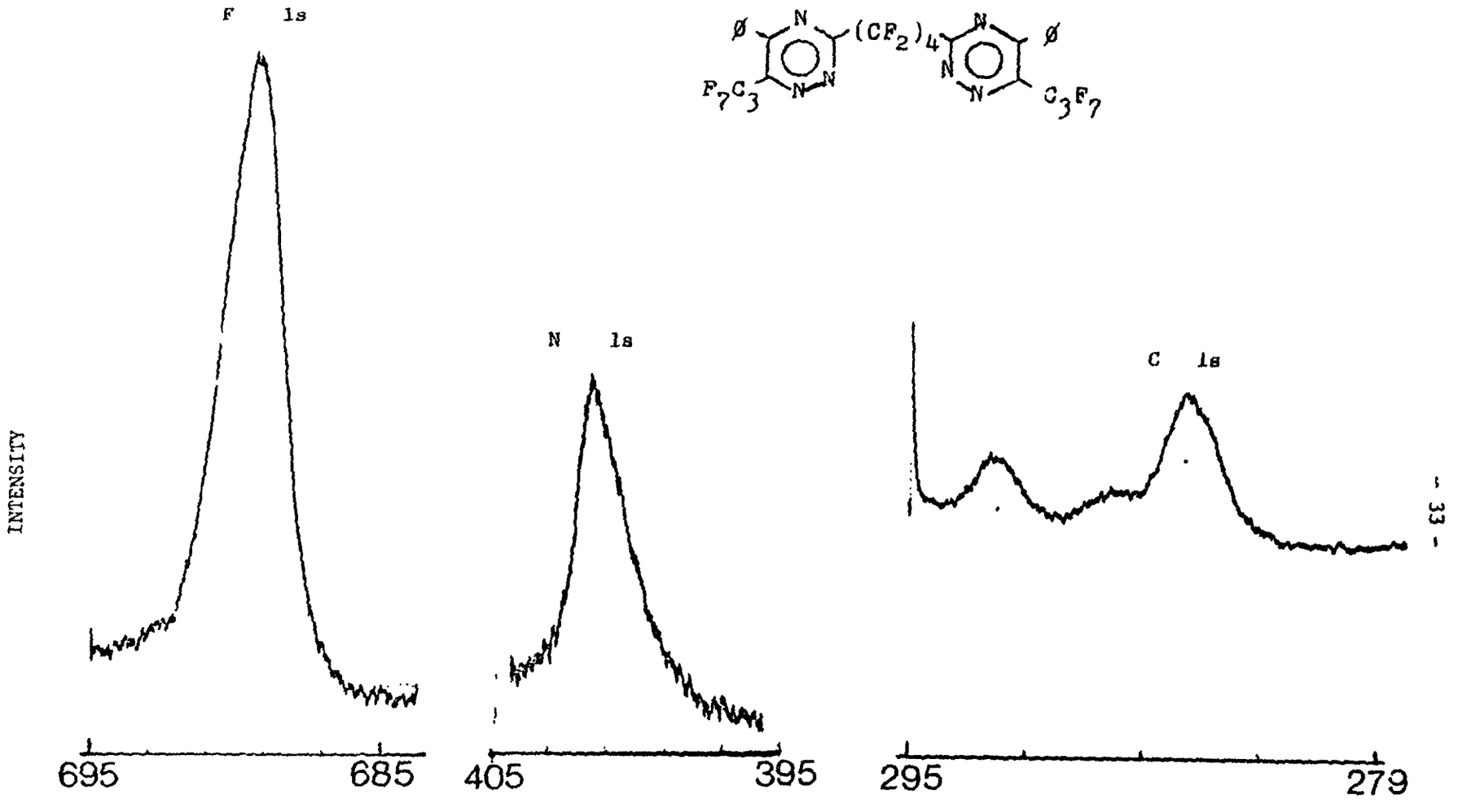

Figure 14. ESCA spectra of PH-57-1

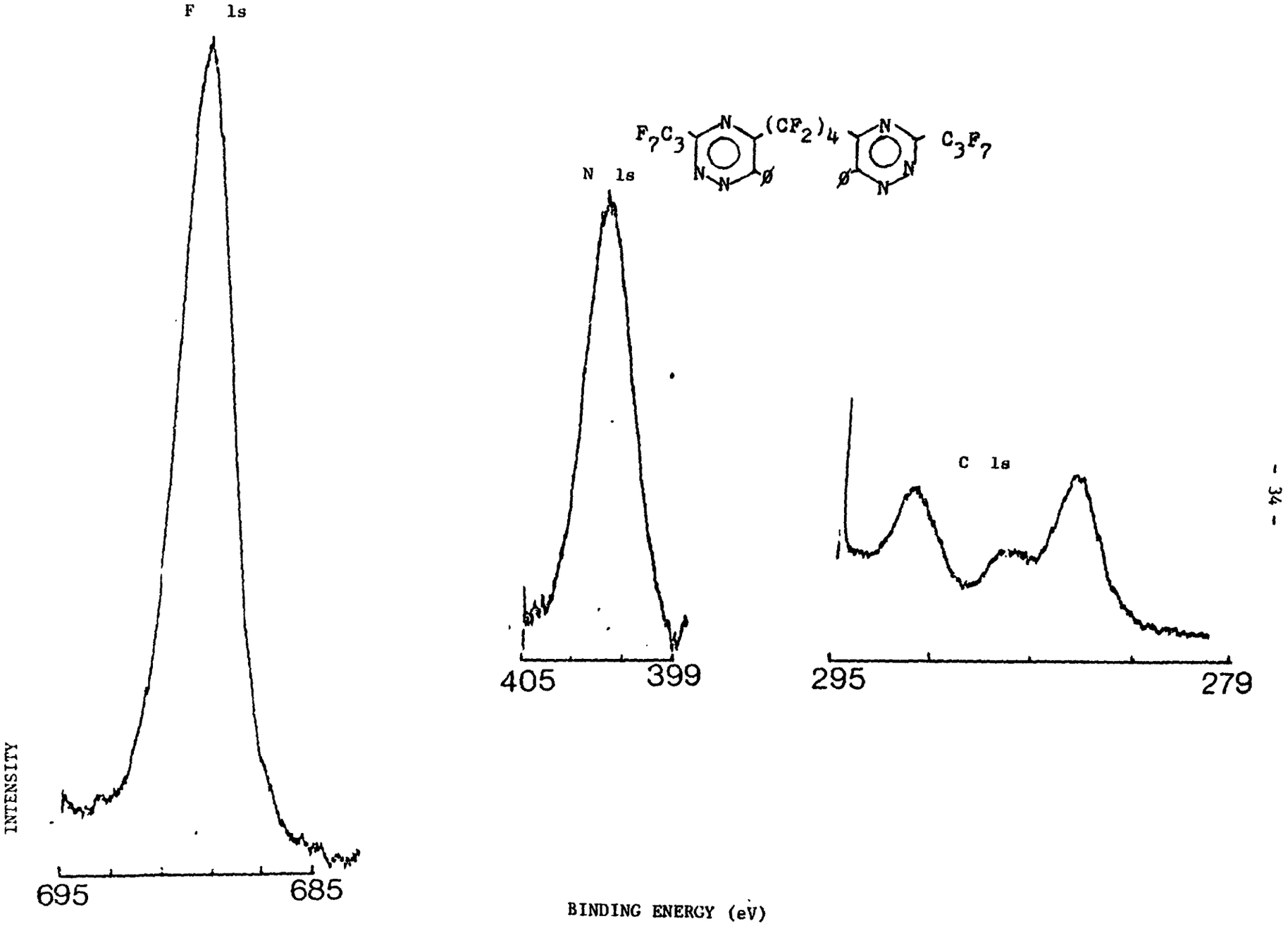

Figure 15. ESCA spectra of PH-82-2.

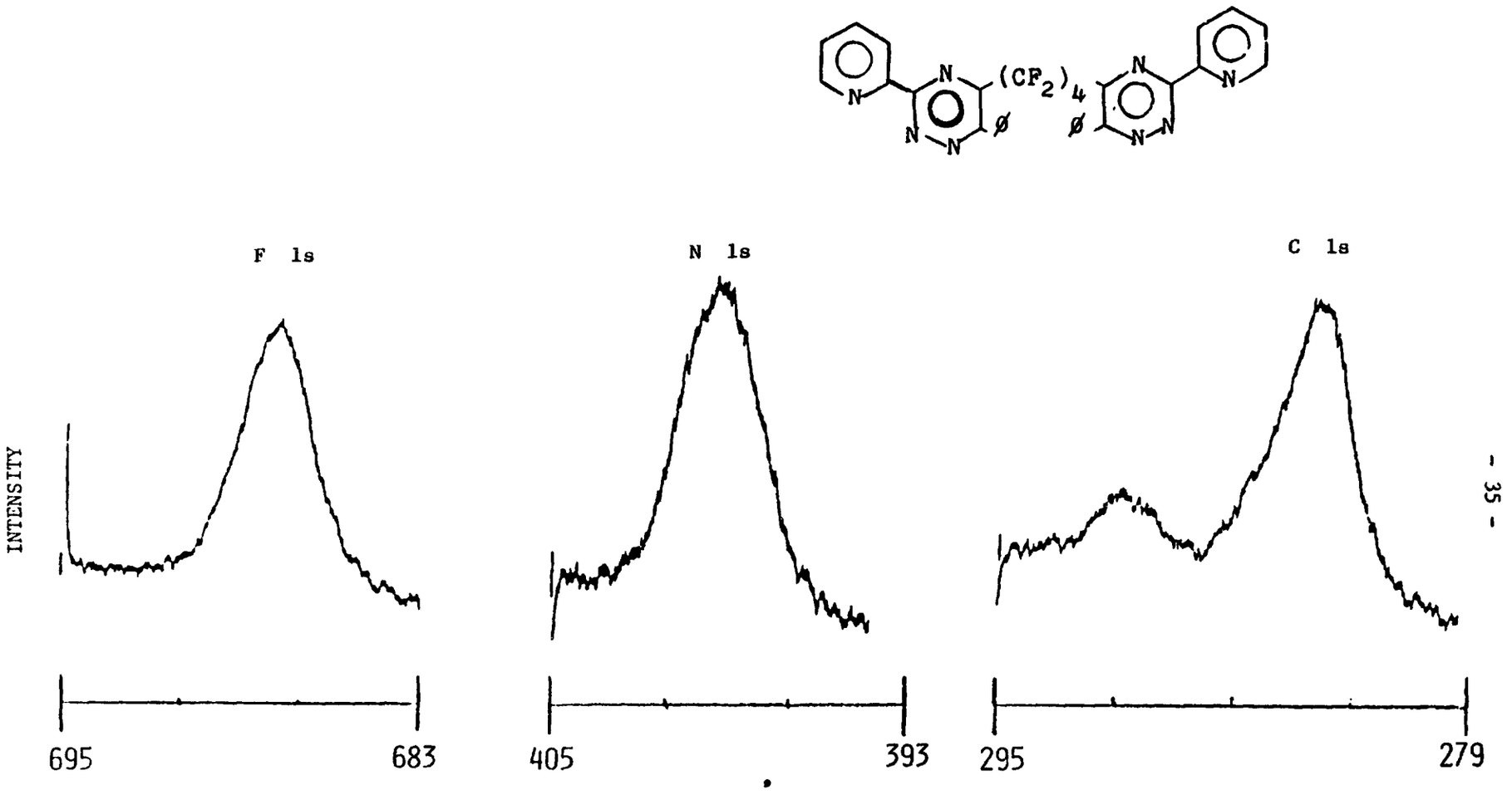

Figure 16. ESCA spectra of PH-82-3.

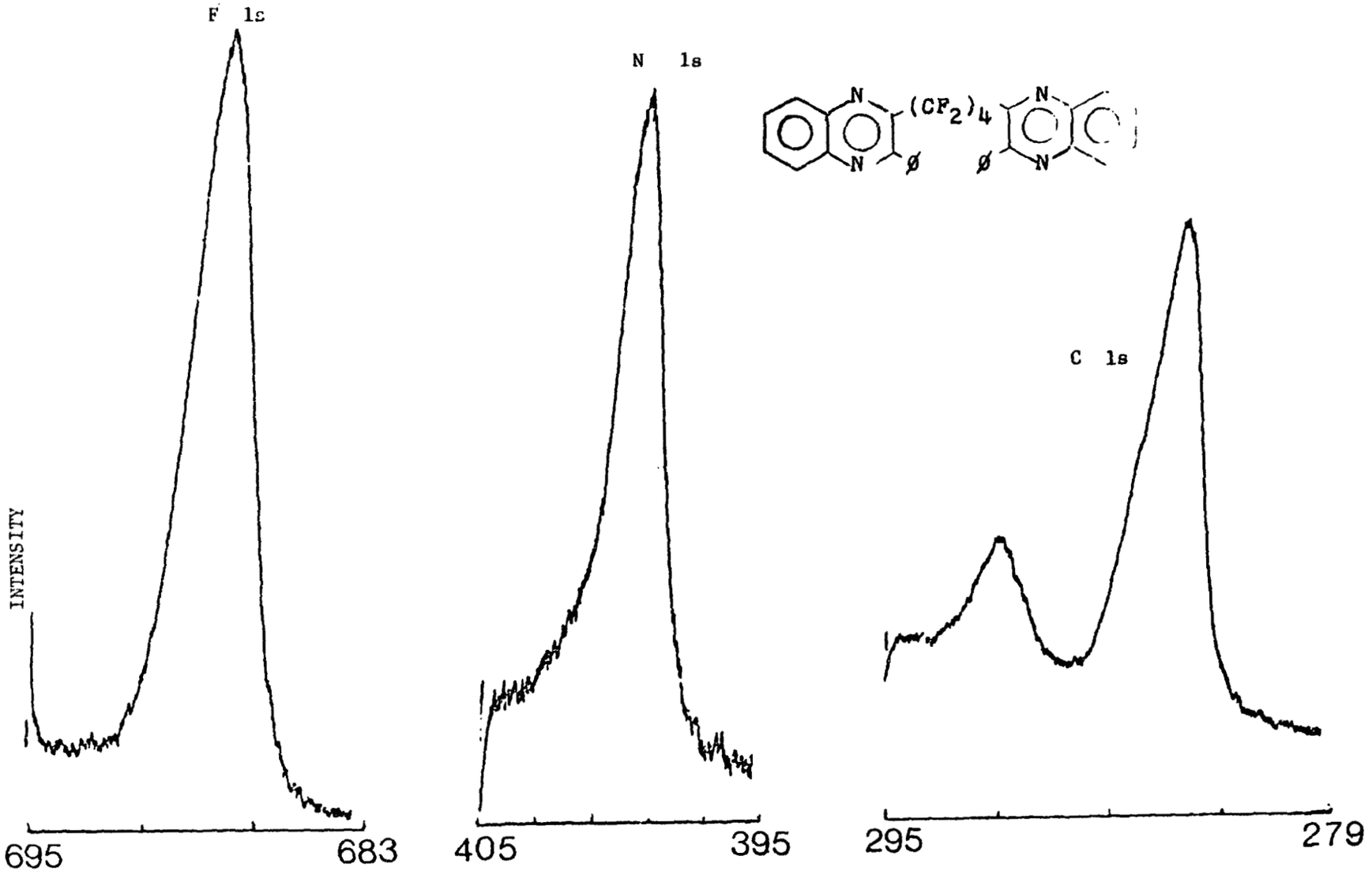

Figure 17. ESCA spectra of PH-84-1.

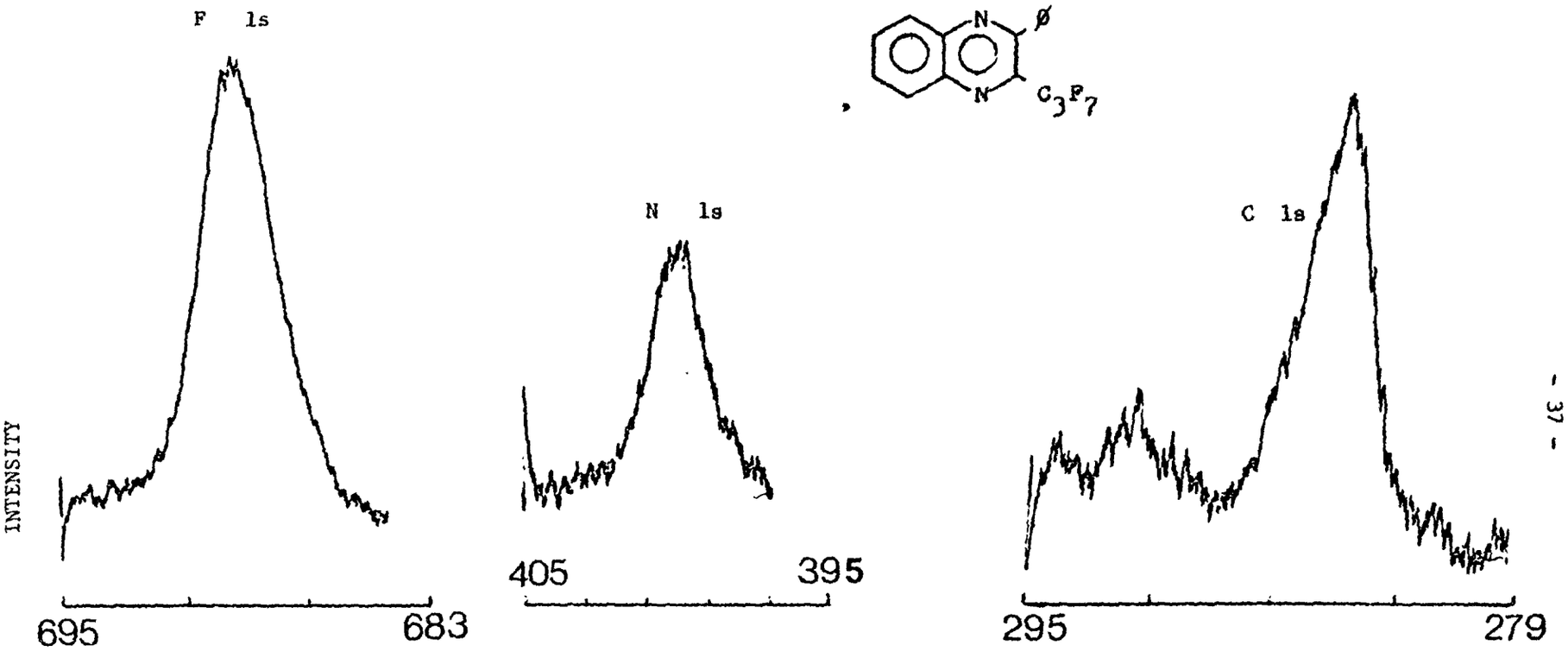

Figure 18.. ESCA spectra of PH-84-2.

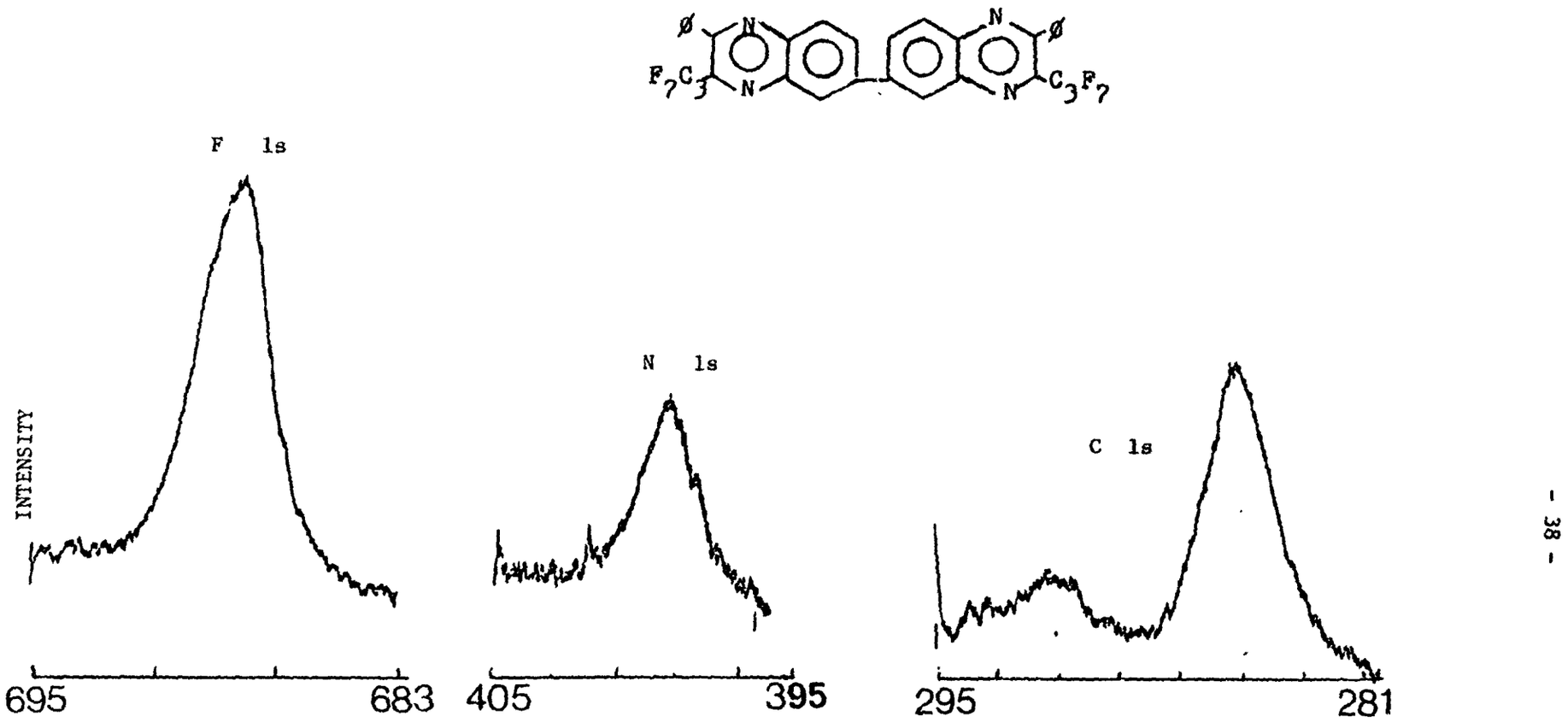

Figure 19. ESCA spectra of PH-85-1.

Table V. ESCA PARAMETERS FOR LaRC MODEL COMPOUNDS

LaRC #	FORMULA	C 1s		N 1s		F 1s	
		BE(eV)	AF	BE(eV)	AF	BE(eV)	AF
pH-57-1	$C_{28}H_{10}F_{22}N_6$	284.0 290.4	0.373 0.140	400.2	0.095	687.6	0.393
pH-82-2	$C_{28}H_{10}F_{22}N_6$	284.0 290.4	0.291 0.179	400.0	0.109	688.0	0.421
pH-82-3	$C_{32}H_{18}F_8N_8$	284.0 290.1	0.533 0.117	398.7	0.13	686.9	0.22
pH-84-1	$C_{32}H_{18}F_8N_4$	284.0 290.0	0.562 0.144	398.7	0.086	687.6	0.208
pH-84-2	$C_{17}H_9F_7N_2$	284.0 290.6	0.62 0.14	398.3	0.077	687.7	0.303
pH-85-1	$C_{34}H_{16}F_{14}N_4$	284.0 290.2	0.50 0.09	398.8	0.076	687.8	0.329
	AVERAGE	290.3±0.3		400.1±0.1 398.6±0.3		687.6±0.7	

Table VI

CONSTITUENT RATIOS FOR LaRC MODEL COMPOUNDS

LaRC #	$(F/C)_E$	$(F/C)_S$	$(N/C)_E$	$(N/C)_S$
PH-57-1	0.77	0.79	0.19	0.21
PH-82-2	0.90	0.79	0.23	0.21
PH-82-3	0.34	0.25	0.20	0.25
PH-84-1	0.29	0.25	0.12	0.12
PH-84-2	0.40	0.41	0.10	0.12
PH-85-1	0.56	0.41	0.13	0.12

D. Contamination of Ti 6-4 (AES/Depth Profiling)

Auger electron spectroscopy (AES) with argon sputtering depth profiling was used to analyze anodized Ti 6-4 and Ti 6-4 after phosphate-fluoride treatment.

1. Anodized Ti 6-4

The AES spectra of anodized Ti 6-4 at the beginning and at the end of depth profiling is shown in Figures 20 and 21, respectively. Trace amounts of sulfur, calcium and fluorine are noted in the sample initially which are removed on argon sputtering. Peaks due to vanadium and argon appear after sputtering. The composition-depth profile for anodized Ti 6-4 is shown in Figure 22. It is noted that the Ti signal increases to a maximum in about 6 minutes corresponding to a surface oxide layer thickness of about 60 nm. There is concomitant decrease in the oxygen signal over this thickness. Only minor changes are noted in the aluminum and vanadium signals. Calcium appears to be a surface contaminant and not identified in the bulk Ti 6-4.

2. Phosphate/fluoride Ti 6-4

The AES spectra of Ti 6-4 after phosphate/fluoride treatment at the beginning and at the end of depth profiling are shown in Figure 23 and 24, respectively. Trace amounts of sulfur, fluorine and sodium are noted in the sample initially which are removed by argon sputtering. Peaks due to vanadium and argon appear after sputtering. The composition-depth profiles for phosphate/fluoride treated Ti 6-4 are shown in Figure 25. The significant difference here is that the surface oxide layer is only about 20 nm thick. Thus, the surface oxide layer on anodized Ti 6-4 is about three times thicker than on phosphate/fluoride treated Ti 6-4. The fluorine content is associated with the surface and not the bulk Ti 6-4.

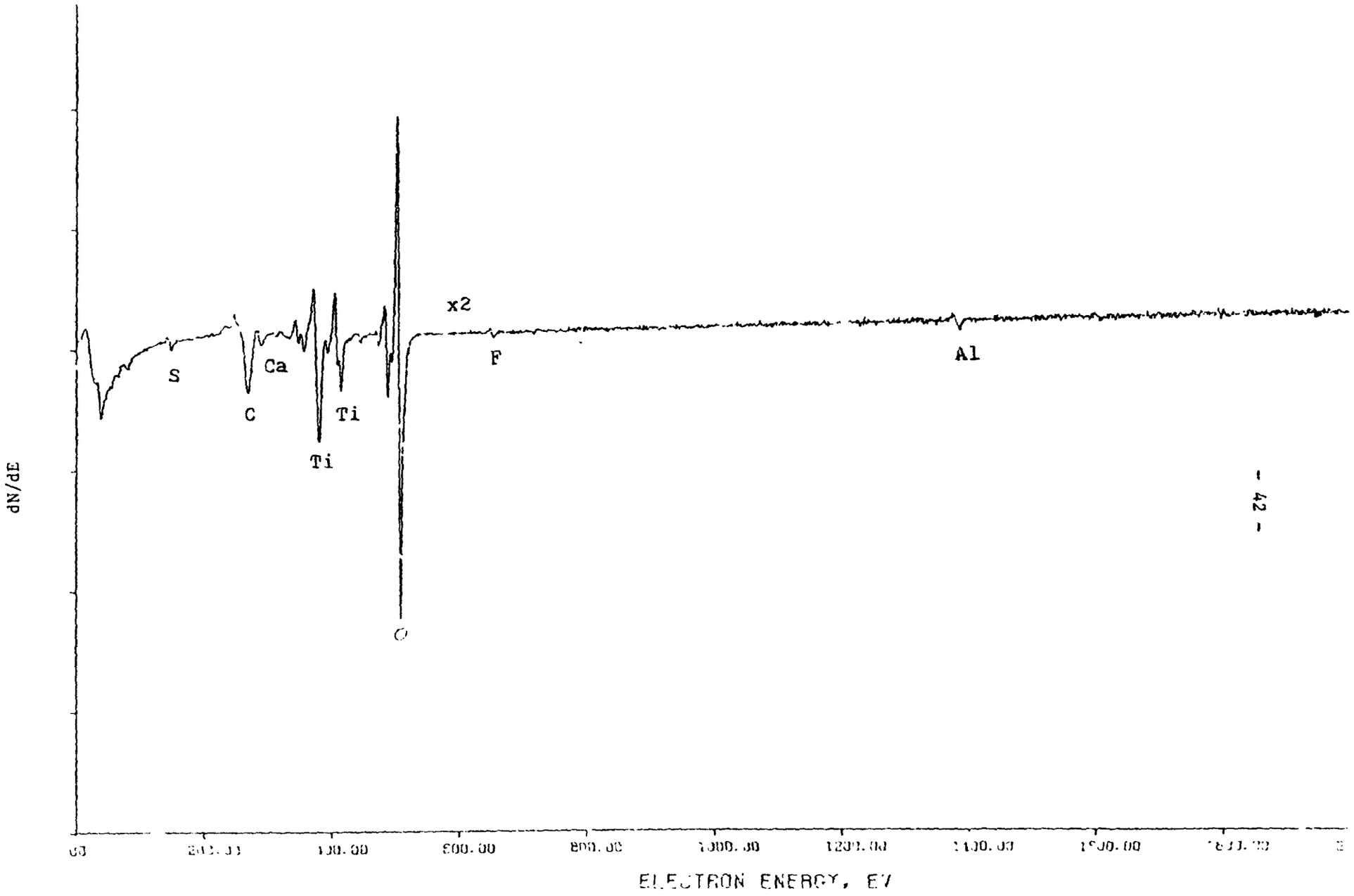

Figure 20. AES spectrum of anodized Ti 6-4.

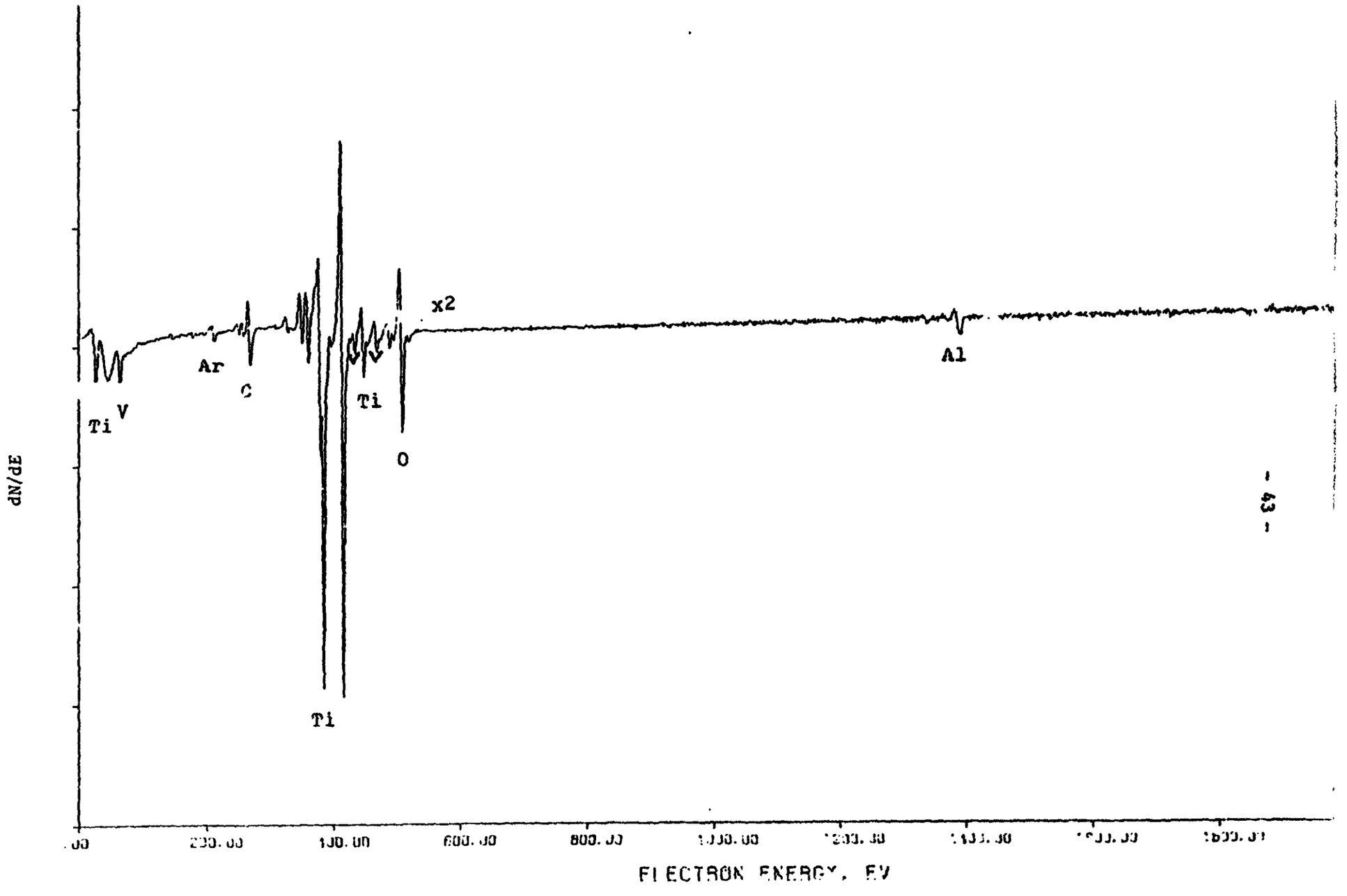

Figure 21. AES spectrum of anodized Ti 6-4 (end of profile).

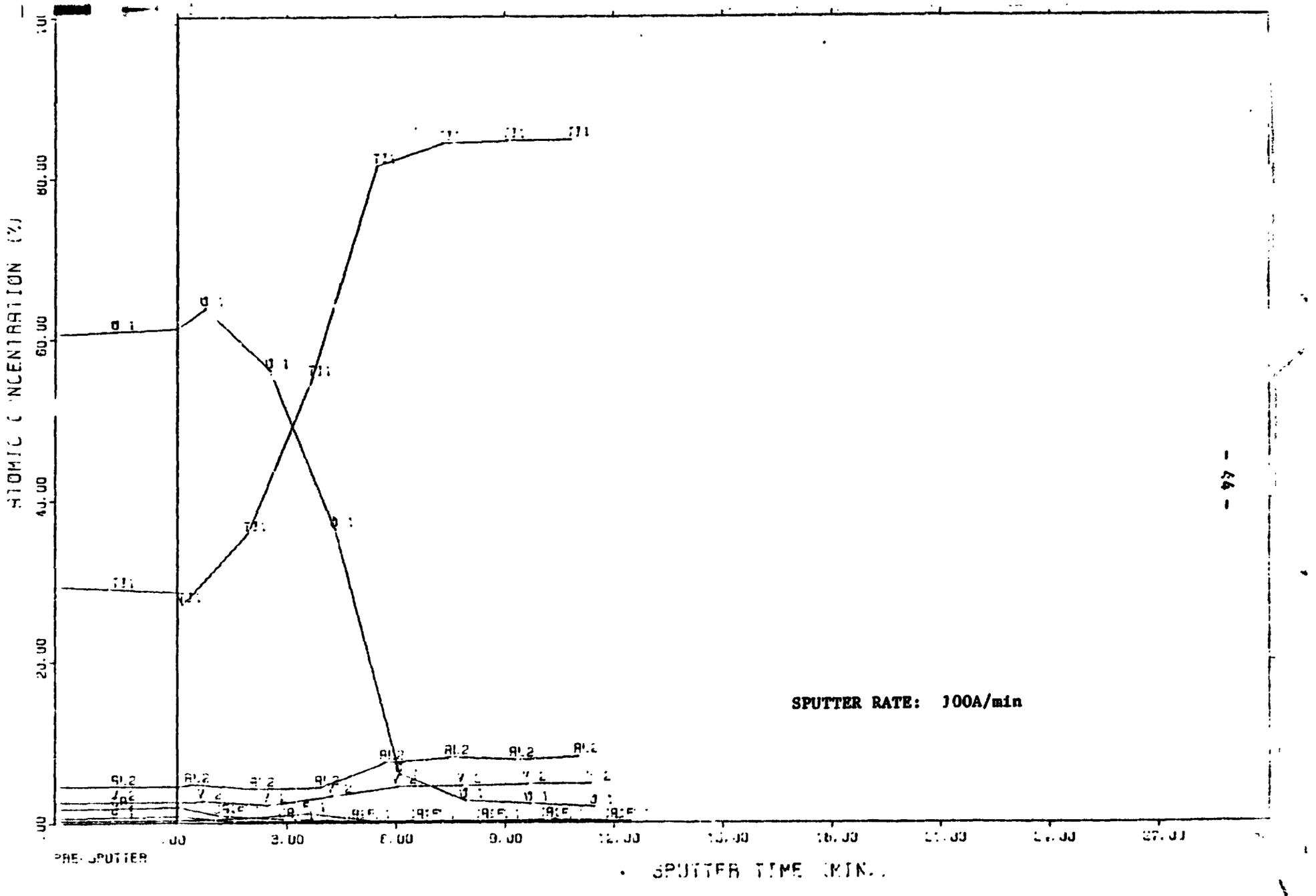

Figure 22. Composition-Depth profiles of anodized Ti 6-4.

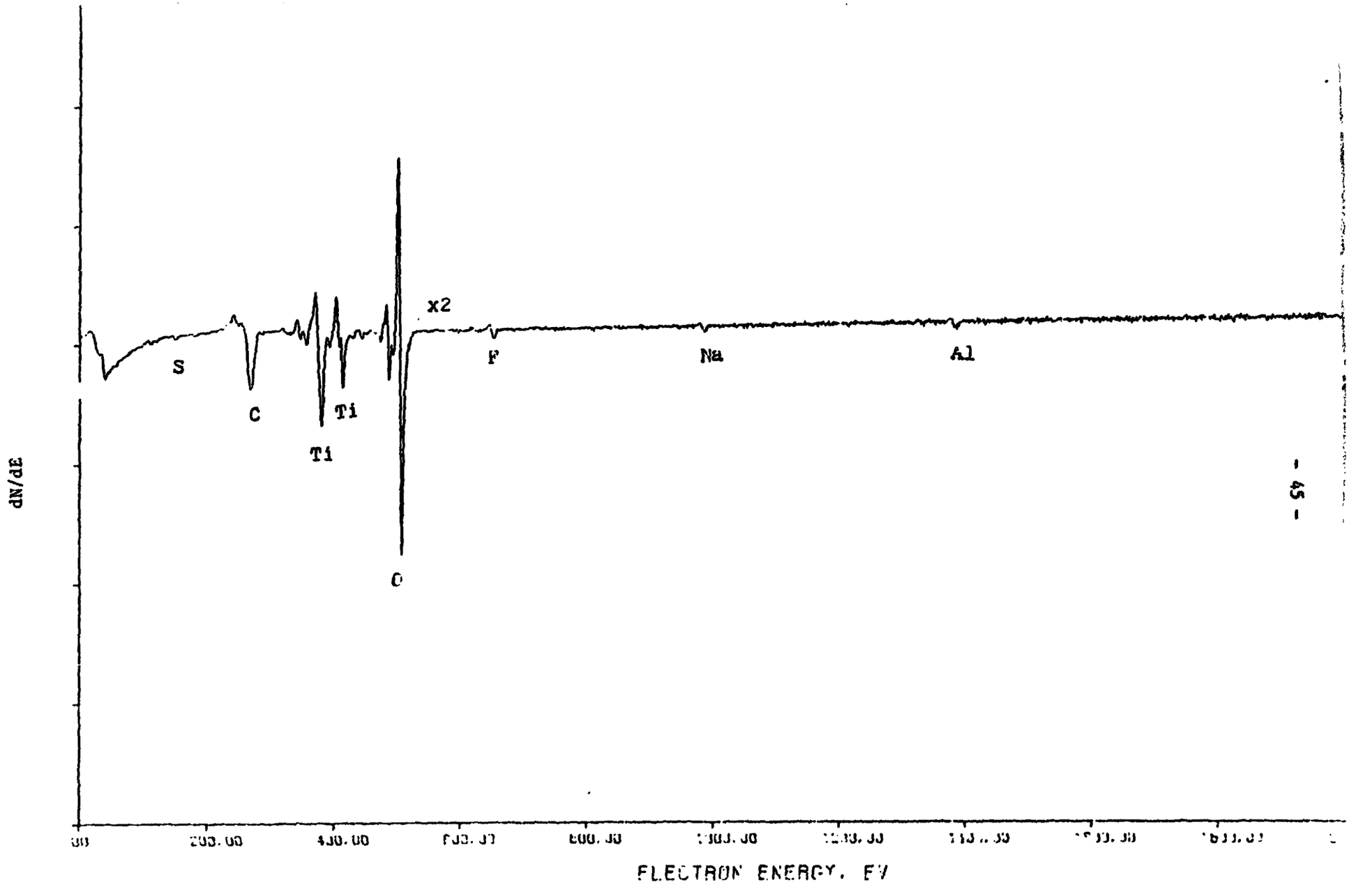

Figure 23. AES spectrum of Ti 6-4 after phosphate/fluoride treatment.

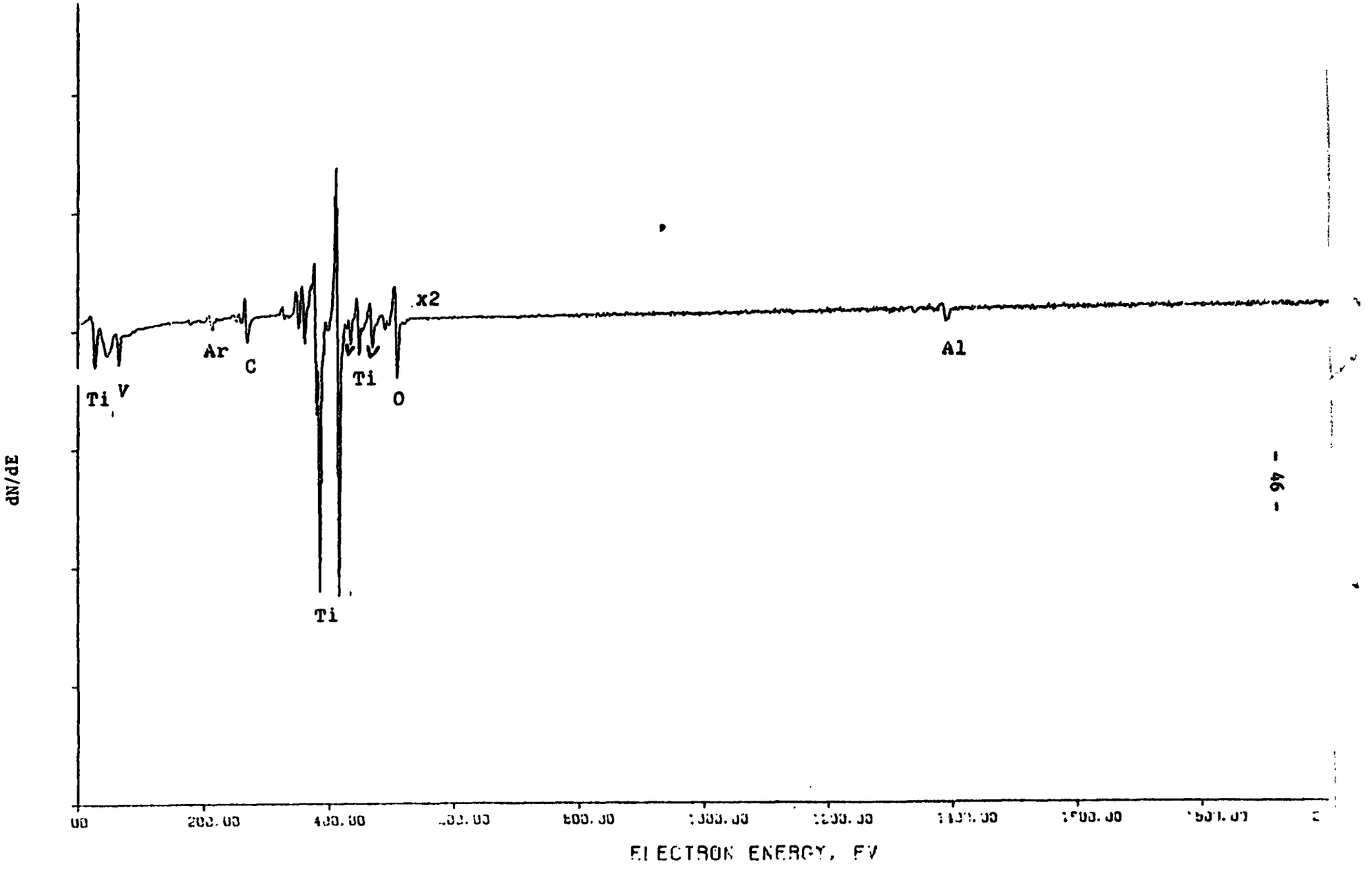

Figure 24. AES spectrum of Ti 6-4 after phosphate/fluoride treatment (end of profile).

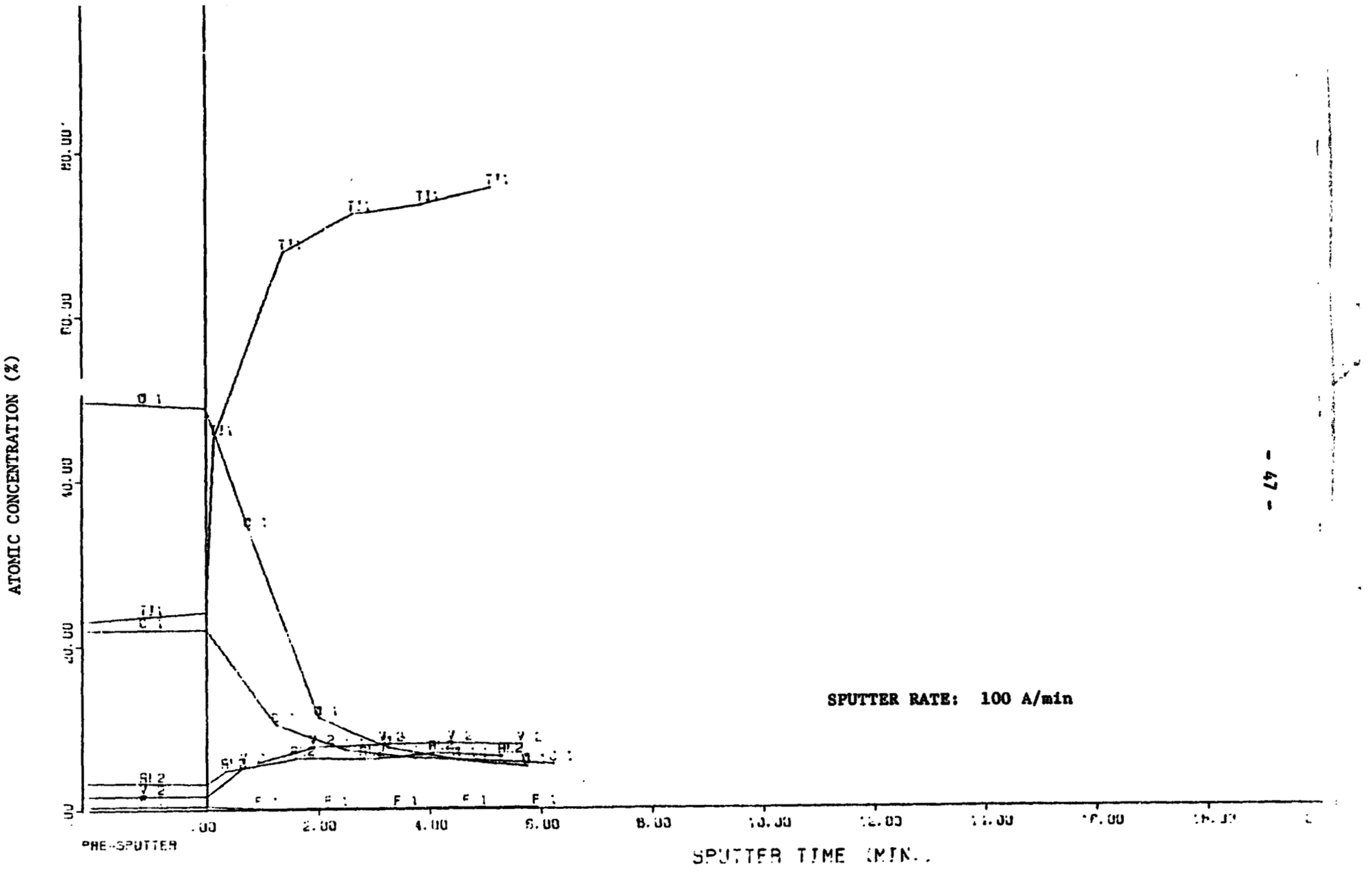

Figure 25. Composition-depth profiles of Ti 6-4 after phosphate/fluoride treatment.

It is of interest to compare the ESCA and AES spectra of Ti 6-4 since the ESCA results are available (3). A qualitative comparison is given in Table VII. Each technique ESCA, AES, and AES/Depth Profiling has its unique contribution and taken collectively define well the surface of Ti 6-4.

E. Fracture Surface Analysis (SEM and ESCA)

1. LaRC-13/No Elastomer.--SEM photomicrographs of opposing sides of a bonded adhesive joint after fracture in a T-peel test are shown in Figure 26. The Ti 6-4 substrate is clearly visible on side B as contrasted to side A where only adhesive and scrim cloth are noted. The ESCA results for both sides are listed in Table VIII. Again, only Ti (IV) is noted on the B side indicative of fracture close to (< 5 nm) the adhesive/adherend interface but not within the surface oxide layer. Otherwise, either a significant peak due to Ti(0) would have been observed at 449.6 eV (3) on the B side and/or a significant peak due to Ti(IV) would have been observed on the A side.

2. LaRC-13/elastomer.--SEM photomicrographs of opposing sides of a bonded adhesive joint after fracture in a T-peel test are shown in Figure 27. The LaRC-13 adhesive in this case contained 15% of a fluorosiloxane elastomer. The fractography is totally different than that noted when no elastomer was present (Fig. 26). No Ti 6-4 substrate is observed on either side. The ESCA results listed in Table VIII support the conclusion that fracture occurred within the adhesive since no Ti signal was observed. In addition, significant increases in the surface concentrations of fluorine and silicon are expected on using a fluorosiloxane polymer.

3. Sample #1499 P-1.--The Ti 6-4 adherend in this case was presumably grit blasted followed by a phosphate/fluoride pretreatment. The strength of the lap shear specimen was minimal. The SEM photomicrographs of two areas of

Table VII

COMPARATIVE ESCA - AUGER RESULTS FOR Ti 6-4

Element	Phosphate/Fluoride			Anodized		
	ESCA	Auger		ESCA	Auger	
		Ar	Profile		Ar	Profile
Ti	X	X	X	X	X	X
O	X	X	X	X	X	X
Al	X	X	X	X	X	X
F	X	X		X	X	
V	X		X	X		X
Cl	X			X		
S		X			X	
K	X					
Na		X				
P	X					
N				X		
Ca					X	
Ar			X			X
C	X	X	X	X	X	X

Figure 26.

SEM photomicrographs of fracture surfaces of Ti 6-4 bonded with LaRC-13 adhesive containing no elastomer.

Figure 26. SEM photomicrographs of fracture surfaces of Ti 6-4 bonded with LaRC-13 containing no elastomer.

A. SEM photomicrographs (100x, 1000x) of the adhesive side. No Ti 6-4 substrate is noted; the scrim cloth is visible.

B. SEM photomicrographs (100x, 500x) of the adherend side. Ti 6-4 substrate is noted with patches of primer/adhesive present.

100μm

0.2mm

1mm

1mm

1

13

Table VIII ESCA ANALYSIS OF FRACTURED T-PEEL AND LAP SHEAR SPECIMENS

SAMPLE	C 1s		O 1s		F 1s		N 1s		Si 2p		Ti 2p		C/Ti
	BE	AP	BE	AP	BE	AP	BE	AP	BE	AP	BE	AP	
LaRC-13/no elastomer (A side)	284.0	85.3	531.4	10.1	686.9	0.9	399.0	2.7	101.4	1.0	-	-	-
LaRC-13/no elastomer (B side)	284.0	68.8	530.1	19.2	686.9	0.5	399.1	2.6	100.9	4.6	463.1 457.3	4.3	15
LaRC-13/elastomer (A side)	284.0 292.2	58.1	531.8	16.6	686.8	7.9	398.8	0.7	101.8	16.7	-	-	-
LaRC-13/elastomer (B side)	284.0 291.8	57.7	531.6	17.3	686.7	7.3	398.2	0.4	101.7	17.3	-	-	-
#1499P-1 (metal side)	284.0	71.6	530.2	17.2	-	-	398.8	2.7	-	-	464.0 458.0	8.5	8.4
#1499P-1 (adhesive side)	284.0	89.0	532.4	7.0	-	-	398.0	4.0	-	-	-	-	-
#1499P-1 (metal side/ Ar discharge)	284.0	43.9	529.6	35.1	-	-	398.8	4.0	-	-	463.9 457.8	17.4	2.5

Figure 27.

SEM photomicrographs of fracture surfaces of Ti 6-4 bonded with LaRC-13 containing 15% of a fluorosiloxane elastomer.

Figure 27. SEM photomicrographs of fracture surfaces of Ti 6-4 bonded with LaRC-13 containing 15% fluorosiloxane elastomer.

A. SEM photomicrographs (100x, 1000x) of one side of fracture. No Ti 6-4 substrate is noted.

B. SEM photomicrographs (500x, 2000x) of opposite side of fracture. Again, no Ti 6-4 substrate is noted; coated scrim cloth seen on both faces.

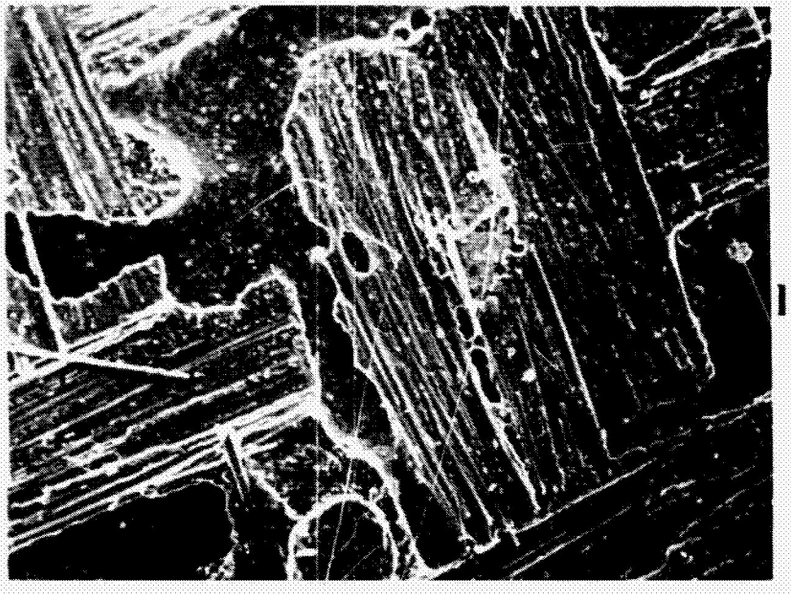

A

1mm

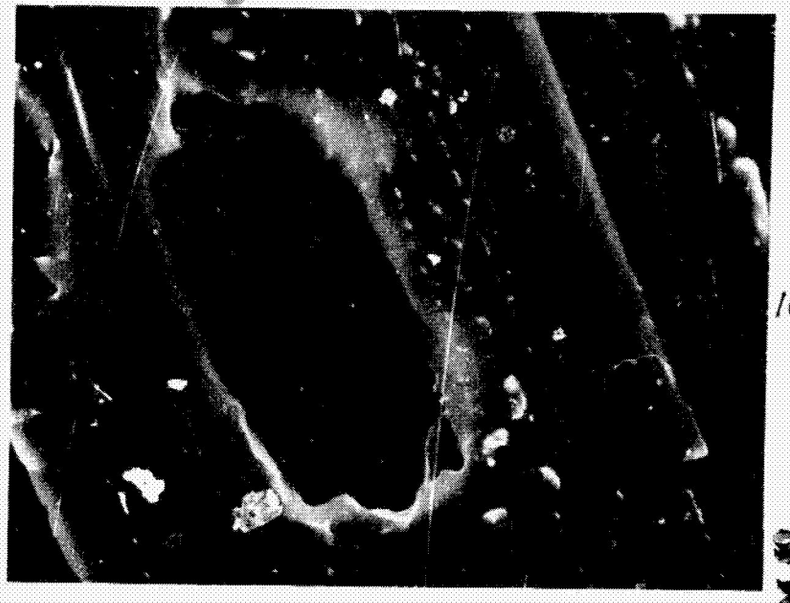

100μm

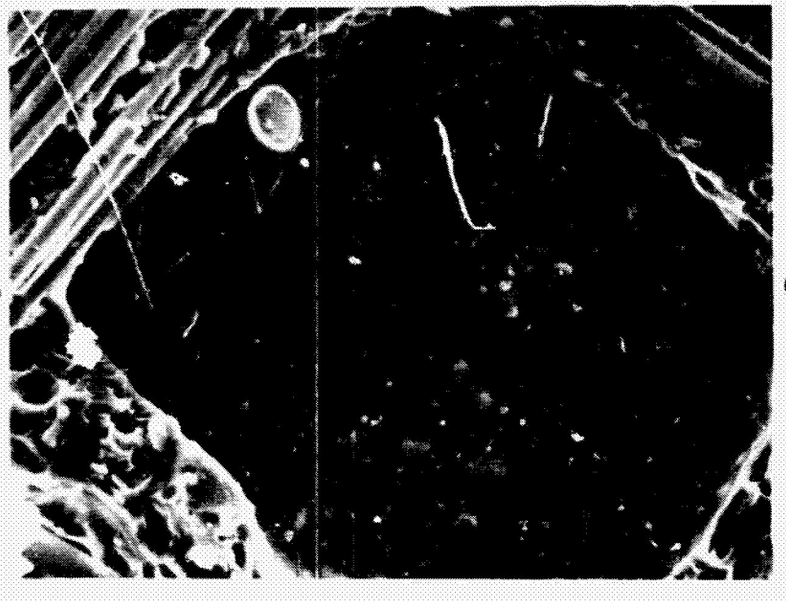

B

0.2mm

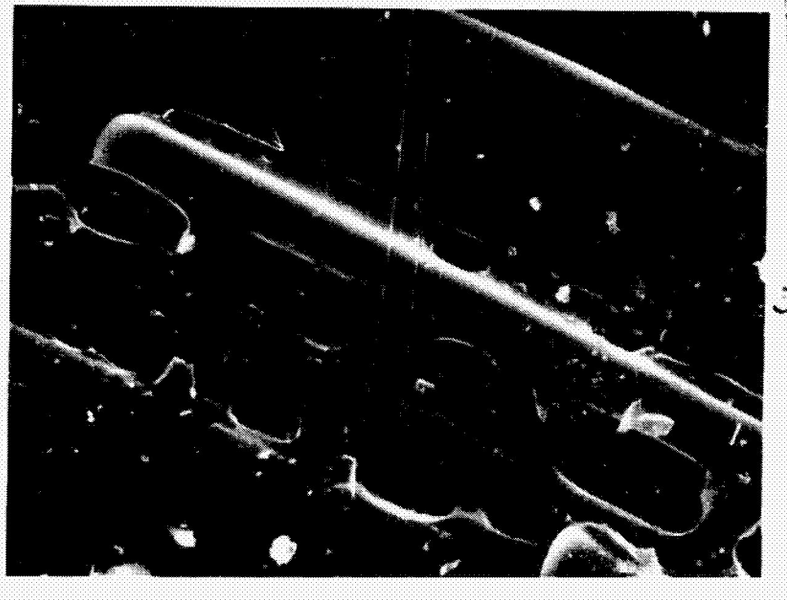

50μm

the fracture surface are shown in Figure 28. Area A was from a "bare" metal area and area B was from an "adhesive" area. It appears from the photomicrographs that the Ti 6-4 was only grit-blasted but given no phosphate/fluoride treatment. This conclusion is based on a comparison with typical grit-blasted and phosphate/fluoride pretreated samples seen in Figures 2 and 5, respectively, in a previous report (3). A typical Ti 6-4 surface after grit blasting and a phosphate/fluoride etch is also seen in Figure 32B of the present report.

The ESCA results for these two samples are listed in Table VIII. A Ti signal was noted from area A but not from area B. The sample containing area A was cleaned subsequently in an argon discharge (6) for 60 seconds resulting in a lower carbon signal and a concomitant larger titanium signal as noted in Table VIII.

F. Surface Analysis of Primed Ti 6-4 (SEM/EDAX and ESCA)

1. MEPPQ primer.--Ti 6-4 specimens (#813-11-5) were primed with MEPPQ (m-cresol/xylene solvent system). When the Ti 6-4 coupon was punched to prepare the SEM/ESCA sample, there was a clean separation of the primer from the adherend. The ESCA results for the top side of the primer are shown in Table IX. No SEM photomicrographs were taken of the primed surface. The SEM photomicrographs in Figure 29 show the primed surfaces which originally was against the metal. The primer appears to replicate the adherend surface which again has only been grit-blasted. The ESCA results are shown in Table IX for this section of primer for which no Ti signal was observed. This result indicates that separation occurred at the primer/oxide interface rather than within the oxide layer.

The SEM photomicrographs in Figure 30A show the adherend surface

Figure 28.

SEM photomicrographs of #1499P-1
fracture surfaces.

Figure 28. SEM photomicrographs of #1499P-1 fracture surfaces.

Sample #1499P-1 is a specimen after fracture in a lap shear test. Ti 6-4 was reportedly given a grit-blast followed by a phosphate/fluoride etch.

A. SEM photomicrographs (1,000x, 10,000x) of an area of the fracture surface showing the bare metal.

B. SEM photomicrographs (1,000x, 5,000x) of an area of the 1499P-1 sample fracture surface showing the adhesive on the metal substrate.

Table IX ESCA ANALYSIS OF PRIMED Ti 6-4 SURFACES

SAMPLE	C 1s		O 1s		N 1s		Ti 2p		P 2p		Al 2s		C/Ti
	BE	AP	BE	AP	BE	AP	BE	AP	BE	AP	BE	AP	
#813-11-5 (primer, top side)	284.0	89.2	532.6	3.0	398.2	7.8	NS		NS		NS		-
#813-11-5 (primer, metal side)	284.0	85.6	531.8	6.0	397.6	7.0	-		-		120.0	1.0	-
#813-11-5 (metal, under primer)	284.0	48.6	529.2	28.5	398.4	2.1	463.5 458.2	14.5	132.8	3.5	120.0	2.6	3.4
#813-11-5 (after $CHCl_3$ rinse)	284.0	70.8	531.1	14.2	398.2	6.8	463.9 458.1	3.5	132.9	1.0	119.1	3.0	20.2
Primed Ti 6-4 MEPPQ	284.0	88.4	532.2	3.4	398.4	8.1	-	-	-	-	-	-	-
Primed Ti 6-4 (after $CHCl_3$ rinse)	284.0	73.5	530.6	12.2	398.8	4.8	463.2 458.0	6.2	134.6	2.7	118.0	1.0	11.9
Primed Ti 6-4/Boeing (MEPPQ)	284.0	88.4	532.2	3.7	398.0	7.9	-	-	-	-	-	-	-
Primed Ti 6-4/Boeing (after $CHCl_3$ rinse)	284.0	88.5	532.2	3.4	398.3	7.9	464.0 457.9	0.2	-	-	-	-	442.5

NS not scanned
- not shown up

Figure 29.

SEM photomicrograph of the primer surface which was against the Ti 6-4 in the #813-11-5 sample.

Figure 29. SEM photomicrographs (200x, 1000x) of the primer surface which was against the Ti 6-4 in the #813-11-5 sample.

MEPPQ primer was coated on a grit blasted Ti 6-4 coupon after a presumed phosphate/fluoride pretreatment. The joints between primer and Ti 6-4 substrate were very weak. The primer separated from the Ti 6-4 substrate in a punch-type cutter.

Figure 30.

SEM photomicrographs of Ti 6-4 substrates of #813-11-5.

Fiture 30. SEM photomicrograph of Ti 6-4 substrates of #813-11-5.

A. SEM photomicrographs (1,000x, 10,000x) of the titanium substrate under the primer. Note that the material appears heavily worked.

B. SEM photomicrographs (1,000x, 10,000x) of the primed surface of #813-11-5 sample after a chloroform solvent rinse for 30 min at ambient temperatures.

which was originally against the primer. The similarity between this photomicrograph and the one for the primer shown in Figure 29 at the same magnification (100 μm) is striking. An aluminum signal was noted in the EDAX spectrum of this sample suggesting the presence of residual grit blast particles. The ESCA results shown in Table IX for this surface show a large Ti signal (C/Ti = 3.4) consistent with the interpretation of a clean failure between primer and metal.

The SEM photomicrograph of the primed adherend after a chloroform rinse is shown in Figure 30 B. Any residual primer coating is not apparent in this figure. However, the ESCA results in Table IX, where only a weak (C/Ti = 20.2) Ti signal was noted, demonstrate the presence of a thin residual primer film.

2. Phosphate/fluoride treatment with BR-34 primer.--In light of the uncertainty in the pretreatment of sample No. 1499 P-1 and #813-11-5, coupons of Ti 6-4 were given a phosphate/fluoride treatment and the SEM photomicrograph is shown in Figure 31 A. This picture is characteristic of Ti 6-4 after an acid etch. A comparison SEM photomicrograph was given in Figure 5A of the previous report (3). The pretreated Ti 6-4 sample was heated in air at 483K for 45 min with no noticeable changes in the SEM photomicrograph (see Fig. 31 B). The Ti 6-4 was subsequently primed with BR-34 and the resultant surface shown in the SEM photomicrograph in Figure 31 C. The primer contains aluminum particles as shown by the EDAX spectrum of this sample in Figure 31 D.

3. Phosphate/fluoride treatment with MEPPQ primer.--Ti 6-4 coupons pretreated with phosphate/fluoride were primed with MEPPQ and heated at 343K for 30 min. The SEM photomicrographs for this primed surface are shown in

Figure 31.

SEM photomicrographs of etched and primed (BR-34) Ti 6-4 specimens.

Figure 31. SEM photomicrographs (1,000x) of etched and primed (BR-34) Ti 6-4 specimens.

A. After phosphate/fluoride treatment. Note the characteristic acid etch pattern.
B. After phosphate/fluoride treatment and thermo-oxidative aging at 483K for 45 min.
C. After phosphate/fluoride etch, sample was primed with BR-34 (Batch no. 169), and heated to 483K for 45 min. Note the many filler particles.
D. EDAX spectrum of primed Ti 6-4 showing presence of Al filler.

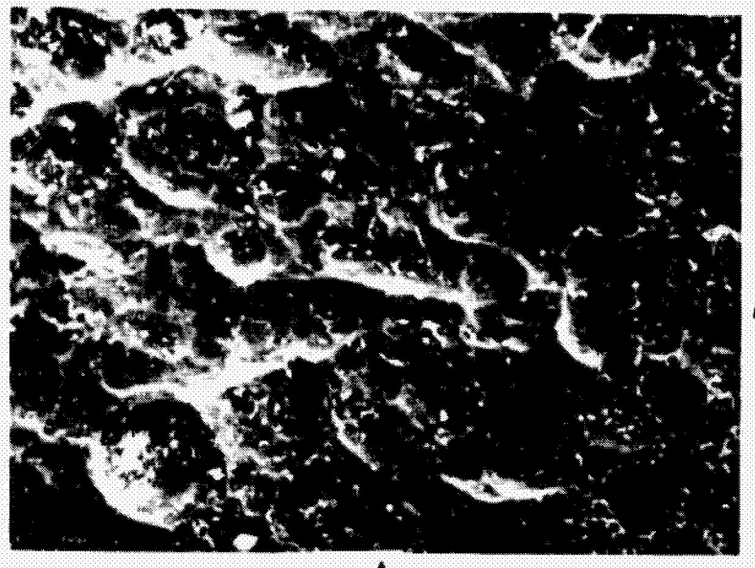

100μm

A

100μm

C

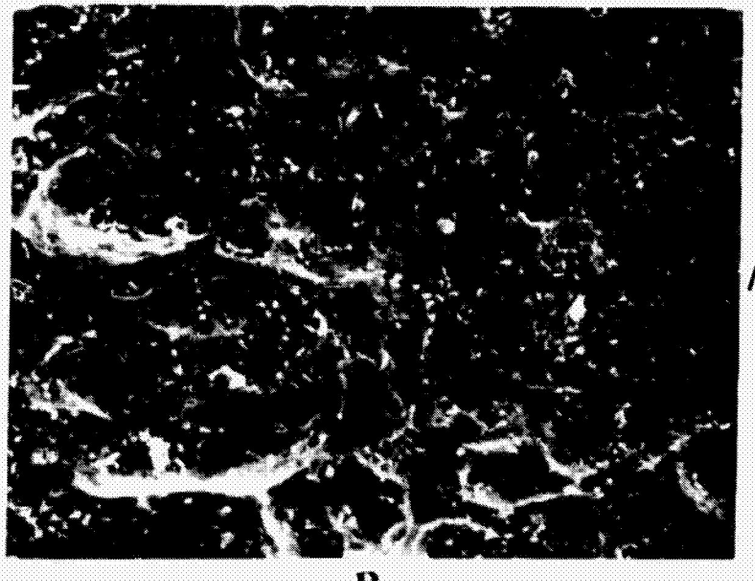

100μm

B

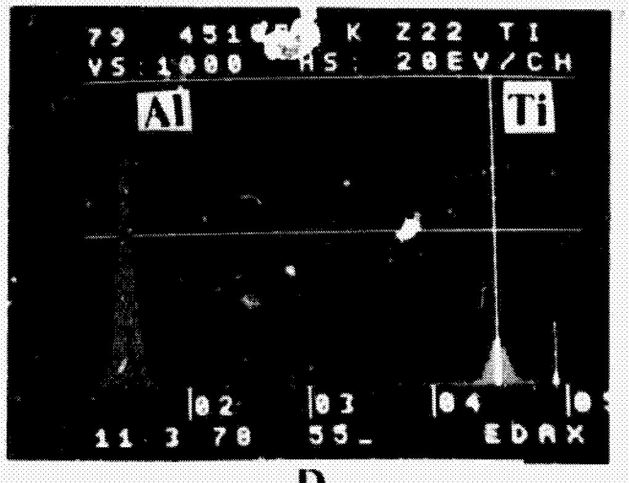

D

Figure 32A. The presence of the primer causes the Ti 6-4 substrate to appear "out-of-focus" particularly noticeable in the high magnification (10 μm) picture. The ESCA results in Table IX show no Ti signal present from this sample consistent with the presence of a thick (> 5 nm) primer film.

The primed coupon was rinsed with chloroform for 30 min at ambient temperatures. The clarity of the SEM photomicrograph in Figure 32B bespeaks the removal of much of the primer film by chloroform. A significant Ti signal is noted in the ESCA results (see Table IX) consistent with the removal of all but a thin (< 5 nm) layer of primer.

4. Phosphate/fluoride treatment with MEPPQ primer-Boeing.—This Ti 6-4 coupon primed with MEPPQ was pretreated with a phosphate/fluoride etch by personnel at the Boeing Aerospace Co. The SEM photomicrograph of the sample shown in Figure 33A indicates the presence of a primer coating. In addition, the striations in the Ti 6-4 substrate suggest that the sample was not grit-blasted before etching. The features in Figure 33A are strikingly similar to those in Figure 1 of the previous report (3) for the 'as received from the supplier' state of Ti 6-4 coupons. It has been standard practice at NASA-LaRC to grit-blast Ti 6-4 coupons prior to chemical pretreatment. The ESCA results in Table IX show again by the absence of a Ti signal, the presence of a thick coating. The primer was rinsed with chloroform for 30 min at ambient temperature. The SEM photomicrograph in Figure 33B suggests removal of the primer coating. However, only a minimal Ti signal was obtained from the ESCA measurements listed in Table IX suggesting gross residual organic contamination.

Figure 32.

SEM photomicrographs of primed (MEPPQ) and rinsed Ti 6-4.

Figure 32. SEM photomicrographs of primed (MEPPQ) and rinsed Ti 6-4.

A. SEM photomicrographs (100x, 1000x) of Ti 6-4 pretreated with phosph_ e/fluoride, primed with MEPPQ, and heated at 343K for 30 min. Note the fuzziness of the 50 μm picture.

B. SEM photomicrographs (1,000x, 2,000x) of Ti 6-4 primed with MEPPQ and rinsed with chloroform for 30 min at ambient temperature. Note the clarity of the 50 μm picture and the characteristic acid etch pattern.

Figure 33.

SEM photomicrographs of primed (MEPPQ/Boeing) and rinsed Ti 6-4.

Figure 33. SFM photomicrographs of primed (MEPPQ/Boeing) and rinsed Ti 6-4.

A. SEM photomicrographs (1,000x, 2,000x) of Ti 6-4 primed with MEPPQ. Note the surface striations and the fuzziness of the 50 μm picture.

B. SEM photomicrographs (1,000x, 2,000x) of Ti 6-4 primed with MEPPQ and rinsed with chloroform for 30 min at ambient temperature. Note the residual chunky overlayer on the substrate.

A

B

IV. CONCLUSIONS

The following conclusions are based on the results in this report on the surface analysis of a variety of materials:

1. There are no significant changes in the morphology of coated, and rinsed graphite fibers as gauged from scanning electron photomicrographs compared to the uncoated fibers.

2. It is possible to differentiate between various graphite fibers and to detect coatings on fibers using the ESCA technique.

3. The chromium coating on metallized Kapton is a thick (< 5 nm) oxide layer whereas the aluminum coating is a thin (< 5 nm) oxide layer over an elemental substrate as concluded from the ESCA results.

4. Depth profiling done simultaneously with AES of the metallized Kapton indicates the thickness of the aluminum and chromium layers were 40 and 14 nm respectively. The oxugen content of both metallic coatings varied significantly.

5. A number of voids are generated on bonding metallized Kapton and LaRC-3 adhesive.

6. The ESCA spectra of each fluoro-containing model compound were unique, either in binding energy of the elements or in constitution.

7. The oxide film on anodized Ti 6-4 is about 60 nm thick whereas on phosphate/fluoride treated Ti 6-4, the oxide layer is only about 20 nm thick. These thicknesses were obtained from depth profiling measurements using AES. Calcium and fluorine were shown to be trace surface contaminants on anodized and phosphate/fluoride etched Ti 6-4, respectively. The ESCA results on the same samples are in qualitative agreement with the AES results.

8. Lap shear testing of Ti 6-4 bonded with LaRC-13 containing no elastomer resulted in interfacial failure as noted by SEM/ESCA techniques.

On the other hand, cohesive failure was noted for LaRC-13 containing 15% of a fluorosiloxane elastomer.

9. The Ti 6-4 adherend in #14499 P-1, which had a minimal lap shear strength, was presumably given a phosphate/fluoride etch prior to bonding. However, the SEM/EDAX results suggest that the sample was only grit-blasted.

10. The primed (MEPPQ) in m-cresol/xylene) Ti 6-4 substrate is S813-11-5 was also presumably given a phosphate/fluoride etch. Again, the SEM/EDAX results suggest that the sample was only grit-blasted. The primer is not removed completely by chloroform rinsing at room temperature.

11. Primed (BR-34) Ti 6-4 substrates show the presence of Al filler particles by SEM/EDAX. The Ti 6-4 substrate before priming had a surface morphology characteristic of an acid etch as seen in the SEM photomicrographs.

12. Primed (MEPPQ) Ti 6-4 substrates after phosphate/fluoride treatment give a characteristic(of an acid etch)surface morphology by SEM. Only a thin residue film of primer is left on the Ti 6-4 surface after chloroform rinsing at room temperature as gauged by ESCA.

13. Primed (MEPPQ) Ti 6-4 substrates supplied by Boeing show SEM evidence of phosphate/fluoride etch but no evidence of a prior grit-blasting step. The removal of the primer film by chloroform is not as effective in this case as gauged by ESCA.

V. REFERENCES

1. P. W. Palmberg, "Combined ESCA/Auger System Based on the Double Pass Cylindrical Mirror Analyzer", J. Electr. Spectrosc. and Related Phenom., 5, 691 (1974).

2. P. M. Hergenrother and M. Hudlicky, J. Fluorine Chem., 12, 439 (1978).

3. W. Chen, D. W. Dwight and J. P. Wightman, "A Fundamental Approach to Adhesion: Synthesis, Surface Analysis, Thermodynamics and Mechanics", Final Technical Report, NASA Grant NSG-1124, VPI & SU, Blacisburg, Va., February, 1978.

4. J. H. Scofield, "Hartree-Slater Subshell Photoionization Cross-Sections at 1254 and 1487 eV", J. Electr. Spectosc. and Related Phenom., 8, 129 (1976).

5. T. A. Carlson, Photoelectron and Auger Spectroscopy, Plenum Press, New York, 1975.

6. W. Chen, D. W. Dwight, W. R. Kiang and J. P. Wightman, "Reduction of Contamination of Titanium Surfaces Studied by ESCA", in Surface Contamination: Its Genesis, Detection and Control", K. L. Mittal, Editor, Plenum Press, New York, June, 1979.

VI. ACKNOWLEDGEMENTS

Most of the work described in this report was performed on samples supplied by personnel in the Polymer Group at NASA-LaRC. Our studies would not have been possible without their efforts, especially Mr. Don Progar, Mr. Paul Hergenrother and Ms. Anne K. St.Clair. Dr. David W. Dwight kindly arranged to have the Auger electron spectroscopy including depth profiling of selected Ti 6-4 samples done at Physical Electronics. The expert operation of the SEM by Frank Mitsianis is acknowledged.

VII. APPENDIX

Paper 1 - David W. Dwight, Wen Chen and James P. Wightman, "Surface Analysis and Adhesive Bonding. III. Titanium 6-4", in Applications of Surface Analysis, L. E. Davis and T. Barr, Editors, ASTM Publication, Philadelphia, PA., in press.

Paper 2 - David W. Dwight and James P. Wightman, "Identification of Contaminants with Energetic Beam Techniques", in Surface Contamination: Its Genesis, Detection and Control, K. L. Mittal, Editor, Plenum Press, New York, June, 1979.

Paper 3 - W. Chen, D. W. Dwight, W. R. Kiang and J. P. Wightman, "Reduction of Contamination on Titanium Surfaces Studied by ESCA", in Surface Contamination: Its Genesis, Detection and Control, K. L. Mittal, Editor, Plenum Press, New York, June, 1979.

SURFACE ANALYSIS AND ADHESIVE BONDING. III. TITANIUM 6-4

DAVID W. DWIGHT, WEN CHEN & JAMES P. WIGHTMAN
Virginia Polytechnic Institute and State University
Blacksburg, Virginia 24061

ABSTRACT

In a program to develop adhesive bonding for fabrication of aerospace structures with titanium 6-4 alloy, we have characterized the physical and chemical constituents of the surfaces using SEM/EDAX and ESCA. The results elucidate the changes that occur from manufacture through surface treatment, bonding and strength-testing.

Ti 6-4 sheet stock had wide variability on the opposite sides, but grit blast destroyed the initial structures, leaving the surface heavily worked and with significantly higher aluminum content. Chemical treatments removed the worked layer and resulted in a thin oxide layer with various structures depending upon the specific treatment. After ten hours aging in air at 505 K (450°F), the oxide layer grew and microstructural changes indicate transformations favoring the α-phase. These observations show a qualitative correlation with adhesive bond durability.

INTRODUCTION

Titanium 6-4 alloy, introduced in 1954, is a highly stabilized, alpha-beta phase alloy, using aluminum as the alpha stabilizer and vanadium as the beta stabilizer (1). These impart toughness and strength at temperatures up to 627 K (750°F). Other alloying elements that favor the alpha crystal structure (hexagonal close pack) at room temperature are gallium, germanium, carbon, oxygen, and nitrogen. The beta crystal structure (body centered cubic) is stabilized by molybdenum, vanadium, tantalum, and columbium. Superior in corrosion resistance to many metals, titanium and its alloys are protected by an inherent oxide film at low and moderate temperatures, but are subject to oxidation above 523 K (480°F) (2).

One of the most important considerations for joining of titanium and its alloys by welding, adhesive bonding, or other techniques is the difficulty of removing contamination. A variety of specialized surface treatments have been developed over the past decade, and increasingly sophisticated measurements are being used to characterize the surfaces involved.

An early report describes the difficulties in working with titanium compared to copper, iron, and aluminum and other metals in common engineering use (3). In a paper which reviewed the application of many

techniques of surface analysis to adherends, the use of both alkaline and phosphate/fluoride surface treatments on titanium 6-4 alloy were characterized. Differences between treatments were seen by SEM and in surface elemental composition as determined by ESCA (4). The suggestion was made that the change from anatase to rutile crystal structure made an 8 to 11 percent change in volume, and affected the long term stability of titanium joints. A number of other surface preparations for titanium have been described in the literature (5), including those designed to increase surface hardness by nitriding (6).

In a study of a proprietary structural adhesive (HT 424) with aluminum 2024-T3 and titanium 6-4, ellipsometry and surface potential difference measurements identified substrates which would result in poor adhesive bonding (7). The use of Auger spectroscopy with ion-sputtering depth-profiling, electron microscopy and diffraction and x-ray diffraction allowed the locus-of-failure in these systems to be determined. The fracture surface alternated between a surface oxide layer, an interface and primer layer, and into the bulk adhesive. Phosphate/fluoride and Turco surface treatments gave similar bond strength and failure loci. Only a nitric acid/fluoride treatment produced low bond strengths, and this treatment gave large copper concentrations in the oxide film.

Another experimental approach to evaluate different surface treatments determined time-to-failure, or durability, at 333 K (140°F) and 95% relative humidity, at various loads (8). This work indicated the phosphate/fluoride treatment gave stress-durability almost an order of magnitude greater than alkaline-cleaned alloys. Outdoor exposure in both stressed and unstressed adhesive joints indicated a similar comparison between the two surface treatments. Non-destructive thermoholography was able to determine the rearrangement of titanium dioxide under the bond from anatase to rutile crystal structure. Electron diffraction was used to determine the surface structures, which were stabilized with ions that promote the anatase form (9). To determine the statistical nature of failure under stress in different environments, Weibull distribution parameters were determined from the data (10). A predictive model for failure times of adhesive bonds at constant stress (11) was developed using multiple regression analysis.

In a program to determine relative durabilities of adhesive bonded structures, nylon-supported FM400 (a modified epoxy adhesive) was used in conjunction with a corrosion inhibiting primer (12). Six different treatments were applied to the titanium 6-4 alloy and exposure lifetimes determined at $1.03 \times 10^{7} Nm^{-2}$ at (1500 psi) stress, 334 K (160°F) and 100 percent relative humidity. Locus-of-failure was determined visually and samples of lowest life time showed the greatest amount of interfacial failure. Longer-lasting surface treatments (lifetimes varied from 15 to over 1000 hours) produced evidence of more cohesive failure in the adhesive layer. The phosphate/fluoride surface treatment showed the lowest lifetime while several other acid treatments (pre-treated with base) produced life-times averaging around 500 hours.

The atomic details of oxidation of titanium surfaces have been described. For example, secondary ion mass spectrometry (SIMS), Auger electron spectroscopy (AES), and X-ray photoelectron spectroscopy (XPS) (or ESCA) were simultaneously used to study the oxidation of titanium in the monolayer range (13). Successive stages of oxidation led to significant changes, first in the AES, then in the SIMS signals, and finally to a chemical shift in XPS. Also a number of treatments of titanium 6-4 alloy and pure titanium were studied with x-ray and electron diffraction, and no anatase form was found (14). The oxidation of titanium by water vapor in the 923 to 1223 K range and from 27 to 2400 Nm^2 (0.5 to 18 torr) pressure has recently been studied (15). Only one oxide form (rutile) was found and SEM examination of oxidized specimens revealed the presence of whiskers. The pure metal oxidized at a rate about double that of the alloy. Ellipsometry has been used to determine the thicknesses of films formed by anodization. Crystal structures were determined by electron diffraction which consisted of either amorphous or the anatase crystal form of TiO_2. The amorphous phase gradually reverted into the rutile structure. An inference was made that this slow, allotropic transformation from anatase to rutile adversely affects the bonding of paint films (16). Low energy electron diffraction (LEED) and AES were used to study the reaction of a clean Ti surface with oxygen at room temperature and dosages between 133 and 1.33×10^4 Nm^{-2}sec (1 and about 100 Langmuirs). The results indicate that the final film is probably not TiO_2 but rather TiO (17). A different approach to the study of high temperature air oxidation of titanium alloy involved the use of mass transport diffusion data in the metallic and oxide phases. A mechanism was determined involving the growth of successive elemental layers. The rate determining step for oxidation was found to be the diffusion of oxygen through a dense elementary layer (18).

In summary, the literature contains useful background information concerning analysis of titanium and its alloys oxidized by oxygen and water, and Ti 6-4 surface treatments and adhesive bond durability. No publications described the parameters of Ti 6-4 after commercial Anodize, Phosphate/Fluoride, Pasa-Jell, or Turco treatments, specifically. Herein we report the morphological aspects of a systematic study of each step in the various preparations for titanium 6-4 surfaces. As a first stage in assessing the relative durability of the different surface treatments, changes occasioned by aging at 505 K (450°F) were monitored. Results of the ESCA studies of the surface chemistry in these specimens, as well as adhesive bond strength experiments have been published elsewhere (19,20).

EXPERIMENTAL

Photomicrographs were obtained using a Polaroid camera back attached to the oscilloscope on the Advanced Metals Research Corporation Model 900 scanning electron microscope. Operating at 20 kV, high magnification views (500X-10,000X) gave information on the details of surface features, while survey scans at 20X-200X provided a check on the distribution of representative features that describe the surface. Most specimens were cut to approximately 1 x 1 cm with a high pressure cutting bar and fastened to SEM mounting stubs with conductive, adhesive-coated,

copper tape. To enhance conductivity of insulating samples, a thin (∿ 20 nm) film of Au-Pd alloy was vacuum-evaporated onto the samples. Photomicrographs were taken with the sample inclined 70° from the incident electron beam. Rapid, semiquantitative elemental analyses were obtained with an EDAX International Model 707A energy-dispersive X-ray flourescence analyzer attached to the AMR-900 SEM. A Polaroid photographic record of each spectrum was made using a camera specially adapted for the EDAX oscilloscope output.

Lap shear coupons of Ti 6-4 were provided by D. Progar, NASA Langley Research Center, both before and after grit blasting. Anodizing was performed by the Boeing Company using a proprietary process. Procedures followed for the three chemical treatments are listed in Tables I-III. Also samples of each of the four treatments were exposed for 10 and 100 hours at 505K (450°F) in an air oven.

TABLE I
PHOSPHATE/FLUORIDE TREATMENT

1. Solvent wipe - methylethyl ketone.
2. Alkaline clean - immerse in SPREX AN-9, 30.1 g/ℓ, 353 K (80°C) for 15 min.
3. Rinse - deionized water at room temperature.
4. Pickle - immerse for 2 min. at room temperature in solution containing 350 g/ℓ of 70% nitric acid and 31 g/ℓ 48% HF.
5. Rinse - deionized water at room temperature.
6. Phosphate/fluoride treatment - Soak for 2 min. at room temperature in solution containing 50.3 g/ℓ of tri sodium phosphate (Na_3PO_4); 20.5 g/ℓ of potassium fluoride (KF); and 29.1 g/ℓ of 48% hydrofluoric acid (HF).
7. Rinse - deionized water at room temperature.
8. Hot water soak - deionized water at 338 K (65°C) for 15 min.
9. Final rinse - deionized water at room temperature.
10. Dry - air at room temperature.

TABLE II
PASA-JELL 107 TREATMENT

1. Solvent wipe - methylethyl ketone.
2. Alkaline clean - immerse in SPREX AN-9, 30.1 g/ℓ, 353 K (80°C) for 15 min.
3. Rinse - deionized water at room temperature.
4. Pickle - immerse for 5 min. at room temperature in solution containing 15g nitric acid (HNO_3) 15% by weight; 3g hydrofluoric (HF) acid 3% by weight; and 82g deionized water.
5. Rinse - deionized water at room temperature.
6. Pasa-Jell 107 Paste - Apply to the titanium surface with an acid resistant brush covering the entire surface by cross brushing.
7. Dry - for 20 min.
8. Rinse - deionized water at room temperature.
9. Dry - air at room temperature.

TABLE III
TURCO 5578 TREATMENT

1. Solvent wipe - methylethyl ketone.
2. Alkaline clean - immerse in Turco 5578, 37.6 g/ℓ, 343-353 K (70-80°C) for 5 min.
3. Rinse - deionized water at room temperature.
4. Etch - immerse in Turco-5578, 419 g/ℓ, 353-373 K (80-100°C) for 10 min.
5. Rinse - deionized water at room temperature.
6. Rinse - deionized water at 333-343 K for 2 min.
7. Dry - air at room temperature.

RESULTS AND DISCUSSION

Sequentially described is the surface characterization of Ti 6-4 alloy, from manufacture through grit blasting, chemical surface treatment and thermo-oxidative aging. The differences between steps were most apparent in the physical structures that composed the surfaces. Surface chemistry was remarkably constant except for the presence of minor constituents apparently adsorbed from the treatment solutions (19).

As Received

Scanning electron micrographs of both sides of titanium 6-4 alloy before grit blasting are shown in Fig. 1. The opposite sides are composed of entirely different structures. Side A appears to have random, short striations that may be derived from surface working during manufacture or subsequent burnishing or deburring. This side appeared relatively shiny to the eye. Side B, on the other hand, shows no signs of mechanical working, but appears dull to the eye. The difference in surface morphology was not removed entirely by chemical treatments, and grit blasting was a necessary, intermediate step to produce titanium 6-4 coupons with identical surface structures on both sides. Clearly, the original differences could cause variations in bond strength values depending upon the side bonded.

Grit Blast

After grit blasting the surface appears heavily worked; Fig. 2 shows there is no resemblance to either of the original sides. This surface is composed of deformed and fractured metal and oxide, covered with fracture debris in the size range 0.1 to 10 μm. None of the particles on this substrate resemble grit blast particles. However, the aluminum content of this surface was unusually high. Fig. 3 compares the EDAX results from Ti 6-4 after grit blast, and subsequent phosphate/fluoride etch, with results from a grit blast particle. The aluminum content of the grit blasted sample is about an order of magnitude greater than titanium 6-4 alloy. Also, the aluminum was uniformly distributed over the surface; the fracture debris particles showed the same EDAX spectrum as the substrate.

Chemical Treatment and Thermo-oxidative Aging

1. Anodize. Scanning electron micrographs of the anodized specimen before and after thermo-oxidative aging for ten hours at 505 K (450°F) are shown in Fig. 4. There appears to be a very thin layer on the top surface with minute cracks or fissures of irregular shape, densely populating the surface. These cracks have sharp edges at the upper surface and where they meet the underlaying substrate. At highest magnification the whole surface

appears to be sponge-like with fine pores of diameter < 0.1 μm. After aging, some connecting of the irregular cracks in the surface oxide layer appears to occur. However, at high magnification it appears that this layer joins the underlying substrate more smoothly.

Simultaneous ion sputtering/Auger analysis showed that the oxide layer was about 60 nm after anodization, while only about 20 nm thick after the phosphate/fluoride treatment (21).

2. Phosphate/Fluoride. Scanning electron micrographs of phosphate/fluoride-etched Ti 6-4 before and after aging are shown in Fig. 5. Before aging (A) there appear fairly well defined alpha gray and beta white phases. At high magnification the beta phase crystals are poorly defined, but the alpha phase shows regularly-spaced edges approximately 100 nm apart. After aging, the surface becomes covered with a dense packing of small nodules approximately 100 nm in diameter. Both alpha and beta phases are still distinguishable; however, it appears that the alpha phase has grown at the expense of the beta during oxidation.

3. Pasa-Jell. Fig. 6 shows scanning electron micrographs of the Ti 6-4 surface after Pasa-Jell treatment and thermo-oxidative aging. The beta phase is larger than in the previous case and more clearly defined in white, plate-like crystallites. On the other hand, the gray, alpha phase shows less distinct crystalline development. An artifact appears in these photomicrographs in the form of "popcorn" particles approximately 50 nm in diameter. These are shown to occur in step 6, Table III, of the Pasa-Jell process as noted in comparing Figures 6 and 7. After aging, the beta phase appears to have diminished dramatically. Those few beta phase particles that still appear seem to have been absorbed into the surrounding alpha-phase matrix.

Figure 7 shows the titanium 6-4 alloy after all but the final application of the acid-jell in the Pasa-Jell process. Clearly, the surface shows less developed alpha and beta phases and appears to consist more of amorphorous oxide in greater thickness. However, the "popcorn" particles do not appear, and thus we conclude that they were artifacts carried on the surface by the specific lot of the Pasa-Jell paste.

Both phosphate/fluoride and Pasa-Jell treatments are acidic, and they result in surface structures that are similar.

4. Turco. The Turco process exposed Ti 6-4 alloy to basic solutions. Scanning electron micrographs of the results are shown in Fig. 8. This surface is entirely different from any of the previous surface treatments morphologies. There is no clear distinction between alpha and beta phases, which leads to the impression that the surface is a pure oxide layer without separate alloy phases. The oxide layer is highly fragmented at the asperities on the surface. The results of thermo-oxidative aging are more dramatic in the case of Turco surface treatments than in the previous cases. It appears that the surface topography has collapsed to some degree into locally-ordered plane or plate-like structures that now appear on the surface. The rearrangements of surface morphology seemed to create further fracture in the oxide layer, shown especially at high magnification. Also, a grainy texture appears after aging, whereas the surfaces were very smooth prior to aging.

In summary, surface treatment and aging cause profound changes in the surface morphology of Ti 6-4. The surface chemical composition remained relatively constant, both in oxidation state and in stoichiometry. The surface morphology can be ranked in the order Turco>Pasa-Jell>phosphate/fluoride>anodize by considering the relative heights-of-asperities (or degree of three-dimensional development), and also the degree of change induced by aging. Thus, there appears an inverse correlation between morphological development and reports that claim basic treatments to be the least durable.

SUMMARY AND CONCLUSIONS

The results demonstrate the utility of surface analysis in adhesive bonding research and development. Surface pretreatments on Ti 6-4 clearly produce different microstructures and brief heating in air induces further change. Such basic data identify components of the system that may be a site of weakness, and serve as controls for diagnostic analysis of fracture surfaces in strength-tested joints. Specifically, we found:

1. Ti 6-4 has totally different morphology on opposite sides before grit blasting. One side has markings that appear to be the result of process working or subsequent deburring.

2. Grit blasting destroys the original structures, leaving the surface heavily worked and fragmented and covered with minute fracture debris. Aluminum content is significantly increased although uniformly and no Al_2O_3 grit blast particles appear.

3. Each of the four chemical surface treatments produced unique surface morphology, with only the two acid treatments bearing any resemblance to each other.

4. A qualitative ranking: Turco>Pasa-Jell>phosphate/fluoride> anodize was made both by considering the degree of roughness and the degree of change in surface morphology after 505 K (450°F) exposure in air.

5. Oxidation generally seems to diminish the size of surface structures and to favor the alpha phase at the expense of the beta phase.

ACKNOWLEDGMENT

The support of the National Aeronautics and Space Administration (NASA Grant NSG-1124) is gratefully acknowledged.

REFERENCES

1. R. F. Muraca and J. S. Whittick, "Materials Data Handbook on Titanium 6Al-4V," NASA Tech Brief B73-10372, October 1973.

2. ASM Committee on Metallography of Titanium and Titanium Alloys, "Microstructure of Titanium Alloys," Metals Handbook, 7, 321 (1972).

3. N. L. Rogers, "Surface Preparation of Metals for Adhesive Bonding," Applied Polymer Symposia 3, 327 (1966).

4. W. C. Hamilton, "Some Useful Techniques for Characterization of Adherend Surfaces," Applied Polymer Symposium 13, 105 (1972).

5. E. D. Newell and G. Carrillo, "A New Surface Preparation Process for Titanium," Materials and Processes for the 1970's, SAMPE Conference, 1973, p. 131.

6. R. H. Shoemaker, "New Surface Treatments for Titanium," Titanium Science and Technology, 4, 2401 (1973).

7. T. Smith and D. H. Kaelble, "Mechanism of Adhesion Failure Between Polymers and Metallic Substrates: Al 2024-T3 and Ti 6-4 with HT 424 Adhesive," Report No. 74-73, Air Force Materials Laboratory, Wright-Patterson Air Force Base, Ohio (1974).

8. R. F. Wegman, "Durability Testing of Adhesive Bonded Joints," Applied Polymer Symposium 19 384 (1972).

9. F. Wegman and J. Bodnar, "Structure Adhesive Bonding of Titanium - Superior Surface Preparation Techniques," Quarterly 5, 28 (1973).

10. D. W. Levi, R. F. Wegman, and M. J. Bondar, "Effect of Titanium Surface Pretreatment and Surface Exposure Time on Peel Strength of Adhesive Bonds," SAMPE Journal, March/April, 32, (1977).

11. W. C. Jones, III, E. McAbee, R. F. Wegman, and D. W. Levi, "Use of Multiple Regression Analysis to Develop Predictive Models for Failure Times of Adhesive Bonds at Constant Stress," Journal of Applied Polymer Science 18, 555 (1974).

12. P. M. Stifel, "Durability Testing of Adhesive Bonded Joints," New Industries and Applications for Advanced Materials Technology, SAMPE Publin., Azusa, CA, 1974, p. 75.

13. A. Benninghoven, H. Bispinck, O. Ganschow, and L. Wiedmann, "Quasisimultaneous SIMS-AES-XPS investigation of the oxidation of Ti in the monolayer range," Applied Physics Letters, 31, 341 (1977).

14. K. W. Allen, and H. S. Alsalim, "Titanium and Alloy Surfaces for Adhesive Bonding," J. Adhesion, 6, 299 (1974).

15. Motte, C. Coddet, P. Sarrazin, M. Azzopardi, and J. Besson, "A Comparative Study of the Oxidation with Water Vapor of Pure Titanium and of Ti6 Al-4V," Oxidation of Metals 10, 113 (1976).

16. F. Dalard, C. Montella et J. C. Sohm, "Adhension Des Peintures Sur Le Titane Anodise," Surface Technology 4, 367 (1976).

17. H. D. Shih and F. Jona, "Low-Energy Electron Diffraction and Auger Electron Spectroscopy Study of the Oxidation of Ti (0001) at Room Temperature," Applied Physics 12, 311 (1977).

18. C. Coddet, "Essai dinterpretation du mechanisme d'oxydation de l'alliage de titane TA6V4 par l'oxygene sec entre 700°C et 1000°C," Journal of the Less-Common Metals 51, 1 (1977).

19. W. Chen, D. W. Dwight, W. R. Kiang and J. P. Wightman, "ESCA Study of Contamination on Titanium," in "Surface Contamination " (K.L. Mittal, Ed.), Plenum, New York, in press.

20. D. W. Dwight, M. E. Counts and J. P. Wightman, "Surface Analysis and Adhesive Bonding. II. Polyimides," in "Colloid and Interface Science, Vol. III," (M. Kenker, Ed.), Academic, New York, 1976, p. 143.

21. D. W. Dwight and J. P. Wightman, "Identification of Contaminants with Energetic Beam Techniques," in "Surface Contamination," (K. L. Mittal, Ed.), Plenum, New York, in press.

FIGURE CAPTIONS

FIGURE 1. SEM photomicrographs (2000X) of both sides of a Ti 6-4 coupon "as received" before grit blasting, showing entirely different physical structures that may produce different results in adhesion.

FIGURE 2. SEM photomicrograph (2000X) of a grit blasted sample of Ti 6-4, which appears to be the heavily worked, fragmented remains of the previous Ti 6-4 sample. Fracture debris, 0.1 μm <d<10 μm, are densely scattered.

FIGURE 3. EDAX Spectra typical of Ti 6-4 Coupon. A. After chemical surface treatments, B. After grit blast, and C. Grit blast particles.

FIGURE 4. SEM photomicrographs (10,000X) of Ti 6-4 surface after anodizing. A. Before and B. After exposure to air at 505 K (450°F) for 10 hours, showing a unique surface morphology that appears to change little after aging.

FIGURE 5. SEM photomicrographs (10,000X) of Ti 6-4 surface after Phosphate/ Fluoride treatment. A. Before and B. After exposure at 505 K (450°F) for 10 hrs. in air, showing gray alpha phase and a discontinuous, white beta phase.

FIGURE 6. SEM photomicrographs (10,000X) of Ti 6-4 surface after Pasa-Jell process. A. Before and B. After aging in air at 505 K (450°F) for 10 hours, showing the white, beta phase particles larger than in the previous sample. The small white "popcorn" particles appear to be artifacts of the last step of process.

FIGURE 7. SEM photomicrograph (10,000X) of Ti 6-4 surface after the Pasa-Jell process except step 6. The clear alpha/beta phase structure has not materialized but the "popcorn" particles are no longer present, indicating they arise during step 6 of the Pasa-Jell treatment.

FIGURE 8. SEM photomicrographs (10,000X) of Ti 6-4 after Turco process. A. Before and B. After exposure to air at 505 K (450°F) for 10 hours, showing surface structures are very different from the preceeding two acid treatments.


50 μm

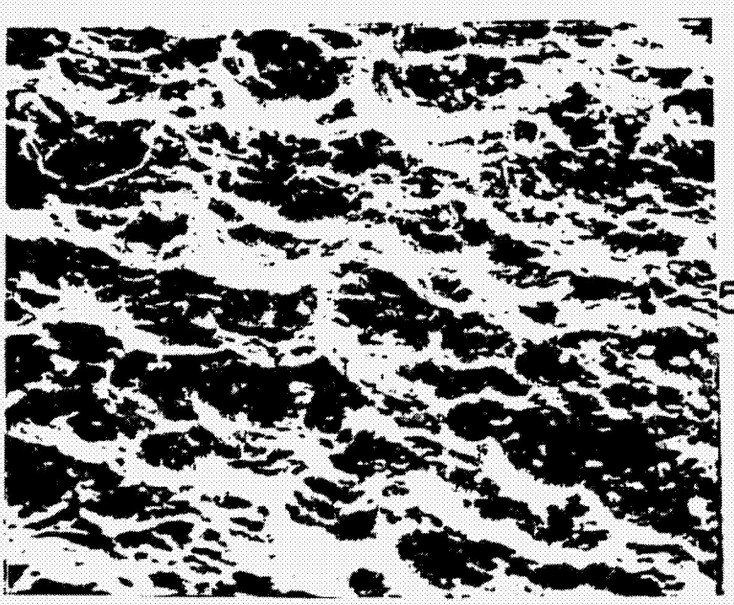
50 μm

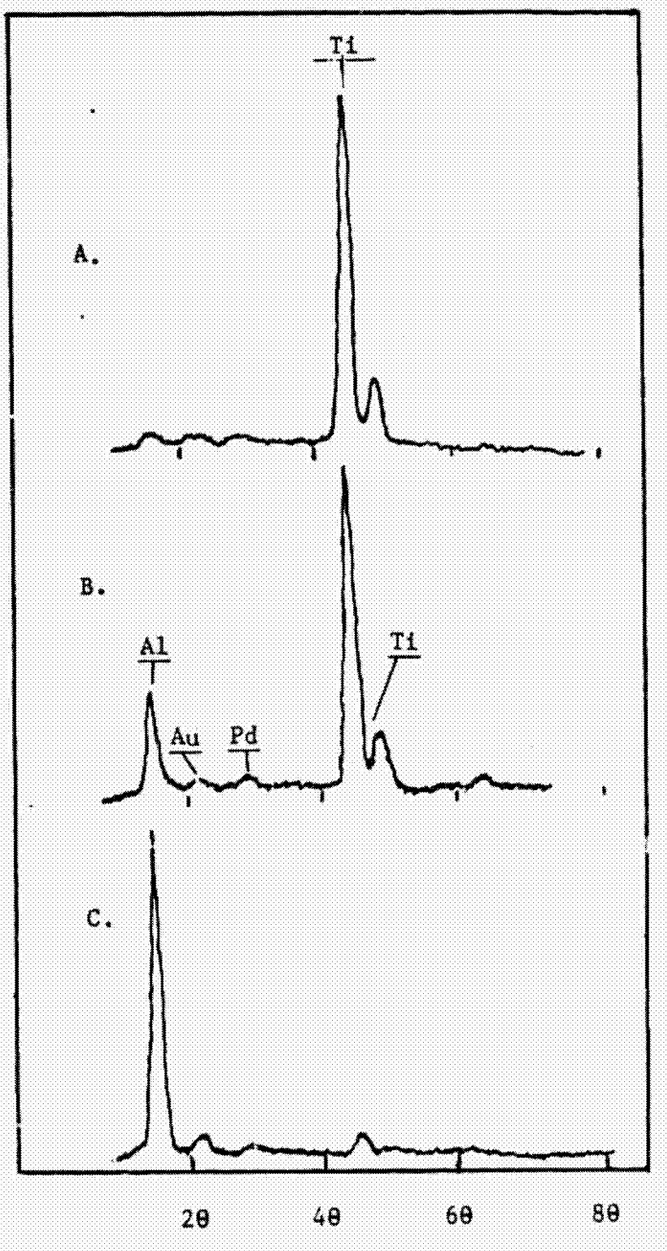
Ti
A.
B.
Al
Au
Pd
Ti
C.
2θ
4θ
6θ
8θ

10 μm

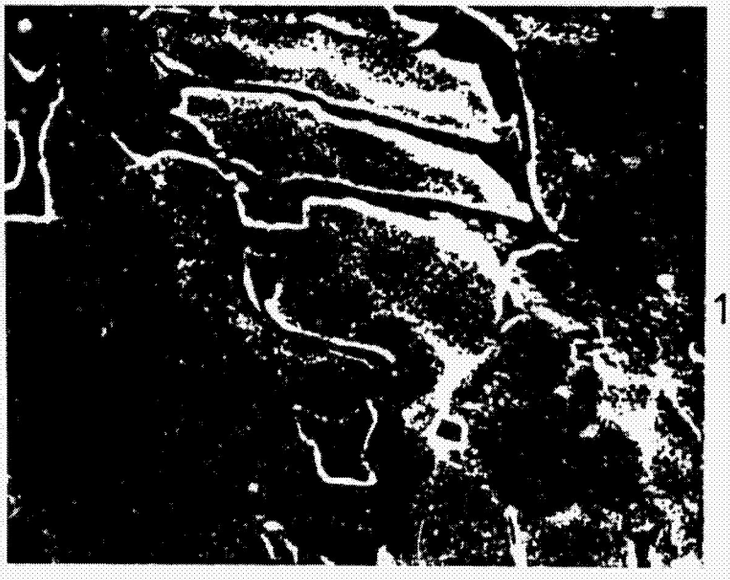

10 μm

10 μm

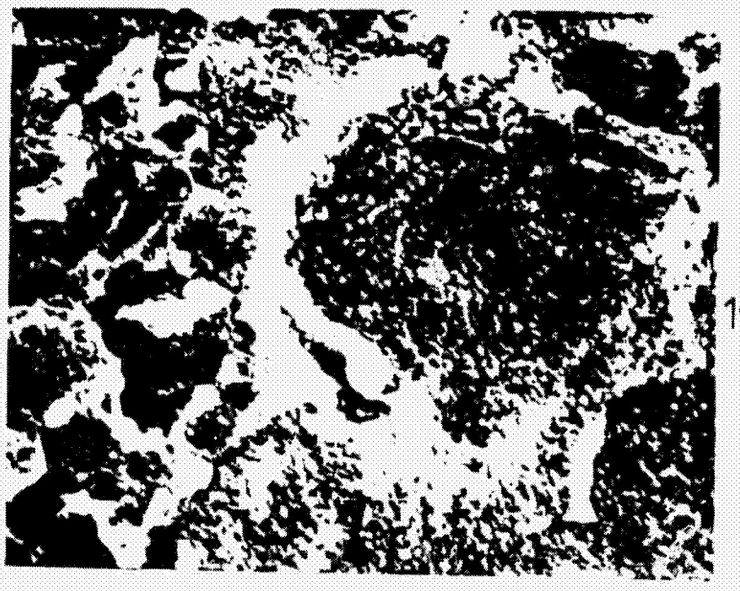

10 μm

Figure 5

10 μm

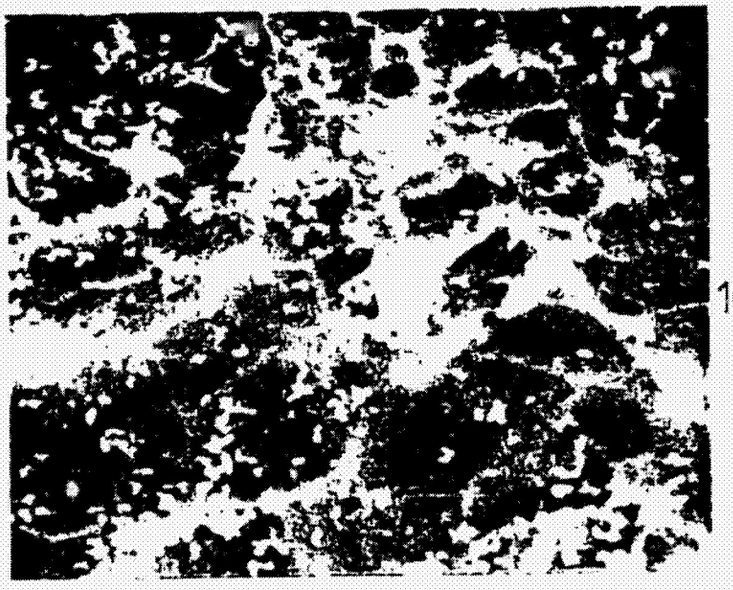

10 μm

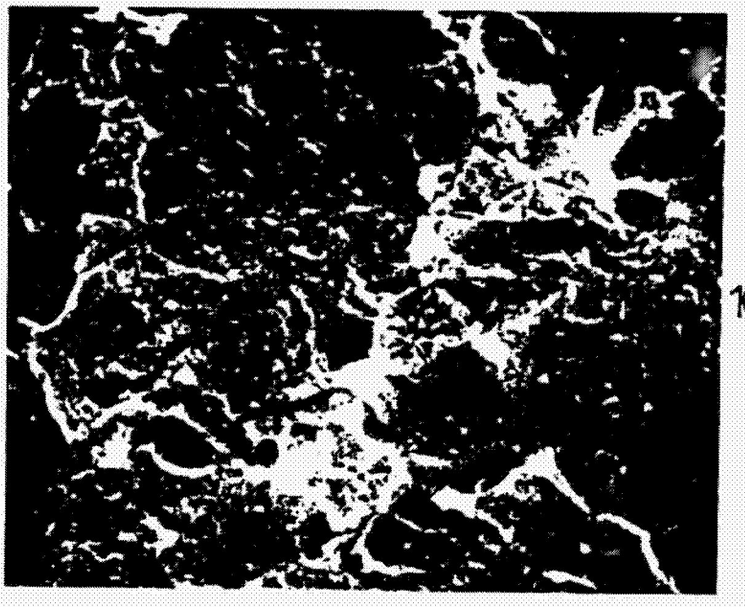

10 μm

Figure 7

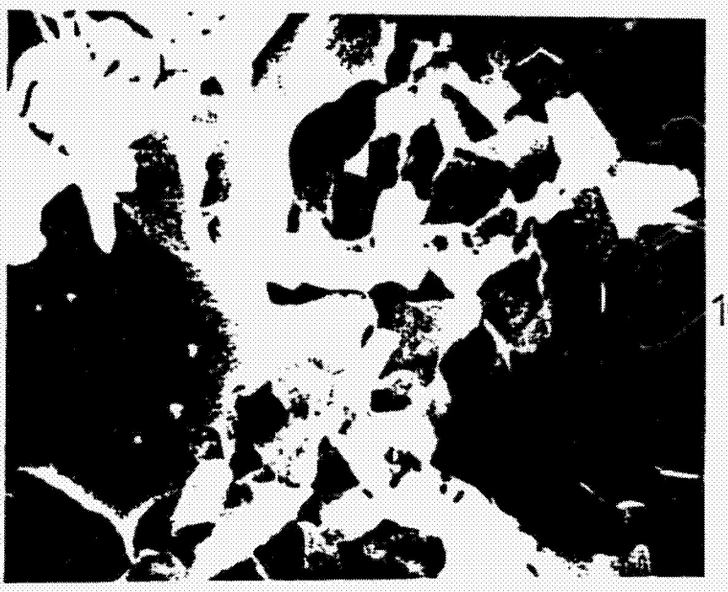

10 μm

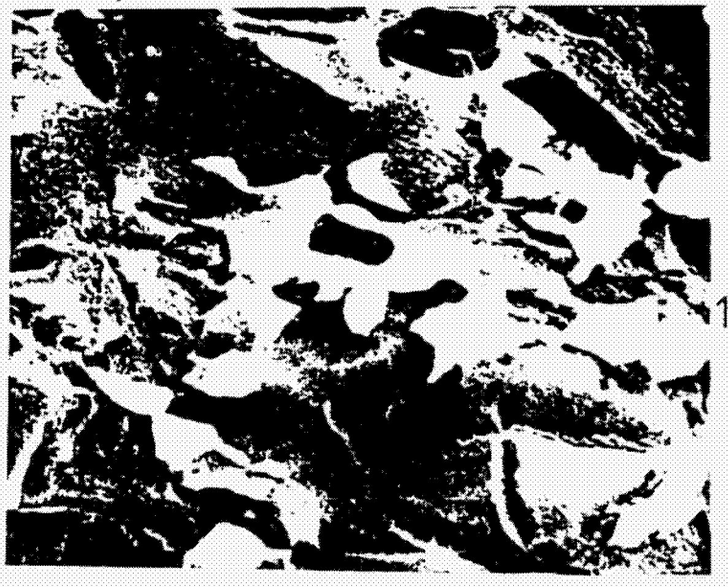

10 μm

IDENTIFICATION OF CONTAMINANTS WITH ENERGETIC BEAM TECHNIQUES

David W. Dwight* and James P. Wightman†

Virginia Polytechnic Institute and State University

Blacksburg, Virginia 24061

A review of techniques to obtain structure and bonding analysis in 1nm-1μm phases with ion, photon, or electron beams emphasizes the advantages and limitations of TEM, SEM, ISS, SIMS, ESCA, AES, and UPS. Highlights from recent applications in the fields of adhesion, corrosion, and wear demonstrate a broad range of new information on structure/property relationships in microphases. Quantitative analysis of segregation from bulk substrates and of weak boundary layers indicates the control of adhesion at the 0.2-0.5nm level. A general model of corrosion postulates electrochemical mechanisms around microscopic heterogeneities at interfaces. Surface analysis in wear experiments shows nearly ubiquitous atomic or molecular-level transfer upon touch, and surface chemical changes inevitably accompany changes in friction and wear behavior.

New results illustrate the importance of depth-profile studies. Angle-resolved ESCA study of ion-sputtered fluoropolymer demonstrate effects confined to the top few atom layers while ion sputter/Auger profiles on titanium 6-4 show three-fold changes in oxide layer thickness within the top 100nm.

---

*Department of Materials Engineering

†Department of Chemistry

INTRODUCTION

For over a century, colloid chemists have studied the structure and properties unique to materials of dimensions 1nm-1μm. Energetic beam techniques promoted major advances in the field, historically in morphology first with Transmission Electron Microscopy (TEM) and Scanning Electron Microscopy (SEM). Chemical analysis in these instruments usually analyzes x-ray emission and is not sensitive to thicknesses <100nm. The current decade has produced a burgeoning of electron, photon, and ion bombardment methods (1), and now two surface science journals are devoted to elucidation of "microscopic force laws that govern the properties of surfaces and interfaces...and the technological implications..."

Ion Scattering Spectroscopy and Secondary Mass Spectrometry (ISS & SIMS) are the most sensitive, but interpretation of the data can be difficult because of complex scattering and ionization processes. Auger Electron Spectroscopy (AES) has sensitivity of a fraction of a monolayer *and* can be focused laterally to identify features <0.5μm in diameter. Scanning the electron beam in coordination with a CRT image allows both physical and chemical heterogeneities of the sample surface to be recorded. Profiles of composition vs depth can be obtained by combining ion-beam milling with simultaneous AES. Unfortunately, ion and electron beams are likely to damage polymer surfaces during the measurement, so photoelectron spectroscopy using x-ray (XPS or ESCA), or ultraviolet (UPS) radiation is the method of choice. These methods give additional chemical bonding information, but cannot resolve lateral heterogeneities easily. Synergistic combinations of some of the methods in one apparatus offer possibilities exemplified by new data on angle-resolved photoemission from an ion-sputtered fluoropolymer and Auger depth profiles on titanium 6-4 alloy after treatments designed to improve adhesive bonding.

The following review describes the principal advantages and limitations of the most utilized energetic beam methods. Selected examples are cited of applications of modern methodology in adhesion, corrosion, and wear.

Techniques

Electron Microscopy. A simplified schematic (Figure 1) illustrates the two types of electron microscopes. Transmission Electron Microscopy has been the mainstay of microstructure analysis since the 1930's. The use of TEM in contamination research usually requires replication; an adhesive tape or solvent-carried polymer placed on the surface of interest produces a negative image of the surface with spacial resolution of 6nm. Consecutive replication of the same contaminated surface with solvent-softened cellulose

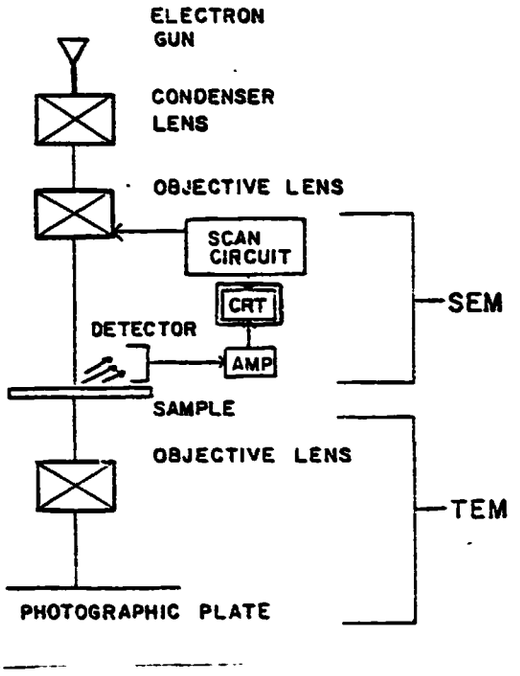

Figure 1. Simplified schematic diagram showing the basic components of Scanning (SEM) and Transmission (TEM) Electron Microscopes.

acetate tape first removes particles, then loosely held contaminants for subsequent analysis in the Scanning Electron Microscope (SEM). Finally, a replica of the underlying substrate can be made, "shadowed" with vacuum evaporated metal and studied with high resolution (2). The SEM has an advantage in depth-of-field, and relatively large sections of material can be fit in the analysis chamber. Practical samples can be analyzed without replication because SEM creates an image from surface emission of secondary or backscattered electrons; thus samples do not need to be transparent to the electron beam as is the case in TEM.

Electron Spectroscopy. In principle, measurement of the electron energy spectrum identifies elemental constituents and bonding states in a material. Figure 2 illustrates the excitation/emission process for three common spectroscopic techniques. In ESCA, x-rays excite core level photoemission while in UPS ultraviolet light excites valence band electrons. After core holes are created, relaxation processes produce both fluorescent x-rays and Auger electrons; probability favors Auger transitions for low

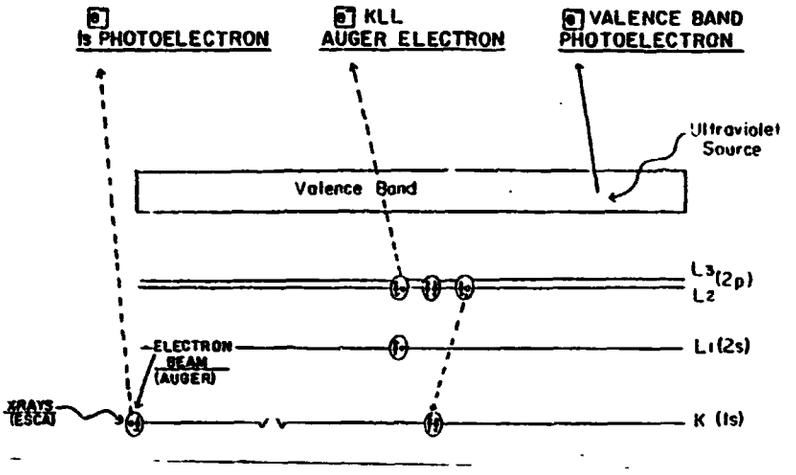

Figure 2. Simplified schematic diagram of the electronic energy levels in any material. Superimposed are illustrations of energetic beams (x-ray, electron, and ultraviolet) commonly used in three types of electron spectroscopy (ESCA, Auger, and UPS).

atomic numbers; only hydrogen cannot be detected. Details of bonding are seen in shifts in the position of photoelectron peaks, and semiquantitative conclusions can be derived from peak intensities.

Electron excitation is used for Auger spectroscopy giving the advantage of a beam that can be focused to very small lateral dimensions to provide resolution of heterogeneities across the sample surface. ESCA and UPS are limited to area greater than $\approx 5mm^2$, but have the advantage of providing less radiation damage to substrates than Auger spectroscopy. During conventional Auger spectroscopy, decomposition of adsorbed species, reduction of surface oxides, diffusion to or from the irradiated area, and electron induced desorption are possible complications (3). These effects are caused by the high electron flux or impurities in the apparatus.

Illustrating the importance of multiple techniques, small amounts of oxygen, fluorine, and chlorine have been found on the sample after collection of a typical Auger spectrum (4). These contaminants were *not* found in the AES or the ESCA spectra, but with the sensitivity of static SIMS. The build-up of these contaminants was proportional to the decrease in the substrates signal obtained from *0-100 eV* by pulse counting of secondary electrons with *low* total electron dose density.

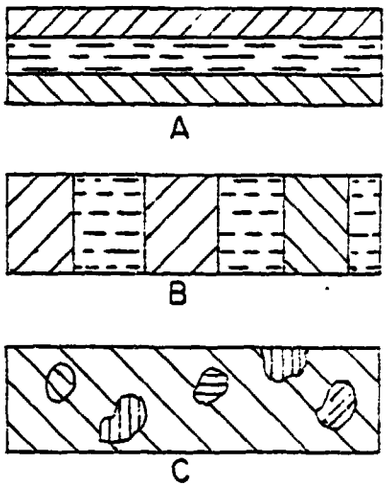

Figure 3. Idealized cross-sections of three major types of samples requiring analysis in contamination research. A. Laterally homogeneous but vertically inhomogeneous, B. Laterally inhomogeneous but vertically homogeneous, C. Inhomogeneous in both dimensions.

In contamination research it is important to determine the variation in composition and morphology with depth. Figure 3 shows simplified cross-sections illustrating the classes of samples encountered. With ESCA one can determine trends with depth (up to at most 10 or 20 atom layers) by changing the photoelectron take-off angle relative to the analyzer, diagrammed on the left in Figure 4. Unfortunately, precise distinctions may be difficult. For example, angle-resolved photoemission studies of a class A sample (carbon contaminating film on gold) determined the ratio of the average contamination layer thickness to the mean free path of photoelectrons, but found that the variable take-off geometry had an error limit of at least $\pm$ 50% (5). Ion bombardment can be used to conduct deeper profile studies, although specimens may be distorted from the true structure (6). In addition to using ion beams to remove atom layers, the sputtered products can be analyzed by mass spectrometer (SIMS). Details of the ion beam methods are covered in other papers in this Symposium, but it should be noted that ion scattering spectroscopy has sensitivity to a small fraction of the first atom layer and can distinguish between isotopes (7).

Other Surface-Sensitive Techniques. Classical methods to characterize surfaces, such as gas adsorption on finely divided solids (8), heat of adsorption (9), contact angles (10), and zeta potential (11) techniques are usually analyzed in terms of thermodynamic interactions between bulk heterogeneous phases. Fundamental interpretation of these measurements in terms of dispersion force

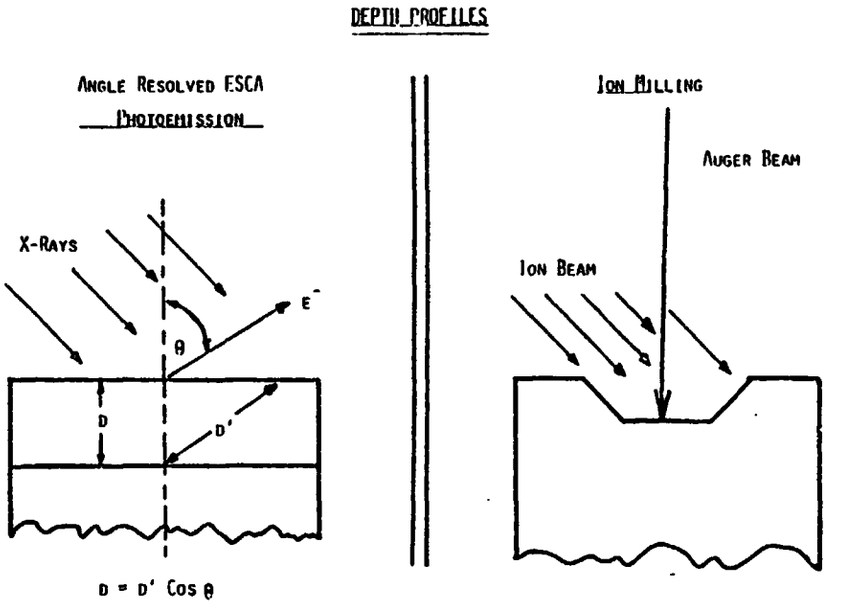

Figure 4. Simplified schematic diagram illustrating two techniques that provide in-depth study of heterogeneous samples. Angle-resolved photoemission (on the left) is non-destructive but limited to the top few monolayers. On the right, milling a crater in the sample surface with an ion beam while analyzing the new surface with Auger electron emission, can provide a chemical profile many μm into the surface but is destructive.

and acid-base interactions between phases at the interface (12) should provide correlations with atomic properties obtained from energetic beam techniques (13).

Many new energetic beam techniques are developing for specific purposes. For example, surface - EXAFS (Extended X-ray Absorption Fine Structures) promises to determine directly the bond lengths and positions of atoms adsorbed on substrates (14). Also Fourier Transform technique and digital substraction promises to expand the use of Infrared analysis of surfaces (15).

Applications

Adhesion. Energetic beam techniques have been used in fractographic analysis of such diverse systems as Ta_2N-TiPdAu films on Al_2O_3 substrates (16) and epoxy adhesives on "Teflon" fluoropolymer (17). A unified theory of adhesion has been promoted which

considers strength as a product of properties representing bulk mechanical behavior and interfacial bonding (18). Qualitative analysis seems to indicate whether the latter is the weak link in adhesive failure. In the case of a structural epoxy adhesive, the initial locus of failure was found to be primarily cohesive through the adhesive, using SEM and electron probe microanalysis with a TiO_2 tracer in the adhesive. However, after water immersion, a complex locus of failure was found. The path of fracture occurred between the oxide surface layer and the epoxy adhesive, alternating onto the adhesive layer (19). Carrying on further, Auger, ESCA, and SIMS were employed to ascertain the mechanism of durability conferred by silane-based primers. Fractures were carried out in the analysis chamber, and profiling more clearly delineated epoxy primer, oxide, or other surface layers. Environmental resistance correlated directly with $FeSiO^+$ radicals detected in SSIMS (20).

D. T. Clark and co-workers at Durham (U.K.) pioneered application of ESCA to structure and bonding studies in polymers (21). A systematic investigation of homopolymers, combined with molecular orbital calculations confirmed the ability of ESCA to elucidate polymer-surface chemistry (22). Critical to precise study of organic surface layers is the mean free path of photoelectrons, now carefully determined to be 1.3nm and 2.9nm at 969 eV and 1430 eV, respectively, for uniformly deposited films of poly-(*p*-xylyene) (23). This background was used to analyze a variety of surface effects in polymers such as contamination from mold release agents, entrained emulsifiers, plasticisers, and catalysts. Further, chemical modification by oxidation and fluorination were defined in terms of kinetics and mechanism as these reactions proceed into the top 3-5nm. Finally, these workers have explicated a variety of effects of inert and reactive gas plasmas upon polymer, including mechanisms of energy transfer, cross-linking, graft polymerization, and oxidative degradation (24).

With more specific interest in adhesive bonding, surface studies showed a thick oxidized film as molded in air against aluminum foil, but if the film was peeled from the foil, essentially bulk failure occurred and the oxidized layer was confined to the top monolayer (25). Composition data from ESCA on commercial polymers subjected to plasmas (26) or chemical etches (27,28) have provided new information to design surface treatments for adhesive bonding applications in particular.

The usefulness of modern energetic beam analysis to microelectronics processing is evidenced by a number of contributions to this Symposium. Holloway has reviewed applications of ESCA, AES, ISS, and SIMS to substrate and substrate processing, deposited films, patterning, interconnection, and compatability (29). Because over 50% of device failures are related to interfacial phenomena, particular effort has been made to understand cleaning techniques.

Generally it has been found that plasmas, ultraviolet radiation, and ozone are more effective than ion sputtering or chemical etches in removing carbon contaminants (30,31). Quantitative AES studies indicated that about 0.5nm was the maximum contaminant thickness allowable and still retain practical bondability, although there was a marked dependence on the type of bonding technique (32).

Troublesome inorganic contaminants, notably Ag and Na, are well known to segregate to the surface from the bulk during processing (33). These effects can lead to device instability and poor adhesion (34). On the other hand, a beneficial effect was found for the adhesion to Al_2O_3 when bulk impurities Ca and Si were found to segregate to the surface (16). In a similar system, the unique properties of high energy in backscattering were used to monitor the migration of silicon through Au, Ag, and Al films at temperatures less than half the eutectic temperature (35). Bulk properties such as ductility minima in Zircaloy seem to be related to carbon segregation and metal carbide formation, as analyzed by AES (36).

Surface cleaning studies on glass (37) and titanium alloy (38) demonstrate that a redeposit of carbon contamination forms on these surfaces in the ambient environment. Storage under ultraviolet light will minimize the effect.

Corrosion. Corrosion is closely related to adhesion; the appearance of corrosion is indicative of loss of adhesion between the paint and the underlying substrate. General corrosion mechanisms have been proposed to account for both anodic (oxidation) and cathodic (reduction) reactions (39). It has been shown that adhesion failure under anodic conditions is due to displacement of the primer by hydroxide ions electrochemically generated at the paint/metal interface (40). Resin composition markedly affected the reaction rate. Recently, the use of photoelectron spectroscopy in corrosion science has been reviewed, including applications to passive films, solid state reactions, electro-chemistry, and aqueous corrosion, concluding with examples of the concurrent use of ESCA and ion beam etching (41).

Figure 5 presents a simplified model of the general corrosion mechanism that can be inferred. Moisture accelerates the electrochemical reactions, and inorganic contaminants may draw moisture through the film as well as conduct current and react with film or substrate. Recent ESCA work on the locus of failure in the loss of paint adhesion specifically identified sapoification of the polymer at the interface by hydroxide ions generated in anodic corrosion (42).

A thorough study of contamination and corrosion will require not only multiple energetic beam techniques, but also *in situ*

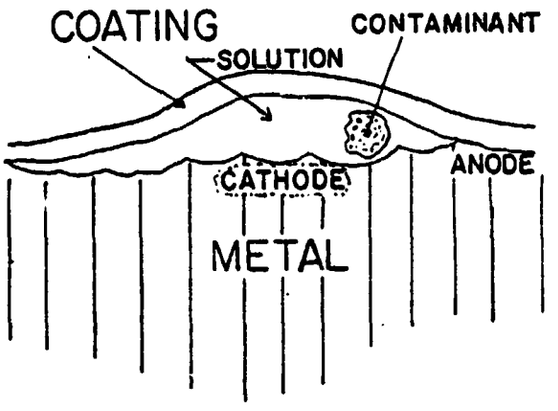

Figure 5. Schematic model of a general mechanism of corrosion. Inorganic contaminants and moisture accelerate electro-chemical reactions that saponify the coating and corrode the substrate.

reactions, to form identifiable derivatives. For example, Ion profiling/Auger spectroscopy revealed the interactions between sulfur dioxide and modified 440C stainless steel at different temperatures (43). SO_2 adsorbed dissociatively with equal quantities of sulfur and oxygen on the surface, and the sulfur did not form a metallic surface phase. Instead the oxide layer thickness increased the presence of SO_2, especially between 500° and 600°C where the oxide became thicker by a factor of seven.

The use of freshly cleaved *in situ* bulk samples as controls for contamination and surface studies is important. This was illustrated in the Auger analysis of E and S glass fibers (44). In S glass, magnesium and aluminum are concentrated on the fiber glass surface, whereas in E glass, chlorine, silica, and aluminum show surface segregation. In order to control progressive beam-induced depletion of cations in soda lime-silica glass analysis, profiles were obtained by making a linear series of analyses along the surface of a sloping ramp etched into the glass in a separate ion bombardment operation (45).

Wear. The interactions between polymers and metals in touch- and sliding-contact were elucidated by Field-Ion Microscopy (FIM) and Auger spectroscopy. Strong adhesion between the organics and all metals (clean or oxidized) was observed (46). Using field-ion microscopy with increasing voltage, electron induced desorption in the vicinity of 20 keV indicated chemical bonding of polymer to the metal surface. ESCA studies in friction, lubrication, and wear are exemplified by a variety of experiments on wear conditions (47). A sulfide was formed at the expense of oxide under severe wear. In

mild wear scars, however, there was no evidence of sulfide or mercaptide, but the oxide layer thickness doubled. Further, it was determined that surface chemistry was a function of wear rate rather than load.

EXPERIMENTAL

Apparatus

A combined ESCA/Auger instrument (PHI Model 550, Physical Electronics Industries, Inc., Eden Prairie, MN), with a double pass Cylindrical Mirror Analyzer (CMA) described by Palmberg (48) was used. Auger depth profiles were obtained with a coaxial electron gun and simultaneous ion beam etching using 2 keV Ar^+ ions from a differentially pumped PHI gun. A magnesium x-ray source (1254 eV) operated at 10 kV and 60ma produced the ESCA results. Differentiation of surface from sub-surface components was made with angle-resolved spectra using Lapeyre's drum/aperature arrangement (49) restricting the cone of acceptance of the CMA to normal or grazing angles.

Materials

The fluoropolymer sample was supplied by NASA Lewis Research Center. A piece of commercial "Teflon" FEP sheet stock was used as a target for ion-beam-sputter modification studies (50). We analyzed both sides of the target: Side 1 represents a case of intensional contamination, while Side 2 had been roughened by an argon beam from an 8cm ion thruster. Also, we collected spectra from a thin fluoropolymer film that was deposited on aluminum foil placed near the target during sputtering.

The titanium 6-4 was obtained from NASA Langley Research Center after grit blasting and degreasing. A variety of oxidative surface treatments were studied in detail (51); a comparison between two types: phosphate/fluoride and anodized was selected to illustrate the importance of depth profiles.

RESULTS AND DISCUSSION

Ion Sputtered Fluoropolymers

The angle-resolved ESCA photoemission from both sides of the "Teflon" FEP ion-sputtering target are shown in Figures 6 and 7. A quick glance at the spectra shows a greater concentration of

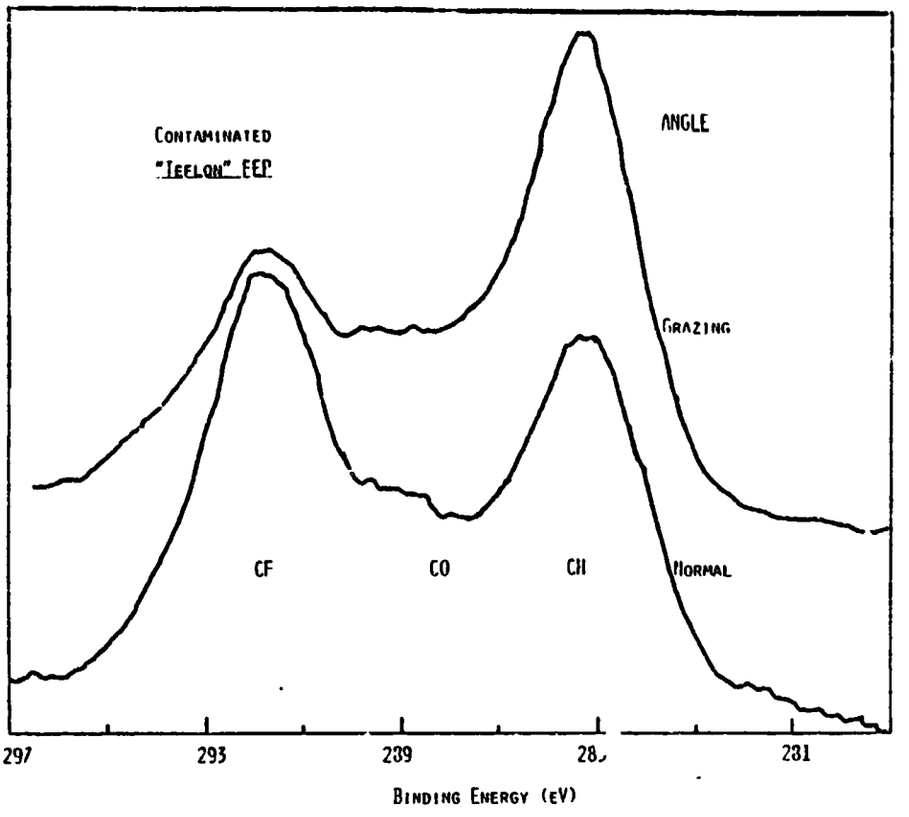

Figure 6. Angle-resolved ESCA photoemission from contaminated "Teflon" FEP showing significant hydrocarbon in the surface and sub-surface layers. Dominance of fluorocarbon signal at normal incidence means the overlying contamination must be <3nm

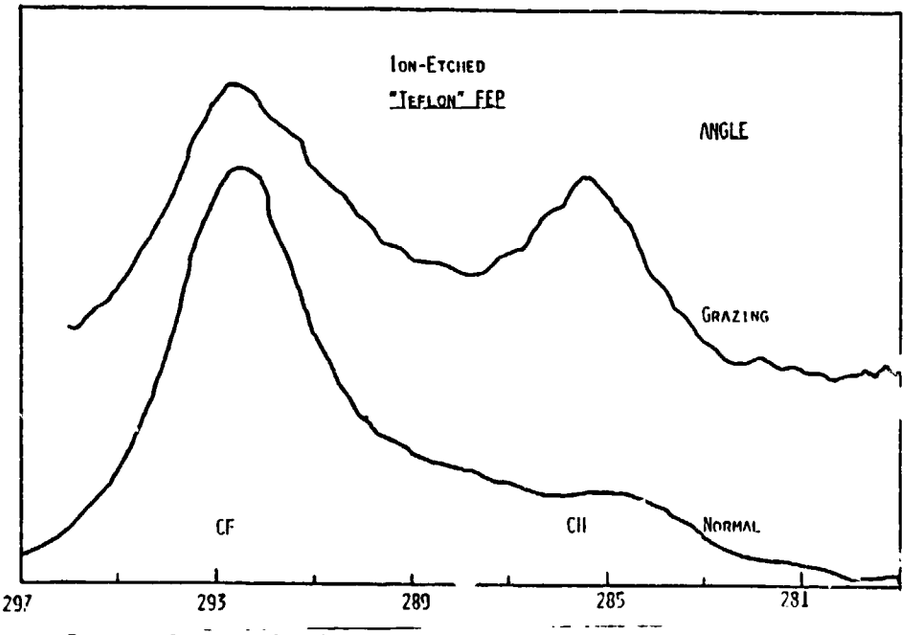

Figure 7. Angle-resolved ESCA photoemission from ion-etched "Teflon" FEP The top monolayer is partially hydrocarbon in nature, whereas the surface appears entirely fluorocarbon.

Table I. Peak Intensity Ratios from Angle-Resolved ESCA Spectra

Sample	ESCA Take-off Angle	$\frac{F}{CF}$	$\frac{CH}{CF}$	$\frac{O}{CO}$
"Teflon" FEP target, side 1 contaminated	Integral	2.7	1.1	1.6
	Normal	2.9	0.9	1.8
	Grazing	2.6	2.0	1.2
"Teflon" FEP target. side 2 ion-etched	Normal	2.6	0.2	-
	Grazing	4.3	0.7	-
"Teflon" FEP, sputter-deposit	Integral	2.6	-	-

hydrocarbon material on the contaminated side of the target. However, the ratio of hydrocarbon to fluorocarbon does change upon normal incidence, indicating a thin contaminating surface layer. The ratio of hydrocarbon:fluorocarbon is quantified in Table I, which also shows fluorine:fluorocarbon and oxygen:oxidized-carbon ratios obtained from three fluoropolymer specimens. Note that "integrated" photoelectron collection (cone of rotation around the CMA axis) produces results thatare closest to those from normal incidence on the contaminated FEP sample. The grazing incidence results are high in hydrocarbon compared to either the normal or integral results, further indicating the top surface concentration of the hydrocarbon material.

The ion-etched FEP has a very rough surface structure, as seen in Figure 8, which may explain the unusual composition results. First, hydrocarbon is present in only the first atom layer or two, because its signal virtually disappears in normal incidence. Moreover, the hydrocarbon:fluorocarbon ratio increases by a factor of 3.5. More interesting is the fact that fluorine:fluorocarbon ratio increases by a factor of 1.7 from normal to grazing incidence. The grazing angle results are higher in fluorine relative to fluorocarbon by a factor of 1.7 compared to any of the other fluoropolymer surfaces. Apparently, an increased concentration of fluorine is trapped in the thin, rough overlayer of crosslinked fluorocarbon polymer.

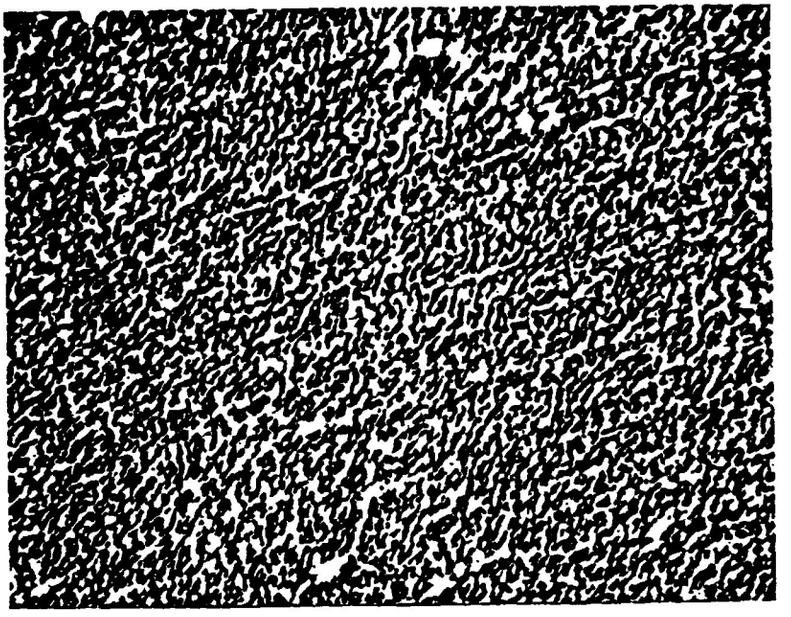

Figure 8. SEM photomicrograph (1000x) of ion-sputtered "Teflon" FEP, for which the ESCA spectra are shown in Figure 7. The surface is rough and pitted to an extreme. Asperities are less than 1μm in diameter and seem to project several micrometers above the surface.

Surface-Treated Titanium 6-4 Alloy

Morphological and structural details of a variety of surface treatments on Ti 6-4 alloy were obtained by SEM and ESCA (51). Further elucidation of these surface structures is shown with Auger depth profiling in Figures 9, 10, and 11. Figure 9 represents the Auger spectrum obtained (in seconds) from the Ti anodized sample at the end of the depth profiling experiment. All of the constituents of the alloy and oxide surface are visible, including a significant carbon component that arises from the surface treatment and an argon component deriving from implantation during the collection of profile data. The contrast between Figures 9 and 10 illustrates that the anodized Ti 6-4 has an oxide surface layer at least three times as thick as the oxide layer produced in the phosphate-fluoride treatment. It is important to note from both profile experiments that a significant carbon contamination exists throughout the oxide layer and is not simply a surface contaminant caused by handling.

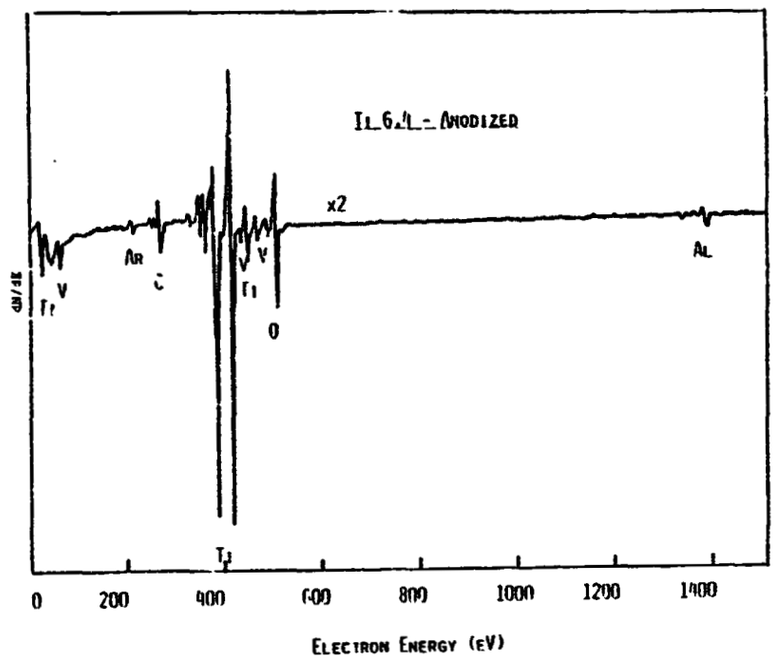

Figure 9. Auger spectrum taken at the end of ion profiling through the oxide layer on anodized titanium 6-4 alloy. The principal elemental constituents appear, including argon implanted during sputtering.

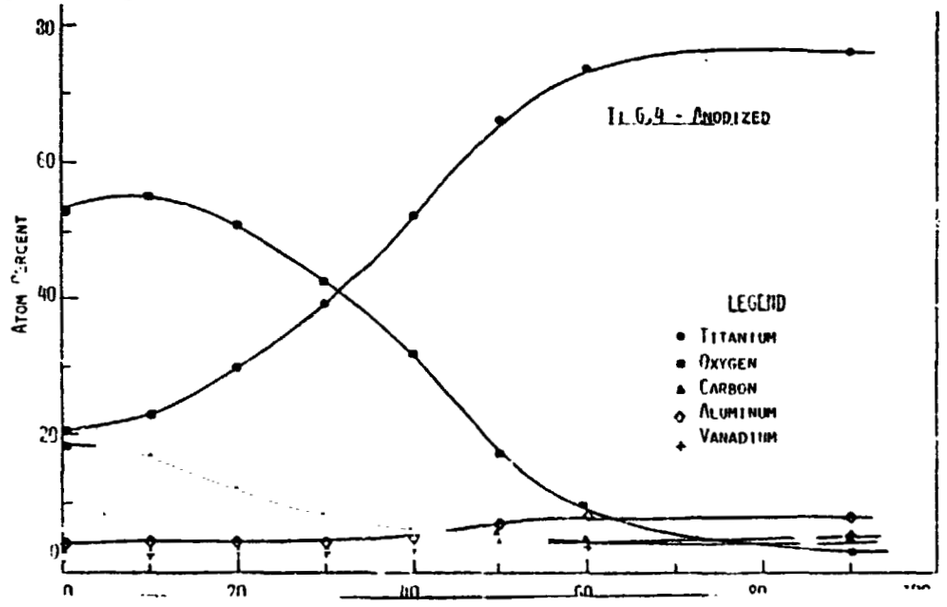

Figure 10. Simultaneous Auger/ion-milling depth profile (calibrated with Ta_2O_5 at 0.1nm/sec.) of anodized titanium 6-4 alloy. An oxide layer thickness of approximately 60nm and a significant carbon percentage throughout the oxide layer are obvious.

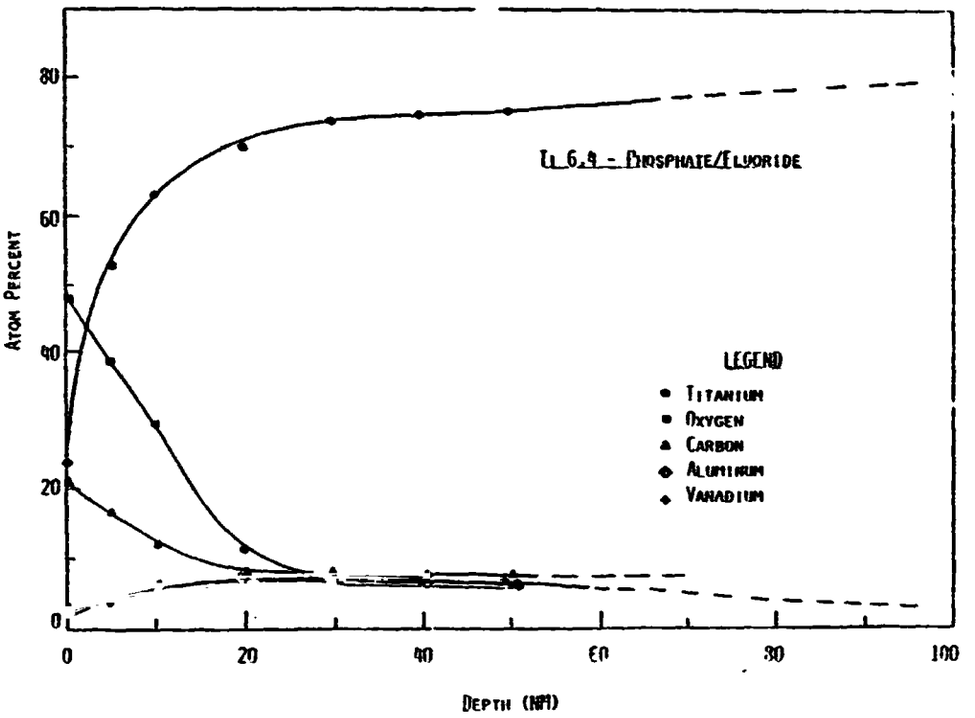

Figure 11. Simultaneous Auger/ion-milling depth profile of phosphate/fluoride treated Ti 6-4 alloy. A very thin oxide layer is apparent, with carbon also penetrating the oxide layer.

CONCLUSION

Modern surface analysis has promoted new understanding of contamination effects in the related fields of adhesion, corrosion, and wear. Successful applications require an understanding of the fundamentals of each energetic beam technique *and* their synergistic combination. Depth profile information is necessary to understand heterogeneous specimens, as illustrated with angle-resolved ESCA photoemission on fluoropolymers and ion-sputter/Auger analysis of oxidized titanium 6-4 alloy.

ACKNOWLEDGEMENTS

The support of the National Aeronautics and Space Administration under Grants NSG-1124 and NSG-3204 is gratefully acknowledged.

REFERENCES

1. C. J. Powell, "Appl. of Surface Sci.," 1, (2), 143 (1977).

2. R. H. Scott, P. B. DeGroot and J. Caron, Mater. Eval., 45, Oct. 1977.
3. M. Gettings and J. P. Goad, AERE-Report #8288, (1976).
4. L. Wiedmann, O. Ganschow and A. Benninghoven, J. Electron Spectrosc., 13, 243, (1978).
5. K. Persy and N. Gurker, J. Electron Spectrosc., 13, 91 (1978).
6. D. E. Williams and L. E. David, in "Characterization of Metal and Polymer Surfaces," (L. H. Lee, Ed.), Academic, New York, 1977, p. 53.
7. A. W. Czanderna, et al., J. Vac. Sci. Technol., 14 227 (1977).
8. D. M. Young & A. D. Crowell, "Physical Absorption of Gases," Butterworths, London, 1962.
9. J. J. Chessick, and A. C. Zettlemoyer, Advances in Catalysis, XI. 263 (1959).
10. K. E. Johnson, Jr. and R. H. Dettre, in "Surface and Collord Science," (E. Matijevic, Ed.) Vol. 2, Wiley, New York, 1969, p. 85.
11. P. C. Hiemenz, "Principles of Colloid and Surface Chemistry," Marcel Dekker, New York, 1977, p. 453.
12. F. M. Fowkes and M. A. Mostafa, Ind. Chem. Prod. Res. Dev., 17, 3, (1978).
13. H. R. Anderson, F. M. Fowkes and F. H. Hielscher, J. Polym Sci., Phys., 14, 879 (1976).
14. P. A. Lee, Phys. Rev., 23, 29 (1978).
15. H. Ishida and J. L. Koenig, J. Colloid and Interface Sci., 64, 555 (1978).
16. R. C. Sundahl, J. Vac. Sci, Technol., 9, 181 (1972).
17. D. W. Dwight, J. Colloid Interface Sci., 59, 447 (1977).
18. E. H. Andrews and A. J. Kinlock, J. Polym. Sci.: Symp. No. 46, 1 (1974).
19. R. A. Gledhill and A. J. Kinlock, J. Adhesion, 6 315 (1974).
20. M. Gettings and A. J. Kinlock, J. Mater. Sci., 12, 2511 (1977).
21. D. T. Clark, in "Handbook of X-Ray and Ultraviolet Photoelectron Spectroscopy," (D. Briggs, Ed.) Heyden & Son, London, 1977.
22. D. T. Clark and H. R. Thomas, J. Polym. Sci., Chem., 16, 791 (1978).
23. D. T. Clark and H. R. Thomas, J. Polym. Sci., Chem., 15, 2843 (1977).
24. D. T. Clark, A. Dilks and H. R. Thomas, in "Developments in Polymer Degradation, Part I.," (N. Grassie, Ed.), Applied Science Pub. Ltd., London, 1977, p. 87.
25. D. Briggs and D. M. Brewis, J. Mater. Sci., 12, 2549 (1977).
26. H. Yasuda, H. C. Marsh, E. S. Brandt and C. N. Reilley, J. Polym. Sci., Chem., 15, 991 (1977).
27. D. W. Dwight and W. M. Riggs, J. Colloid and Interface Sci., 47, 650 (1974).
28. D. Briggs, D. M. Brewis, and M. B. Konieczo, J. Materials Sci., 11, 127, (1977).
29. P. H. Holloway, "Application of Surface Analysis for Electronic

Devices," Pittsburgh Conference on Analytical Chemistry and Applied Spectroscopy, Cleveland, OH, May 12-16, 1978.
30. M. G. Yang, K. M. Koliwad and G. E. McGuire, J. Electrochem. Sol., 122, 675 (1975).
31. P. H. Holloway and D. M. Bushmire, Proc. 12th Ann. Intl. Conf. Reliability Physics, Las Vegas, 1974, p. 180.
32. D. W. Bushmire and P. H. Holloway, Proc. 1975 Int. Micro-Electronics Symp., p. 402.
33. F. J. Grunthaner, in "ARPA/NBS Workshop IV; Surface Analysis for Silicon Devices," NBS Spec. Publ. 400-23 (A. G. Lieberman, Ed.) p. 151.
34. H. L. Marcus, et al., J. Electrochem. Soc., 119, 1348 (1972).
35. A. Hiraki and E. Lugujjo, J. Vac. Sci. Technol., 9, 145 (1972).
36. G. J. Dooley, J. Vac. Sci. Technol. 9, 145 (1972).
37. R. R. Sowell, et al., J. Vac. Sci. Technol. 11, 474 (1974).
38. T. A. Bush, M. E. Counts and J. P. Wightman, in "Adhesion Science and Technology, Part A." (L. H. Lee, Ed.) Plenum, New York, 1975, p. 365.
39. E. L. Koehler, Corrosion, 33, 209 (1977).
40. A. G. Smith and R. A. Dickie, Ind. Eng. Chem. Prod. Dev., 17, 42 (1978).
41. J. E. Castle, Surface Sci., 68, 583 (1977).
42. J. S. Hammond, J. W. Holubka and R. A. Dickie, "Polym. Prepr.," 39, 506 (1978).
43. J. Ferrante, NASA Technical Note TN D-7933, Washington, (1975).
44. J. P. Rynd and S. K. Rastogi, Ceramic Bull. 53, (9), 631 (1974).
45. R. A. Chappell and C. T. H. Stoddart, J. Mater. Sci.. 12, 2001 (1977).
46. D. H. Buckley and W. A. Brainard, "Advances in Polymer Friction and Wear," Vol. 5A, (L. H. Lee, Ed.), Plenum, p. 315.
47. D. R. Wheeler, Wear, 47, 243 (1978).
48. P. W. Palmberg, J. Electron Spectrosc., 5, 691 (1974).
49. G. L. Lepeyre, R. J. Smith and J. Anderson, J. Vac. Sci. Technol., 14, 384 (1977).
50. A. J. Weigand and B. A. Banks, J. Vac. Sci. Technol., 14, 326 (1977).
51. W. Chen, D. W. Dwight and J. P. Wightman. "Surface Analysis and Adhesive Bonding III Titanium 604," Pittsburg Conference on Analytical Chemistry and Applied Spectroscopy, Cleveland, OH, May 12-16, 1978.

REDUCTION OF CONTAMINATION ON TITANIUM SURFACES STUDIED BY ESCA

W. Chen*, D. W. Dwight+, W. R. Kiang+ and J. P. Wightman*

Virginia Polytechnic Institute and State University

Blacksburg, Virginia 24061

X-ray photoelectron spectroscopy (ESCA) was used to determine compositions of some titanium and Ti 6-4 alloy surfaces before and after a variety of cleaning pretreatments. Although ubiquitous carbon contaminating layers were present, trace elements characteristic of specific etching solutions were detected. When the same specimens were analyzed in the AEI ES-100 and the duPont 650 photoelectron spectrometers, excellent agreement was obtained in binding energy values, but peak intensities were significantly different. Two types of argon plasmas (external to the spectrometer) were rapid and effective to reduce carbon contaminants to a minimum, promoting identification of trace elements associated with the substrate.

*Department of Chemistry
+Department of Materials Engineering

INTRODUCTION

Titanium 6-4 alloy is a highly stabilized, alpha-beta phase alloy, using 6% aluminum as the alpha stabilizer and 4% vanadium as the beta stabilizer, imparting toughness and strength at temperatures up to 627 K (750°F) (1). The general corrosion resistance of titanium alloys is superior to many common engineering metals, because of its natural, tenacious, self-healing oxide film, usually developed in the environment of water (2). However, in joining titanium alloys by welding, adhesive bonding, or other techniques, it is difficult to clean and prepare good bonding surfaces. A variety of specialized surface treatments have been developed over the past decade (3), and increasingly sophisticated measurements are being used to characterize the surfaces involved.

The use of alkaline and phosphate/fluoride surface treatments on Ti 6-4 were characterized in a review of surface analysis applied to several adherends. Differences between treatments were seen by Scanning Electron Microscopy (SEM) and in surface elemental composition as determined by Electron Spectroscopy for Chemical Analysis (ESCA) (4). Other surface preparations for titanium have been described, but without detailed analysis (5). In a study of a proprietary structural adhesive (HT 424) with aluminum 2024-T3 and Ti 6-4, ellipsometry and surface potential difference measurements identified substrates which would result in poor adhesive bonding (6). The use of Auger Electron Spectroscopy (AES) with ion-sputtering depth profiling, electron microscopy and diffraction and x-ray diffraction showed that the locus-of-failure alternated between the surface oxide layer, the interface and primer layer, and into the bulk adhesive. Phosphate/fluoride and Turco surface treatments gave similar bond strength and failure loci. Only a nitric acid/fluoride treatment produced low bond strengths, and this treatment left large copper concentrations in the oxide film.

Determination of time-to-failure (durability) at 333 K (140°F) and 95% relativity humidity at various loads, indicated stress-durability almost an order of magnitude greater with phosphate/fluoride treatment that with alkaline-cleaned alloys. Outdoor exposure in both stressed and unstressed adhesive joints provided a similar comparison. By non-destructive thermohology the rearrangement of titanium dioxide from anatase to rutile crystal structure was detected under the bond. Electron diffraction determined surface structures that were stabilized with ions that promote anatase formation (7). Similar observations have been made by other workers who comment that ~ 10% volume change accompanies the phase change, and may adversely affect bond durability (8).

Nylon-supported FM400 (modified epoxy) adhesive was used in conjunction with a corrosion inhibiting primer in a bond durability study of six different treatments on Ti 6-4 alloy. Lifetimes determined at $1.03 \times 10^7 Nm^{-2}$ (1500 psi) stress, 334 K (160^oF) and 100% relative humidity. Samples of lowest lifetime showed the greatest amount of interfacial failure, and longer-lasting surface treatments (lifetimes varied from 15 to over 1000 hr) produced evidence of more cohesive failure in the adhesive layer. The phosphate/fluoride surface treatment showed the lowest lifetime while several other acid treatments (pre-treated with base) produced lifetimes averaging around 500 hr (9). AES/ESCA/SIMS were used simultaneously to study the oxidation of titanium in the monolayer range (10). Successive stages of oxidation led to significant changes, first in the AES, then in the SIMS signals, and finally to a chemical shift in XPS. Also a number of treatments of titanium 6-4 alloy and pure titanium were studied with x-ray and electron diffraction, and no anatase form was found (11). Another study found oxidation of the metal was twice as fast as the alloy in water vapor at high temperature and pressure, and only rutile was found (12).

We concluded that the literature contains useful information on titanium, its alloys, surface treatments and adhesive bonding, but specific details of chemical and morphological structures that result from several commercial processes are not available or the data are conflicting. Thus we undertook a systematic study of many common treatments steps using scanning electron microscopy (SEM) with energy dispersive analysis of x-ray fluorescence (EDAX) and x-ray photoelectron spectroscopy (ESCA). As a first stage in accessing the relative durability of the different surface treatments, changes occasioned by aging at 505 K (450^oF) were monitored.

In general, our results showed that surface chemical composition was relatively constant, while profound changes occurred in morphology. The SEM results have been published elsewhere (13), but can be summarized briefly as follows: Ti 6-4 coupons had totally different morphology on opposite sides before grit blasting; that destroyed the original structures, leaving the surface heavily worked and fragmented and covered with minute fracture debris. Aluminum content significantly increased (uniformly and no Al_2O_3 grit blast particles appeared). Each of the four chemical surface treatments produced unique surface morphology, and only the two acid treatments bore any resemblance to each other. A qualitative ranking: Turco>Pasa-Jell>phosphate/fluoride>anodize was made by considering both (1) degree of roughness, and (2) degree of change in surface morphology after a 10 hr, 505 K (450^oF) exposure. Oxidation diminished the size of surface structures generally, and favored the alpha phase at the expense of beta.

Initial ESCA results on those samples indicated that 25-75% of the photoemission derived from a contaminating carbon overlayer. Plasmas have been demonstrated more effective than liquid reagents in reducing carbon contamination on rhodium and iron-cobalt alloy (14). Water contact angles and AES data were correlated in determining the amount of residual contamination after each type of cleaning. AES was used to monitor the relative efficacy of cleaning boron-doped silicon (111) semiconductor wafers by several liquid reagents, plasmas, and ion-beam sputtering (15). Again, inert gas plasmas were superior. Therefore we employed argon plasmas to reduce the carbon contamination prior to ESCA analysis.

The results reported below bear upon three points: (1) Semi-quantitative analysis of Ti 6-4 alloy surfaces before and after four commercial surface treatments and thermo-oxidative aging, (2) Comparison between results obtained in two photoelectron spectrometers (AEI ES-100 and duPont 650), and (3) Time study of both custom and commercial plasma cleaning on pure titanium metal.

EXPERIMENTAL

Materials. Lap shear coupons of Ti 6-4 were provided by D. Progar, NASA Langley Research Center, both before and after grit blasting. Pure titanium foil was obtained from the Alfa Division of Ventron Corporation, Danvers, MA 01923. Anodizing was performed by the Boeing Company using a proprietary process. Procedures followed for the three chemical treatments are listed in Tables I-III. Also samples after each of the four treatments were exposed for 10 and 100 hours at 505 K (450°F) in air.

Table I. Phosphate/Fluoride Treatment

1. Solvent wipe - methylethyl ketone.
2. Alkaline clean - immerse in SPREX AN-9, 30.1 g/ℓ, 353 K (80°C) for 15 min.
3. Rinse - deionized water at room temperature.
4. Pickle - immerse for 2 min. at room temperature in solution containing 350 g/ℓ of 70% nitric acid and 31 g/ℓ 48% HF.
5. Rinse - deionized water at room temperature.
6. Phosphate/fluoride treatment - Soak for 2 min. at room temperature in solution containing 50.3 g/ℓ of tri sodium phosphate (Na_3PO_4); 20.5 g/ℓ of potassium fluoride (KF); and 29.1 g/ℓ of 48% hydrofluoric acid (HF).
7. Rinse - deionized water at room temperature.
8. Hot water soak - deionized water at 338 K (65°C) for 15 min.
9. Final rinse - deionized water at room temperature.
10. Dry - air at room temperature.

Table II. Pasa-Jell 107 Treatment

1. Solvent wipe - methylethyl ketone.
2. Alkaline clean - immerse in SPREX AN-9, 30.1 g/ℓ, 353 K (80°C) for 15 min.
3. Rinse - deionized water at room temperature.
4. Pickle - immerse for 5 min. at room temperature in solution containing 15g nitric acid (HNO_3) 15% by weight; 3g hydrofluoric (HF) acid 3% by weight; and 82g deionized water.
5. Rinse - deionized water at room temperature.
6. Pasa-Jell 107 Paste - Apply to the titanium surface with an acid resistant brush covering the entire surface by cross brushing.
7. Dry - for 20 min.
8. Rinse - deionized water at room temperature.
9. Dry - air at room temperature.

Table III. Turco 5578 Treatment

1. Solvent wipe - methylethyl ketone.
2. Alkaline clean - immerse in Turco 5578, 37.6 g/ℓ, 343-353 K (70-80°C) for 5 min.
3. Rinse - deionized water at room temperature.
4. Etch - immerse in Turco-5578, 419 g/ℓ, 353-373 K (80-100°C) for 10 min.
5. Rinse - deionized water at room temperature.
6. Rinse - deionized water at 333-343 K for 2 min.
7. Dry - air at room temperature.

Plasma Cleaning. Both custom and commercial apparatus were used to reduce the carbon contamination on the titanium alloy coupons and pure foils. A "Plasmod" (Tegal Industries, 360 Wharf St., Richmond, CA 94804) with argon gas at 1 torr employed a crystal-controlled 13.6 MHz discharge at about 50 watts. The custom apparatus used argon at 5 torr and a Tesla coil (∿5 MHz) discharge. In this setup specimens were electrically grounded while they were not in the Plasmod. The effects of the custom discharge were studied both before and after mounting the specimens on ESCA probes.

ESCA Analysis. Spectra on some samples were obtained on an AEI ES-100 photoelectron spectrometer with an aluminum anode ($K\alpha_{1,2}$ = 1486.6 ev) and digital data acquisition. Rectangular (5×20^{-2} mm) samples were mounted on the sample probes using double-sided adhesive tape. In addition, ESCA spectra on all samples were obtained on a duPont 650 spectrometer with a magnesium anode ($K\alpha_{1,2}$ = 1253.6 eV) and analog display on an X-Y recorder. The carbon 1s level at 284.0 eV was used to evaluate the work function of both spectrometers (16). Circular (d = 6.4 mm) samples were

mounted on the sample probes using double sided adhesive tape.

Wide-scan spectra for each sample were obtained using the duPont spectrometer, attempting to detect all surface components present in significant amounts. The duPont spectrometer is especially suited for rapid analysis; a wide scan (0-700 eV) can be obtained in about one hour. Narrow scan spectra were obtained to establish precisely the binding energy and intensity of each peak noted in the wide scan.

Elemental assignments for each peak were based on standard binding energy tables (16). Further analysis of the ESCA results is possible using the measured intensities (I_i) in counts/sec and tabulated photoelectric cross sections (σ_i) (17). Using several assumptions the following equation was derived to approximate the atomic fraction (AF_i) of a given surface species (i):

$$AF_i = \frac{I_i/\sigma_i}{\Sigma(I_i/\sigma_i)}$$

It should be emphasized that these calculations are semi-quantitative at best, and primarily serve to reduce the data to comprehensible tables.

RESULTS AND DISCUSSION

The ESCA results discussed below represent two separate contamination studies. The first relates to four common chemical treatments designed to clean and etch Ti 6-4 for bonding. Interference of carbon contamination with ESCA analysis prompted the second study of argon plasmas to reduce that contamination.

Pretreatment and Thermal Aging

The ESCA results for these samples in Table I show that the grit-blasted sample has the highest aluminum content, in agreement with FDAX results (13). The large carbon content indicates organic contamination from the grit-blast operation.

Anodize. Organic contamination from environmental exposure and sample handling prior to analysis, as well as deposition during analysis, invariably gave rise to a large carbon 1s photopeak. Indicative of tetravalent oxide, the major titanium $2p_{1/2}$ and $2p_{3/2}$ oxide photopeaks were observed at 464.0 and 457.7 eV, respectively. The separation of the two peaks by 5.8 $\pm$ 0.4 eV is in excellent agreement with a previously published separation of 6.0 eV (16). Oxygen 1s photopeaks (529.6 $\pm$ 0.4 eV) were observed for each sample: a relatively thick oxide layer for the anodized sample was deter-

Table I. ESCA Peak Parameters for Ti 6-4 Before and After Chemical Surface Treatments

Peak Assignment	As-received		Anodized		Phosphate/Fluoride		Pasa-Jell		Turco	
	BE	%	BE	%	BE	%	BE	%	BE	%
F 1s	684.2	2	684.1		684.2	3	684.7	1	685.0	2
Cr $2p_{3/2}$	———	—	———	—	———	—	576.3	2	———	—
O 1s	530.0	24	529.9	13	529.5	41	529.6	42	529.4	32
V $2p_{3/2}$	514.2	1	515.0	1	515.5	1	514.6	1	515.7	1
Ti $2p_{3/2}$	457.9	6	457.9	7	457.0	17	457.6	14	457.9	10
N 1s	———	—	399.2	1	———	—	———	—	———	—
Ca $2p_{3/2}$	346.6	1	———	—	———	—	———	—	———	—
K 2p	———	—	———	—	287.9	1	———	—	———	—
C 1s	(284.0)	59	(284.0)	77	(284.0)	35	(284.0)	36	(284.0)	53
Cl 2p	———	—	197.6	1	197.3	1	———	—	———	—
P $2p_{3/2}$	———	—	———	—	132.6	1	———	—	———	—
Al 2s	118.5	8	118.2	1	118.2	1	118.0	2	119.1	2
Si 2p	———	—	———	—	———	—	103.2	2	———	—

BE = Binding Energy (eV)

% = Atomic Percent, from normalized peak intensity.

mined by ion milling/AES profiling (18). The O/Ti ratio of 1.9 is close to the expected value for TiO_2. Vanadium is a 4% bulk component of Ti 6-4, but its surface concentration was generally less than one percent, and the stoichiometric ratio of Al/V is greater than 1.5 determined from the bulk composition. A small nitrogen 1s photopeak at 399.4 ± 0.2 eV was noted. Fluorine was present as a fluoride with 1s binding energy of (684.4 ± 0.4 eV). Chloride ion was detected by a very weak 2p photopeak at 197.9 ± 0.3 eV.

Phosphate/Fluoride. The ESCA results (Table I) show traces of phosphorous, fluorine, potassium and chlorine from the surface treatment process, retained in the surface through the rinsing step.

Pasa-Jell. The results show that chromium and silicon (in the Pasa-Jell 107 paste) are residual surface components after this treatment.

Turco. The results in this case indicate minimum residual contamination. Fluorine is the only element not associated with the substrate, and its origin is unclear.

Thermal Aging. A small amount of nitrogen was detected in each of the samples after aging for 10 hours at 505 K (450°F); otherwise, there were no significant changes in the ESCA spectra of any of the samples after 100 hr of thermal aging. The binding energy values above agree closely with preliminary results on similar specimens reported earlier (19).

It should be re-emphasized that the calculated surface compositions are accurate to ± 15% at best, and care should be exercised in interpreting the results. On the other hand, most analytical techniques provide bulk elemental analyses, while the ESCA technique probes the composition of the surface layer (<10nm) only, where attention is focused in many problems. For example, in adhesion the definition of the interfacial region is tantamount to understanding bond failure. The ESCA technique has shown the presence of different trace elements in the interfacial region after specific chemical pretreatments. Some of these trace elements could serve as catalysts in polymer degradation and/or substrate corrosion, and thereby influence bond durability.

Comparison of AEI and DuPont Spectrometers

Since ESCA was collected for some of the anodized samples on both the AEI and duPont spectrometers, it is of interest to compare the results. A tabulation of average binding energies and intensities for Ti, Cr, F, O and C obtained from both spectrometers on three different anodized samples is given in Table II. There

Table II. ESCA Parameters for Anodized Ti 6-4 in two Spectrometers

Peak Assignment	AEI ES-100 BE (eV)	AEI ES-100 %	duPont 650 BE (eV)	duPont 650 %
F 1s	684.4±0.1	4	684.5±0.2	7
Cr	577.2	1	———	—
O 1s	529.7±0.2	37	529.8±0.2	19
Ti (IV) $2p_{3/2}$	458.0±0.3	15	458.1±0.3	7
C 1s	(284.0)	43	(284.0)	73
C/Ti	2.9		10.0	

BE = Binding Energy (eV) % = Atomic Percent, from normalized peak intensity

is remarkable consistency in the binding energies; also peak shapes were similar as gauged by a comparison of the peak widths at half-height. Chromium was detected in the AEI ES-100 but not in the duPont 650. In this case where the chromium surface concentration was <1%, the repetitive scan, digital acquisition used with the AEI ES-100 offered an advantage over the analog mode. The duPont multichannel analyzer was not in operation during this work, but appears necessary for analysis where the signal-to-background ratio is small. The C/Ti ratios are 2.9 and 10.4 for the AEI and duPont spectrometers, respectively. This may be caused by variations in either sample contamination, x-ray beam effects, or instrument geometry.

Significant difference in peak intensities were noted with different spectrometers. The duPont 650 signals were typically 30 times greater than those obtained with the AEI ES-100. The AEI ES-100 uses a slit between the sample and analyzer reducing transmission compared to the duPont 650; differences in intensity were expected. This results in faster analysis in the duPont spectrometer. For example, actual analysis time for the five principal elements was 33 minutes in the duPont 650 spectrometer and 210 minutes in the AEI ES-100 spectrometer. Sample contamination occurred to a greater extent in the duPont spectrometer as gauged by the larger C/Ti ratio. Recent studies on the build up of contamination during ESCA measurements shows that the vacuum level and instrumental factors governing neutralization of hole site are important factors (20). Peak intensity differences between our AEI ES-100 and duPont 650 spectrometers could be due to similar factors.

Figure 1. The decrease in C/Ti atomic ratio (determined from ESCA peak heights) as a function of exposure time to Ar^+ plasmas generated by three methods convenient for subsequent ESCA analysis.

Comparison of Plasma Techniques for Cleaning Titanium

The ESCA results suggest that the removal of a carbonaceous overlayer might enhance the intensity of substrate photopeaks, and permit detection of trace elements associated with the titanium surface. Without *in situ* argon ion cleaning, the question is, can an argon plasma external to the spectrometer significantly reduce the carbon contamination? Three timed series of ESCA studies were made on pure titanium foil, with Ar^+ plasmas generated under different conditions. Figure 1 shows the C/Ti ratio *vs* time of plasma exposure. It is clear that most of the cleaning action is accomplished within one minute. Furthermore, the ESCA probe seems to lead to additional residual contaminants, as can be seen in Table III.

Table III. ESCA Parameters for P e Titanium Foil Exposed tc Argon Discharges for 70 sec.

	As-Received		Custom (probe)		Custom (no probe)		Plasmod	
Element	BE	%	BE	%	BE	%	BE	%
O	529.4	5	529.4	10	529.3	31	529.3	32
Ti	457.5	1	457.6	4	457.3	13	457.7	13
N	———	—	400.2	1	———	—	399.0	1
Ca	———	—	346.8	1	346.6	1	346.5	1
C	(284.0)	88	(284.0)	66	(284.0)	53	(284.0)	50
Cl	197.9	2	197.7	7	———	—	197.6	1
Al	———	—	———	—	———	—	118.5	1
Si	102.2	3	101.7	3	101.4	2	101.4	1

BE = Binding Energy (eV)

% = Atomic Percent, from normalized peak intensities.

Custom rf discharge with sample on grounded probe. The ESCA results obtained in this case detected calcium, nitrogen, potassium, sulfur and zinc after argon cleaning, each at less than 1%. It is likely that these trace elements resulted from sputtered constituents of the sample probe and the glass walls of the plasma apparatus. The C/Ti ratio for the as-received Ti was 67, and it decreased significantly to 19 after 70 sec. exposure to the argon plasma. There is no further significant decrease in the carbon signal even after a 1 hr. exposure. Since the sample was mounted on a grounded probe, removal of carbon contamination is due to the action of both electrons and argon ions.

Custom rf discharge with sample grounded (no probe). When the Ti sample was grounded, but not mounted on a sample probe, only calcium was observed as a trace contaminant after argon plasma cleaning.

Plasmod. The custom and PLASMOD rf discharge appear equally effective in removal of the carbon contamination from titanium surfaces.

SUMMARY

Collectively the data suggest that the major carbonaceous contamination of metal oxides occurs prior to analysis, rather than deposition in the spectrometer. It is obviously desirable to have

in situ cleaning, but in lieu of this capability, external argon plasma cleaning can reduce carbon contamination significantly, leading to improved detection of trace constituents on the substrate of interest.

Binding energy values obtained with two different designs of commercial photoelectron spectrometers were in excellent agreement, but the relative intensities of photopeaks showed no correlation.

Trace contaminants, characteristic of different processes used in the pretreatment of titanium 6-4 alloy remain in the surface and are detected readily by ESCA.

ACKNOWLEDGEMENTS

Support for this work under NASA Grant NSG-1124 including a graduate research assistantship for one of us (WC) and the assistance of Mr. D. J. Progar at the NASA Langley Research Center are acknowledged gratefully.

REFERENCES

1. R. F. Mura[illegible] J. S. Wittick, "Materials Data Handbook on Titanium 6[illegible] NASA Tech Brief B73-10372, October 1973.
2. ASM Committe[illegible]n Metallography of Titanium and Titanium Alloys, Metals Handbook 7, 321 (1972).
3. R. H. Shoemaker, Titanium Sci. and Technol. 4, 2401 (1973).
4. W. C. Hamilton, Appl. Polym. Symp. 13, 105 (1972).
5. E. D. Newell and G. Carrillo, Materials and Processes for the 1970's, SAMPLE Conference, 1973, p. 131.
6. T. Smith and D. H. Kaelble, Report No. 74-73, Air Force Materials Laboratory, Wright-Patterson Air Force Base, Ohio (1974).
7. R. F. Wegman and M. J. Bodnar, SAMPLE Quarterly 5, 28 (1973).
8. F. Dalard, C. Montella and J. C. Sohm, Surf. Technol. 4, 367 (1976).
9. D. M. Stifel in "New Industries and Applications for Advanced Materials Technology," SAMPLE Pubs. Azuza, CA., 1974, p. 75.
10. A. Benninghoven, H. Bispinck, O. Ganschow and L. Wiedmann, Appl. Phys. Lett. 31, 341 (1977).
11. K. W. Allen and H. S. Alsalim, J. Adhesion 6, 299 (1974).
12. A. Motte, C. Coddet, P. Sarrazin, M. Azzopardi, and J. Besson, Oxid. of Metals 10, 113 (1976).
13. W. Chen, D. W. Dwight and J. P. Wightman in Symposium on Surface Analysis, Pittsburgh Conference on Analytical Chemistry and Applied Spectroscopy, Cleveland, OH, May 12-16, 1978, ASTM Publication, in press.

14. D. F. O'Kane and K. L. Mittal, J. Vac. Sci. Technol. 11, 567 (1974).
15. M. G. Yang, K. M. Koliwad and G. E. McGuire, J. Electrochem. Soc. May, 675 (1975).
16. K. Siegbahn, et al.,"ESCA Atomic, Molecular and Solid State Structure Studied by Means of Electron Spectroscopy," Almquist and Wiksells, Uppsalla, 1967.
17. J. H. Schofield, J. Electron Spectrosc. 8, 129 (1976).
18. D. W. Dwight and J. P. Wightman, in "Surface Contamination," (K. L. Mittal, Ed.), Plenum, New York, this volume.
19. T. A. Bush, M. E. Counts and J. P. Wightman in "Adhesion Science and Technology, (L. H. Lee, Ed.), Plenum, New York, 1975, p. 365.
20. E. S. Brandt, D. F. Untereker, C. N. Reilley, and R. W. Murray, J. Electron Spectrosc. 14, 113 (1978).

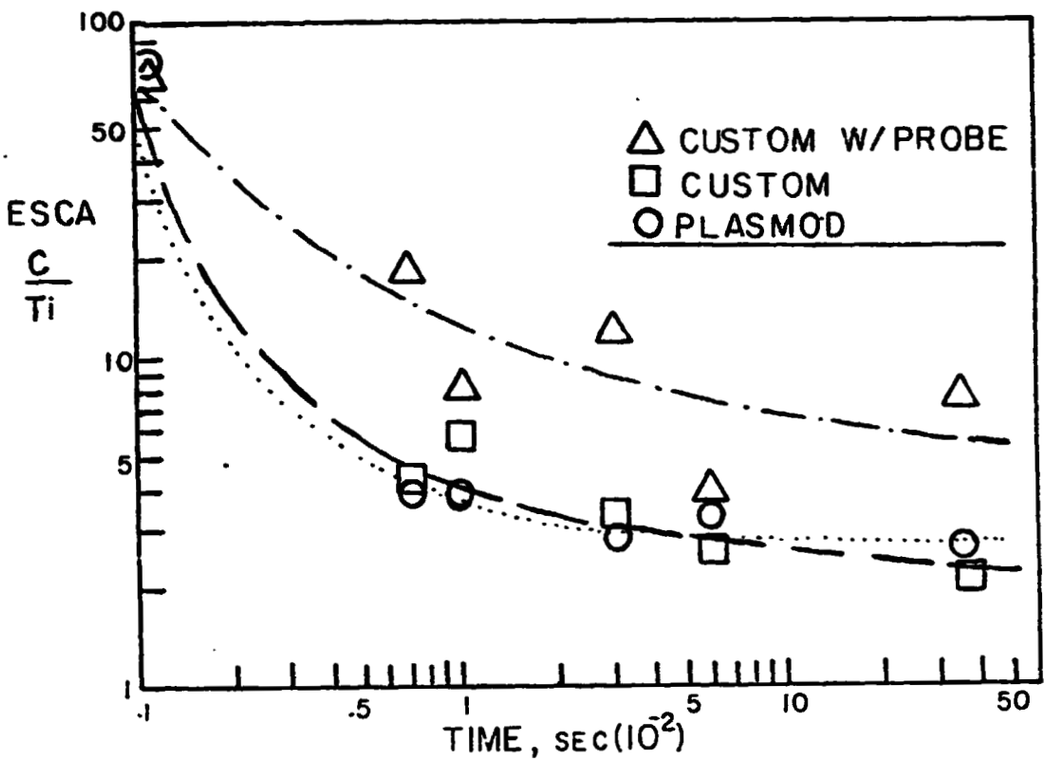
100
50
10
5
1
ESCA
C
Ti
CUSTOM W/PROBE
CUSTOM
PLASMOD
.1
.5
1
5
10
50
TIME, SEC(10-2)